Modeling the kinetics of nanoparticle formation

Rebeka Szabó

PhD thesis

Supervisor: Dr. Gábor Lente

full professor

University of Pécs
Doctoral School of Chemistry
Pécs, Hungary
2024

No problem can be solved until it is reduced to some simple form. The changing of a vague difficulty into a specific, concrete form is a very essential element in thinking.

(J.P. Morgan)

Contents

Notions used

M monomer unit (symbol only)

n the smallest number of monomer units that can form a kinetically effective nucleus (positive integer)

i, j auxiliary variables, i is typically the number of monomer units in a specific nanoparticle (non-negative integers)

C_i nanoparticle containing exactly i monomer units (symbol only)

P external inductor (symbol only)

t time

v_M the rate of nucleation ($\mathrm{mol\,dm^{-3}s^{-1}}$)

$v_{\mathrm{g},i}$ the growth rate of a nanoparticle with i monomer units ($\mathrm{mol\,dm^{-3}s^{-1}}$)

v_P the rate of the induced nucleation ($\mathrm{mol\,dm^{-3}s^{-1}}$)

k_M the rate constant of nucleation ($\mathrm{mol^{1-n}dm^{3n-3}s^{-1}}$)

k_g the second order rate constant of particle growth ($\mathrm{mol^{-1}dm^3s^{-1}}$)

k_P the rate constant of the induced nucleation ($\mathrm{s^{-1}}$)

$K(i)$ the kernel function describing how the growth rate constant of a nanoparticle depends on its size

c_i dimensionless concentration of nanoparticle C_i

m dimensionless concentration of monomer units

p_0 dimensionless concentration of the external inductor

τ dimensionless time

α dimensionless ratio of nucleation and growth rate constant

β dimensionless ratio of the induced nucleation and growth rate constant

μ_q the qth moment of variable c_i

r_{C} the cube-root number-average size of the nanoparticles

r_{A} the number-average size of the population of the nanoparticles

r_{W} the mass-average size of the nanoparticles

r_{Z} the Z-average size of the nanoparticles

$\bar{M}$ the average number of monomer units present in a nanoparticle

PD* polydispersity of nanoparticles

x_0 the number of monomer unit particles

x_i the number of c_i particles

N the total number of monomer units in the system

Q the number of realizations

$p(N)$ the partition function

$\mathbf{S}$ the stoichiometric matrix

p_i the propensity of i reaction step in dimensionless time

rnd_i the random numbers with uniform distributions between $[0, 1]$

$S_1, S_2, \ldots, S_N$ species

$R_1, R_2, \ldots, R_M$ reactions

y_m, y'_m vectors of the source and product complex

C_m reaction vector

s_m stoichiometric vector

κ_i stochastic rate constant

Δ time change

T_m internal time

L the number of firing reactions in a τ-leap

b_m individual reaction count

Λ_m independent sample of a tau-leap algorithm

Y_m unit Poisson process

S_m new jump time of the firing reaction of the mNRM algorithm

T temperature (K)

k_{B} Bolzmann constant (1.38×10^{-23}J/K)

D_i density of nanoparticles

V volumen ([dm^3])

η viscosity of fluid (Pa $*$ s)

$f(t)$ transformed phase fraction of the Johnson–Mehl–Avrami–Kolmogorov model

$(a+1)$ Avrami's exponent

θ shaping factor ($4\pi/3$ for spherical particles)

1 Introduction

Nanoparticles hold tremendous potential for a wide range of applications, from catalysis[1, 2] and electronics[3] to medicine[4–8] and environmental remediation[9–11]. Spherical nanoparticles, typically ranging from 1 to hundreds of nanometer in diameter, exhibit remarkable characteristics distinct from their bulk counterparts. Due to their small size and large surface area-to-volume ratio, nanoparticles possess enhanced reactivity[12] and unique optical, magnetic, and electrical properties, making them highly desirable for numerous applications. Nanoparticles can be obtained from both natural and synthetic sources[13]. Natural sources such as volcanic eruptions, forest fires, and cosmic dust produce nanoparticles through physical and chemical processes in the environment. On the other hand, synthetic methods involve the deliberate fabrication of nanoparticles in laboratories using techniques such as chemical precipitation, and vapor condensation. The ability to precisely control their size, shape, and composition is crucial for tailoring their properties to specific needs. In this context, understanding the kinetics of nanoparticle formation becomes paramount, as it directly influences the size distribution and overall characteristics of these particles.

Nanoparticles have emerged as valuable tools in the field of green chemistry[9–11, 14–16], providing specific opportunities to develop more sustainable and environmentally friendly processes. Their large surface area-to-volume ratio and tailored properties enable efficient catalysis[1], reducing the need for harsh reaction conditions and toxic reagents. The particles can act as catalysts, accelerating chemical reactions and promoting selective transformations, while minimizing waste production. Additionally, nanoparticle-based catalysts can often be more easily recovered than homogeneous ones, enhancing the overall efficiency of chemical processes. By harnessing the potential of nanoparticles, green chemistry aims to develop greener and more sustainable pathways for the synthesis of chemicals[11], pharmaceuticals[16], and materials[9], contributing to a cleaner and more environmentally conscious ap-

Figure 1.1: Illustration representing different types of spherical nanoparticles across a size spectrum spanning from 1 to 1000 nanometers. (*Illustration edited using BioRender*)

proach to chemical synthesis.

Nanomedicine[4–7, 16–18], the field that combines nanotechnology and medicine, holds great promise for innovating healthcare by enabling precise diagnosis, targeted therapy, and advanced drug delivery systems. Nanoparticles play a pivotal role in nanomedicine, providing distinct characteristics that render them well-suited for a wide range of biomedical applications. Their small size and large surface allow efficient interaction with biological systems at the cellular and molecular levels. One key area of nanomedicine is targeted drug delivery[6–8, 17] as they can be functionalized with specific ligands or antibodies that selectively bind to biomarkers present on the surface of diseased cells, such as cancer cells. These particles can also find applications in medical imaging[4, 5], providing enhanced contrast and resolution compared to traditional imaging techniques, and they can be used for various imaging modalities, including magnetic resonance imaging (MRI), and computed tomography (CT). Moreover, they have shown potential in regenerative medicine and tissue engineering[4, 19] because they can serve as scaffolds for cell growth and tissue regeneration, offering structural support and promoting cellular interactions.

It is also important to note that, although nanoparticles hold significant possibilities for various applications, it is essential to take into account their potential toxicity[3, 12, 13, 19, 20] and environmental consequences[9, 11, 15]. Due to their special physicochemical properties, they may pose risks to human health and the environment. When these tiny particles are released into the environment, either through intentional applications or as byproducts, they can interact with living organisms and ecosystems. The small size allows nanoparticles to penetrate biological barriers, such as cell membranes, and interact with cellular components, potentially

leading to cellular dysfunction or damage[13]. Furthermore, nanoparticles are able to induce oxidative stress, inflammation, and genotoxicity, which can have adverse effects on living organisms[15]. Moreover, nanoparticles can accumulate in the environment and bioaccumulate in the food chain, leading to potential long-term effects on ecosystems and biodiversity[9]. It is essential to thoroughly assess the toxicity and environmental behavior of nanoparticles to ensure their safe and sustainable use. Robust studies are needed to understand the mechanisms of nanoparticle toxicity, evaluate their potential risks, and develop appropriate mitigation strategies. By addressing the potential risks associated with nanoparticles, we can harness their benefits while minimizing their adverse effects, promoting the responsible development and application of nanotechnology.

2 Literature overview

2.1 Thermodynamic versus kinetic control

The dynamic process of nanoparticle formation is influenced by both thermodynamic and kinetic factors, which has long been a subject of debate in the scientific literature. Understanding the balance between them is essential for controlling the size, shape, and properties of nanoparticles.

The thermodynamic control in nanoparticle formation refers to a situation where the formation of the particles is primarily driven by the thermodynamic stability of the resulting system, which is determined by the lowest free energy, corresponding to the most stable configuration[21]. Nanoparticles with appropriate size, shape, and composition could be achieved using thermodynamically controlled synthesis because the system can reach a stable configuration with improved thermal stability, minimizing the propensity for aggregation or phase transformation[22].

In the kinetic control scenario, the reaction conditions and the kinetics of the process primarily determine the final nanoparticle structure. The most thermodynamically favored state may not be reached in a sufficient time, leading to the formation of kinetically favored particles instead. Using kinetic factors allows for the synthesis of metastable or non-equilibrium nanoparticles with distinctive properties.

The reaction conditions, such as reactant concentrations, temperature, time, presence of stabilizing agents or additives, and the nature of the precursor materials, primarily influence the dominance of either kinetic or thermodynamic control in particle formation[23, 24]. By carefully manipulating them, we can influence the reaction to achieve a desired kinetic state. Another important aspect is to comprehend the importance of the balance between the thermodynamic and kinetic control[25] which is essential for nanoparticle synthesis and design. The ability to adjust the characteristics of nanoparticles relies on manipulating the formation methods and

controlling the stability of the particles. By understanding the thermodynamics and kinetics involved, the synthesis conditions can be optimized properly to achieve the desired nanoparticle attributes, leading to applications in fields such as catalysis, electronics, energy storage, and biomedicine.

Continued research is needed to uncover the underlying mechanisms to explore new synthesis strategies, and to elucidate the relationship between the properties of nanoparticles and the kinetic and thermodynamic factors[26]. By harnessing the interplay between thermodynamic and kinetic factors, the field of nanoparticle synthesis continues to evolve, offering exciting opportunities for scientific developments and technological innovations.

2.2 Mechanisms of nanoparticle formation

2.2.1 Smoluchowski model

Studies on nanoparticle formation initially focused on kinetic models that could explain the underlying processes and factors influencing particle size and distribution. The Smoluchowski model, based on the Einstein–Smoluchowski theory, is a valuable tool for understanding and predicting the diffusion and aggregation behavior of nanoparticles in a fluid environment. However, this approach requires some simplifying assumptions, such as spherical nanoparticle shapes. More complex scenarios may require more sophisticated models[27–29].

The Einstein–Smoluchowski theory interprets the random motion of particles suspended in fluids, known as Brownian motion. It derives a mathematical relationship between the mean square displacement of a particle and the time elapsed. The Smoluchowski equation explains how particles disperse and cluster together in a fluid. The Langevin equation serves as a link between the two approaches[30].

The Smoluchowski model can be approached both stochastically and deterministically[31], depending on the type of process needed to be described. Under stochastic conditions, the molecular aggregation and fragmentation steps in a finite system can be correctly depicted. There is already a modified version of the Smoluchowski model[32], which fails for smaller systems but becomes available when it converges to infinity. Some researchers have used the Bayesian inference method to discretize the equation in one dimension as a system of rate equations[33]. On the other hand, the deterministic description ignores the influence of fluctuations, and although there are several equilibrium states, the deterministic process relaxes at one of them. For some simple cases, analytical solutions can be derived. The model uses kernel functions for the aggregation and fragmentation to represent the size dependence of the

rate constant. The influence of these kernels depends on the type of aggregation. For example, in the reaction-limited aggregation process, the effect of the self-assembly of the particles is less pronounced than in the diffusion-limited case[34].

The process describing the model can take into consideration reversible or irreversible reactions, both of which start with the formation of small clusters ($[C_i]$), and the latter can be given in the following way:

$$\begin{aligned} C_j + C_{i-j} &\xrightarrow{k_{i-j,j}} C_i \\ C_i + C_j &\xrightarrow{k_{i,j}} C_{i+j} \end{aligned} \tag{2.1}$$

where C_i and C_j represent the two spherical particles with size i and j, respectively, and which ones collide and form a new aggregate. The time evolution of the reaction is given by the differential equation below:

$$\frac{d[C_i]}{dt} = \frac{1}{2}\sum_{j=1}^{i-1} k_{i-j,j}[C_j][C_{i-j}] - [C_i]\sum_{j=1}^{\infty} k_{i,j}[C_j] \tag{2.2}$$

Here, the 1/2 is for a correction to avoid the double counting of the particle collisions, and the $k_{i,j}$ is the second-order rate constant of the bimolecular reaction.

The reversible case can be assumed to be an extended version of the aforementioned one. Here, the formation of small clusters also involves the fragmentation process. The rate constant of the fragmentation of the clusters is represented by $f_{i,j}$.

$$\begin{aligned} C_j + C_{i-j} &\underset{f_{i-j}}{\overset{k_{i-j,j}}{\rightleftharpoons}} C_i \\ C_i + C_j &\underset{f_{i,j}}{\overset{k_{i,j}}{\rightleftharpoons}} C_{i+j} \end{aligned} \tag{2.3}$$

The time-dependence of $[C_i]$ is modified accordingly:

$$\frac{d[C_i]}{dt} = \frac{1}{2}\sum_{j=1}^{i-1}\left(k_{i-j}[C_j][C_{i-j}] - f_{i-j}[C_i]\right) - \sum_{j=1}^{\infty}\left(k_{i,j}[C_i][C_j] - f_{i,j}[C_{i+j}]\right) \tag{2.4}$$

2.2.2 From the Becker–Döring equations to the Lifshitz–Slyozov–Wagner equation

It is possible to describe the size distribution of stable particles/clusters from supersaturated solutions using the well-known Becker–Döring equations, which model a

reversible coagulation process with non-zero rate constants (k_n, f_n, k_i, f_{i+1})[35]:

$$\begin{aligned} n\,\mathrm{M} &\underset{f_\mathrm{n}}{\overset{k_\mathrm{n}}{\rightleftharpoons}} \mathrm{C}_n \\ \mathrm{M} + \mathrm{C}_i &\underset{f_\mathrm{i+1}}{\overset{k_\mathrm{i}}{\rightleftharpoons}} \mathrm{C}_{i+1} \end{aligned} \tag{2.5}$$

The model was first established by Becker and Döring[36], and their version of the model requires the monomer concentration to be constant, while the total particle concentration can vary. From a chemical perspective, this aligns with the Classical Nucleation Theory, which originally explains the formation of stable nuclei/particles from supersaturated solutions[37]. The theory outlines five key steps involved in the formation of particles from a supersaturated solution (or vapor[38]). Obviously, the first step regards reaching the supersaturated solution, in which the individual monomers can start to aggregate and form small nuclei or clusters (second step) that are thermodynamically unstable. The third step is the critical nucleus size[39] representing the minimum number of monomers required for further growth. Above all these, for the formation of stable nuclei, the energy barrier must be overcome. Finally, the last step is the growth step which occurs by attracting additional monomers from the surroundings.

Later, the model was modified by Penrose et al.[40]. This version assumes the total concentration of the monomers in all particles to be constant. From a deterministic point of view, the system is spatially homogeneous with a large number of nanoparticles and reckons mass action kinetics. On the other hand, the stochastic version is a continuous time Markov chain model on a finite state space[41]. Here, the time evolution of the concentration of the species is given by the number of particles per unit of volume, so the infinite system of differential equations can be represented in this manner:

$$\begin{aligned} \frac{\mathrm{d}m(t)}{\mathrm{d}t} &= -nk_n m(t)^n - \sum_{i=n}^{\infty} k_i m(t) c_i(t) + f_{i+1} \sum_{i=n}^{\infty} c_{i+1}(t) + n f_n c_n(t) \\ \frac{\mathrm{d}c_i(t)}{\mathrm{d}t} &= k_{i-1} m(t) c_{i-1}(t) - f_i c_i(t) - k_i m(t) c_i(t) + f_{i+1} c_{i+1}(t) \qquad \infty > i \geq n \end{aligned} \tag{2.6}$$

In the above equations, $m(t)$ means the number of monomer units, and consequently $c_i(t)$ is the number of nanoparticles containing i monomer units.

The classical Becker–Döring model is designed to conserve density over finite time, ensuring the total number of particles (N) remains constant, as has been

already explained:

$$m(t) + \sum_{i=n}^{\infty} ic_i(t) = m(0) + \sum_{i=n}^{\infty} ic_i(0) = N = const. \qquad t \in [0, \infty) \tag{2.7}$$

The model is also known as digestive ripening resulting in small particles that grow at the expense of the larger ones, and the rate constant for the growth step is of the order of $1/N$:

$$k_i \sim \mathcal{O}(1/N) \tag{2.8}$$

This implies that at the end of the process, numerous small monodisperse nanoparticles are produced[42].

While the classical model has various steady-state solutions, it is more practical to consider solutions with long lifetimes. Numerous research groups have investigated this aspect over the past 30 years[40, 43, 44].

From an alternative perspective, the Becker–Döring equations describe the early stages of the growth step, and so then the Lifshitz–Slyozov–Wagner model gives the late stages of the growth, i.e. coarsening[45], so the latter can be interpreted as the limit case of the first model[43, 46, 47]. Moreover, it can also be viewed as a numerical representation of the Ostwald ripening process[48–50], where larger particles grow by dissolving smaller ones. In nanoparticle formation, this often characterizes the aging process[26, 51], involving aggregation and the Ostwald ripening.

These processes typically occur near equilibrium conditions, resulting in the final state of a single large particle in equilibrium with the solution. Considering the fluctuations of the process, it would be more appropriate to approach this model stochastically rather than deterministically[52, 53]. Since the resulting growth process is reversed to the Becker–Döring equations, the scaling of the coarsening rate constant is taken in the following way:

$$k_i \sim \mathcal{O}(N) \tag{2.9}$$

The classical Lifshitz–Slyozov–Wagner model for spherical particles corresponds to the following continuity equation:

$$\frac{\partial N(t,r)}{\partial t} + \frac{\partial \left(v(t,r)N(t,r)\right)}{\partial r} = 0 \qquad (t,r) \in \mathbb{R}_+^2 \tag{2.10}$$

where N refers to the number of particles, while v is the growth rate of the particles, and r is the radius of the particle. Solutions can be found in several ways, one method usually selects globally stable solutions from all the allowed ones[50], and

some others approach the problem by expressing the size distribution in terms of the mass, rather than the radius[54, 55], not to mention that the generalized model is assumed to be independent of the particle size.

2.2.3 Johnson–Mehl–Avrami–Kolmogorov model

The well-established Johnson–Mehl–Avrami–Kolmogorov model is often applied to the isothermal ($\Delta T = 0$) crystallization process and hydrolysis reactions which play through nucleation and growth steps of spherical particles[56]. The rates of these two steps are assumed to be constant throughout the reactions, and the predicted transformed fraction can only be correct if the system is large enough[57]. This transformed phase fraction ($f(t)$) is depicted by the given equation:

$$f(t) = 1 - \mathrm{e}^{-(kt)^{a+1}} \tag{2.11}$$

Here, k denotes the overall rate constant:

$$k = \left(\frac{\theta \upsilon_{\mathrm{M}} \upsilon_{\mathrm{g}}^{a}}{a+1} \right)^{1/a+1} \tag{2.12}$$

where υ_{M} and υ_{g} are the rate of the nucleation and growth, respectively. The nucleation rate is often referred to as a Dirac delta function leading to a process where the nuclei start growing simultaneously[58], other than that, the determined critical size of the nucleus has to be reached in order to grow further steadily[59–61]. The growth rate is often calculated from the half-life of the reaction. $(a + 1)$ is the Avrami's exponent which is related to the dimensionality of the growth process, i.e. the dimension of the crystal domain, usually, it should be between 3 and 4[62]. Furthermore, θ is a shaping factor, which is obviously $4\pi/3$ for spherical particles as it appears in the volume of a particle:

$$V(r, z) = \theta r^3 \tag{2.13}$$

By the aforementioned concepts, the rate equation has to be determined as:

$$\frac{\mathrm{d}f(t)}{\mathrm{d}t} = (a+1)k\left(1 - f(t)\right)\left[-\ln\left(1 - f(t)\right)\right]^{a/a+1} \tag{2.14}$$

Regarding nanoparticles, the model is often used to describe the size distribution of the nanoparticles[63, 64]. Using the Fokker–Planck evolution law leads to lognormal distribution, specifically in the case of ferrite nanoparticles[65], and in the growth process of some gold nanoparticles, a modified version of the model involv-

ing the Ostwald ripening can be applied[66]. Nonetheless, there are some proven results for nonisothermal case[67], as well. Beyond materials science, the model has turned out to be useful in the fields of cancer and genetics studies, ecology, and epidemiology, too[68].

2.2.4 LaMer model

The LaMer model[69, 70] expresses the formation of nanoparticles through instantaneous nucleation followed by subsequent growth steps with the addition of monomers. The key point in this scheme is that the two steps are supposed to be separated in time. It was first applied to the theory and production methods of colloidal suspensions with uniform sizes. The chemical reaction can be shown in this form:

$$\begin{aligned} n\,\mathrm{M} &\xrightarrow{k_1} \mathrm{C}_n \\ \mathrm{C}_n + \mathrm{M} &\xrightarrow{k_2} \mathrm{C}_{n+1} \\ \mathrm{C}_i + \mathrm{M} &\underset{f_{i+1}}{\overset{k_i}{\rightleftharpoons}} \mathrm{C}_{i+1} \end{aligned} \tag{2.15}$$

In these equations, M denotes the n number of monomer species and C means the growing nanoparticle with size i. The rate constants are denoted by k_1, k_2, k_i, respectively, and f_{i+1} is the rate constant of the fragmentation step. The so-called "burst" nucleation is usually a second-order step (so n=2), and it decreases the concentration of the monomers in the solution, even though, it is described as "effectively infinite", so the rate of this step is proportional to infinity (υ_{M}), and after the step, there are hardly any monomers left to form a nucleus but to grow the others. Some experimental studies, however, show this process to be an autocatalytic step[71]. The growth step is considered to happen under a diffusion-controlled reaction. The system of ordinary differential equations describing this model is given as follows:

$$\begin{aligned} \frac{\mathrm{d}[\mathrm{M}]}{\mathrm{d}t} &= -nk_1[\mathrm{M}]^n - k_2[\mathrm{M}][\mathrm{C}_n] - \sum_{i=n}^{\infty}\left(k_3[\mathrm{M}][\mathrm{C}_i] + f_3[\mathrm{C}_{i+1}]\right) \\ \frac{\mathrm{d}[\mathrm{C}_n]}{\mathrm{d}t} &= k_1[\mathrm{M}]^n - k_2[\mathrm{M}][\mathrm{C}_n] \\ \frac{\mathrm{d}[\mathrm{C}_i]}{\mathrm{d}t} &= k_{i-1}[\mathrm{M}][\mathrm{C}_{i-1}] - f_i[\mathrm{C}_i] - k_i[\mathrm{M}][\mathrm{C}_i] + f_{i+1}[\mathrm{C}_{i+1}] \end{aligned} \tag{2.16}$$

The last equation is the same as the already presented growth step of the Becker-Döring model.

According to LaMer et al., the size distribution of the particles can be controlled by manipulating the rates of nucleation and growth. Moreover, this final distribution

is a lognormal distribution. This theoretical framework is still in use, especially in the study of metal and semiconductor nanoparticles[49].

2.2.5 Finke–Watzky model

The general two-step Finke–Watzky model describing nanoparticle formation consists of a slow nucleation step followed by a fast autocatalytic growth step, and the two steps are well-separated in time[72, 73]. The second step is a monomer addition until the agglomeration becomes kinetically competitive. In the nucleation step, species M forms a kinetically effective nucleus (C).

$$\begin{aligned} \mathrm{M} &\xrightarrow{k_1} \mathrm{C} \\ \mathrm{M} + \mathrm{C} &\xrightarrow{k_2} 2\,\mathrm{C} \end{aligned} \tag{2.17}$$

There are two important assumptions in the Finke–Watzky model:

1. $k_1 << k_2[\mathrm{M}]_0$, showing that the rate of nucleation is much slower than the rate of the second step[73]

2. $[\mathrm{M}] < [\mathrm{M}]_0$, specifying that the concentration of species M decreases over time

The differential equation of the time-dependence of the monomer units and the nanoparticles is given as follows:

$$-\frac{\mathrm{d}[\mathrm{M}]}{\mathrm{d}t} = \frac{\mathrm{d}[\mathrm{C}]}{\mathrm{d}t} = k_1[\mathrm{M}] + k_2[\mathrm{M}][\mathrm{C}] \tag{2.18}$$

The exact analytical solutions for the monomer unit and the nanoparticle can be found analytically:

$$\begin{aligned} [\mathrm{M}]_t &= \frac{\frac{k_1}{k_2} + [\mathrm{M}]_0}{1 + \frac{k_1}{k_2}[\mathrm{M}]_0 \exp\left(k_1 + k_2[\mathrm{M}]_0\right) t} \\ [\mathrm{C}]_t &= [\mathrm{M}]_0 \left(1 - \frac{k_1 + k_2[\mathrm{M}]_0}{k_2[\mathrm{M}]_0 + k_1 \exp\left(k_1 + k_2[\mathrm{M}]_0\right) t}\right) \end{aligned} \tag{2.19}$$

This model is often applied in the study of transition-metal nanoclusters (e.x., $\mathrm{Ir}(0)_{\sim 300}$), where the size is monodisperse (narrow size distribution)[74]. By Finke et al., it was shown that it can be an alternative solution to the Avrami–Erofe'ev model for describing the kinetics of nanoparticle formation[75]. The Avrami–Erofe'ev model assumes random nucleation and growth processes despite the Finke–Watzky model. Another important result by them is that a bimolecular nucleation step is still possible, while a termolecular step has been proven not to be feasible[76, 77].

The technique used in this model is called lumping, whose aim is to reduce the dimensionality of the model by combining species and/or reactions. This is a sort of simplification that allows us to have an easier interpretation of the system. The model also incorporates pseudo-elementary steps[78], which are representations of complex systems. Above these, there are several extensions and modified versions of the original two-step Finke–Watzky model[79], some take into account the aggregation[80], or some contain one or two additional steps, such as the following here:

$$\begin{aligned} \mathrm{M} &\xrightarrow{k_1} \mathrm{C} \\ \mathrm{M} + \mathrm{C} &\xrightarrow{k_2} \mathrm{D} \\ \mathrm{M} + \mathrm{D} &\xrightarrow{k_3} 1.5\,\mathrm{D} \end{aligned} \tag{2.20}$$

In this particular model, M is still the monomers, while C represents the "small" particles, and D gives the "larger" nanoparticles. According to this model, the smaller nanoparticles grow faster than the larger ones, i.e. $k_2 > k_3$.

A significant achievement in the field is the use of mechanism-enabled population balance modeling, which has been extensively studied in Handwerk's works [79, 81, 82]. This technique allows for the accurate prediction of particle size and distribution based on various initial conditions and reaction parameters. Using this special technique, all the processes of nucleation, growth, and aggregation can be accounted for. The nucleation can be explained through an nth order step, and the main assumption is that the growth reaction can only be considered as a monomer addition if the aggregation process is not kinetically effective.

2.2.6 Exploring beyond classical models

Understanding the process of nucleation, growth, and aggregation is inevitable for nanoparticle synthesis since it not only influences the particle size distribution but also plays a significant role in determining their behavior and toxicity. While many approaches have been proposed in the literature to describe these processes, none of them is a universal method that can be applied. Several factors have a huge impact on these steps, such as the temperature, pH, solvent properties, concentrations, surface properties, and the presence of stabilizing agents or surfactants[49, 83, 84].

The initial and most fundamental step in nanoparticle formation is the nucleation process [38], which typically occurs much more rapidly than the following growth steps, involving the emergence of the critical size nuclei[39, 85]. The nucleation step can happen through a heterogeneous or a homogeneous process, i.e. either on a pre-existing surface or in a uniform medium spontaneously. Furthermore, a preliminary

step can occur before the nucleation, which could be necessary for certain cases[78]. Nucleation can also be classified as either spontaneous or induced, where external factors, conditions, or reagents trigger the reaction[86, 87], and in some cases, like with quantum dots, the reversible nucleation step can also be possible[88].

The slower reactions are the growth steps[71, 89] in nanoparticle synthesis, which can be categorized by different mechanisms. The more favorable one is the monomer addition, where individual monomer units are added step-by-step to the growing nanoparticle. In this way, precise nanoparticle size distribution and composition can be achieved.

The other possibility is called the coalescence of smaller nanoparticles, i.e. when two particles collide with each other, the repulsive force between them is overcome by their Brownian motion, leading to their fusion. However, coagulation often gives broader size distributions of nanoparticles[90].

Aggregation is another widely studied phenomenon[83, 85], involving the formation of larger clusters through the attraction of nanoparticles. This type of reaction can occur in reversible (then fragmentation also occurs)[91, 92], or irreversible form. The agglomeration reactions usually depend on factors, such as the collision speed of the different particles and the size of the attractive forces between them[28]. The literature describes many types of aggregation models that can be differentiated based on their mechanism. In reaction-limited aggregation[93], the attachment of particles is determined by chemical reactions. The diffusion-limited aggregation is governed by the Brownian motion and the diffusion of the particles. Another current type is cluster-to-cluster aggregation[84] in which the pre-existing clusters collide and attach.

In the context described, population balance modeling[90, 92] seems to be a valuable method for predicting the size distribution of the particles. The modeling equations form a system of partial differential equations which are generally solved numerically using computational methods, but in certain cases, analytical solutions may be obtained.

Sometimes, the aggregation kernels can be introduced, which describe the probability of two clusters coming into contact to form larger aggregates[28, 93]. The rate of diffusion-limited aggregation can be defined using the following equation:

$$v_{\mathrm{AG}}(1,2) = K_{\mathrm{AG}}\ D_1 D_2 = \left[\frac{3\eta}{2k_{\mathrm{B}}T(1/r_1 + 1/r_2)(r_1 + r_2)} + \frac{1}{k_{\mathrm{AG}}}\right]^{-1} * D_1 D_2 \quad (2.21)$$

Here, D_i represents the density of the nanoparticles of hydrodynamic radius r_i, η means the viscosity of the fluid [Pa s], k_{B} is the Boltzmann constant with temper-

ature T[K], while k_{AG} implies a constant [$\mathrm{m^3 s^{-1}}$] which depends on the solution composition and the radii, and K_{AG} gives the aggregation kernel. In the case of reaction-limited aggregation, the latter term can be simplified to:

$$K_{\mathrm{AG}} = k_{\mathrm{AG}} \tag{2.22}$$

2.3 Stochastic kinetic approach

Stochastic chemical kinetics plays an important role in having a more accurate description of chemical processes by taking into account the inherent fluctuations and randomness in molecular interactions. Its significance mostly appears in small systems characterized by low molecule numbers where the effects of molecular discreteness and stochasticity cannot be ignored. The application of stochastic modeling involves various biological processes, including gene regulation[94, 95], virus kinetics[95], enzyme kinetics[94–97], ligand migration in biomolecules[98], and membrane noise[99], as well as chirality[100–102], and the Frank model[103, 104], asymmetric autocatalysis[105–109], all of which heavily rely on the discrete nature of molecular interplays.

Stochastic modeling emerged from the investigation of fluctuation phenomena, notably the renowned research on Brownian motion by Einstein[110]. This work paved the way for the initial development of the fluctuation-dissipation theorem. By regarding the movement of Brownian particles as a trajectory that lacks memory and differentiability, a significant result was achieved in establishing the groundwork for the theory of stochastic (Markovian) processes. Early advancements in stochastic kinetics were reached by Leontovich[111], Delbrück[112], Kramers[113], and Rényi[114], and since then, huge progress has been achieved in this field.

Stochastic chemical kinetics puts a great emphasis on understanding and modeling the effects of noise and fluctuations[115]. In this context, noise refers to the irregularities and disturbances in the system, while fluctuations arise from the random behavior of molecules. Two types of noises can be given in the case of stochastic kinetics: external noise, which is outside the control of the observer, and internal noise, which is directly related to the internal structure of the system.

2.3.1 Continuous time discrete state stochastic model

The needed reaction network is composed of N chemical species denoted by $S_1, \ldots,$ S_N and M reactions denoted by $R_1, \ldots, R_M$. Each reaction R_i can be represented

as:

$$\sum_{i=1}^{N} y_{im} S_i \to \sum_{i=1}^{N} y'_{im} S_i \tag{2.23}$$

where $y_m, y'_m \in \mathbb{Z}^N_{\geq 0}$ are vectors representing the source and product complexes[95, 99, 116, 117], respectively, and $C_m := y'_m - y_m \in \mathbb{Z}^N$ is the reaction vector giving the change in the number of molecules for each species. The system state at time t is represented by the vector $X(t) = (X_1(t), \ldots, X_N(t)) \in \mathbb{N}_0^N$ whose ith component $X_i(t)$ is the number of molecules of S_i at time t.

In the continuous-time discrete-state stochastic approach, the system consists of a discrete set of states connected by transitions, each with an associated rate of an exponential distribution[94, 95, 98, 99, 116, 117]. In each state, transitions compete in a race condition: the fastest one determines the new state and the time elapsed. The next reaction only depends on the current configuration of the system, exhibiting a memoryless property.

The propensity function[117] (or intensity function[95]) $p_i(x)$ determines the rate at which reaction R_i fires when the system is in state x, where $p_i : \mathbb{N}_0^N \to \mathbb{R}_{\geq 0}$. If the reaction i fires at time t, the system's state jumps from $X(t)$ to $X(t^+ = X(t) + s_m$ where $s_m = (y'_{1m} - y_{1m}, \ldots, y'_{Nm} - y_{Nm})$ is the stoichiometric vector representing the change in the state due to the reaction. From this, the stoichiometric matrix can be given in the following form: $S = N \times M$ for the reaction network by $S = [s_1 s_2 \ldots s_M]$. The column of this matrix is the stoichiometric vector for all the reactions. The propensity function $p_i(x)$ is generally arbitrary but must satisfy the condition that if $p_i(x) > 0$ for a given state $x \in \mathbb{N}_0^N$, then $(x + s_m) \in \mathbb{N}_0^N$, ensuring that the model stays inside the nonnegative integer orthant, $\mathbb{N}_0^N$. The general form of this function can be defined in the following way:

$$p_i(x) = \kappa_i \prod_{i=1}^{N} y_{im}! \binom{x_i}{y_{im}} = \kappa_i \prod_{i=1}^{N} \frac{x_i(x_i - 1)\ldots(x_i - y_{im} + 1)}{y_{im}!} \tag{2.24}$$

for each $x = (x_1, \ldots, x_N) \in \mathbb{N}_0^N$. Here $\kappa_i > 0$ denotes the rate constant for the ith reaction.

Often mass-action kinetics is assumed. This form of propensities implies that the rate at which the reaction fires is proportional to the number of ways the required number of reactant molecules can be chosen from the population[118]. This makes sense if the system is well-stirred.

The order of reaction i is the total number of reactant molecules it requires, i.e. $\sum_{i=1}^{N} y_{im}$. Reactions with order three or more are considered untypical[119, 120].

From rate functions, we can derive a set of differential equations that gives how the probability of being in different states varies over time, and this is the chemical master equation (or Kolmogorov forward equation)[95, 99, 116, 117]. The CME is described by a set of differential equations that determines how the probability distribution of being in different states changes over time:

$$\frac{\mathrm{d}\mathbb{P}(X,t)}{\mathrm{d}t} = \sum_{i=1}^{M} \underbrace{p_i(X-s_m)\mathbb{P}(X-s_m)}_{\text{A reaction } R_i \text{happened in time } [t,t+\mathrm{d}t]} - \sum_{i=1}^{M} \underbrace{p_m(X)\mathbb{P}(X)}_{\text{No reaction happened in } [t,t+\mathrm{d}t]} \tag{2.25}$$

While the master equation provides a complete description of the stochastic process, solving it is actually impossible or at least challenging. To find the solution, it might be helpful to know the number of states, which can be found as the number of solutions of a Diophantine equation[117]. There are some approaches that can be employed, like the symbolic Laplace transformation[116], the numerical direct matrix operation, or the Poisson representation[117] as an approximate method. In many applications, only the first two moments (mean and variance) of the probability distribution[95, 116, 117] are necessary, reducing the computational complexity.

2.3.2 The link between stochastic and deterministic kinetics

In the deterministic approach, the system of ordinary differential equations represents the rates of change of concentrations with respect to time and it considers a continuous variation in concentration is often used for large volumes or concentrations[119–121]. On the other hand, the stochastic model assumes discrete states and probabilistic transitions between these states, plus it takes into account the particulate nature of matter. Regarding the Kurtz theorem[122–124], the stochastic model provides a microscopic description that becomes increasingly consistent with macroscopic behavior described by the deterministic model as the size of the system increases. In other words, as the volume of the system approaches infinity, the stochastically described model converges to the deterministic one. This theorem helps us to understand the relationship between these two approaches and to bridge the gap between the continuous and discrete descriptions of the systems.

Deterministic kinetics uses autonomous and non-linear differential equations that describe the time-dependent rates as a function of concentrations. Each concentration of the particles can be altered at most in M different reactions, resulting in each differential equation having a maximum of M additive terms. On the other hand, this property can be described in the stochastic kinetics by a Markov process. The transition rates here are independent of time and instead depend on the molecule

numbers. The master equation is always linear and homogenous, and the positive transition rates incorporate the probabilities of M states, while the negative term does as well.

In this section, the concept of deterministic continuation[117] needs to be mentioned, which involves solving the deterministic differential equation directly using the initial concentration vector obtained from stochastic calculations. In this approach, the particle numbers are treated as dependent variables adjusting them by Avogadro's constant and the volume. Because of the autonomous nature of the master equation, time dependence can sometimes be omitted and one of the particle numbers can be selected as an independent variable. The significance of this technique can be evident in situations when a static property of the system, such as the final state, holds more importance than the time dependence of the particle numbers. However, this technique requires selecting a type of particle number that changes monotonously over time. By doing so, the numerical integration methods get improved in more accurate and efficient solutions.

2.3.3 Simulation methods

As it is known, finding an explicit solution to the master equation can be extremely difficult, especially for complex systems with large state space, simulation methods are crucial as an effective alternative. By generating multiple random trajectories, the following simulation methods can approximate the probability distribution. Monte Carlo simulations[95, 98, 99, 116, 117] are usually applied to simulate stochastic processes.

Monte Carlo estimator is based on the law of large numbers, which states that if we have independent realizations as a random variable X, denoted as $X_{[1]}, X_{[2]}, \ldots$, when the number of realizations converges to infinity, the average of the function $f(X)$ over these realizations approaches to the expected value of $f(X)$. To approximate the expected value of $f(X)$, a large number of independent realizations can be generated, represented as $\{X_{[i]}\}_{i=1}^{Q}$, and use the approximation where the expected value is estimated by the average of $f(X)$ over these realizations. The estimate is given by:

$$\mathbb{E}[f(X)] \approx \frac{1}{Q} \sum_{i=1}^{Q} f(X_{[i]}) \tag{2.26}$$

As the number of realizations Q is increased, the standard deviation of the approximation scales inversely with the square root of Q, while the computational costs increase linearly with Q.

The Stochastic Simulation Algorithm (SSA), also known as Gillespie's algo-

rithm[94, 95, 116, 125–127], operates by simulating a discrete time Markov chain embedded within the model, considering transition probabilities to account for state transitions. At each jump time, two random variables are needed to be generated. The first random number is used to determine the time of the next reaction, while the second one is for finding which specific reaction takes place at that time.

Gillespie's algorithm

Given: Initial time t_0, Final time t_f, Initial state $X(t_0) = x_0 \in \mathbb{Z}^N_{\geq 0}$.

Step 0: Set the jump counter $j = 0$, the initial time $t_0 = 0$, and the initial state $X(t_0) = x_0 \in \mathbb{Z}^N_{\geq 0}$.

Step 1: Calculate $p_m(X(t_j))$ for all $m \in \{1, \ldots, M\}$.

Step 2: Set $p_0(X(t_j)) = \sum_{m=1}^{M} p_m(X(t_j))$.

Step 3: Generate two independent random numbers rnd_1 and rnd_2 from a uniform distribution over the interval $(0, 1)$.

Step 4: Set $\Delta = \ln(1/rnd_1)/p_0(X(t_j))$.

Step 5: Find $\sigma \in [1, \ldots, M]$ such that

$$\frac{1}{p_0(X(t_j))} \sum_{m=1}^{\sigma-1} p_m(X(t_j)) < rnd_2 \leq \frac{1}{p_0(X(t_j))} \sum_{m=1}^{\sigma} p_m(X(t_j)) \tag{2.27}$$

Step 6: Update the state as $X_{j+1} = X_j + s_m$ and $t_{j+1} = t_j + \Delta$.

Step 7: If $t_{j+1} > t_f$ STOP; otherwise, set $j = j + 1$ and go to Step 1.

Output: The list of jump times and states (t_j, X_j) for $j = 0, 1, \ldots, (j + 1)$.

When the reaction rates are relatively high, the First Reaction Method[98] (or First Reaction Monte Carlo method) can be applied, which is less efficient than Gillespie's direct method but is still quite efficient and capable of handling complex systems with large numbers of reactions and species. In this case, M independent exponential random variables need to be generated.

First Reaction Method

Given: Initial time t_0, Final time t_f, Initial state $X(t_0) = x_0 \in \mathbb{Z}^N_{\geq 0}$.

Step 0: Set the jump counter $j = 0$, the initial time $t_0 = 0$, and the initial state $X(t_0) = x_0 \in \mathbb{Z}^N_{\geq 0}$.

Step 1: Calculate $p_m(X(t_j))$ for all $m \in \{1, \ldots, M\}$.

Step 2: Draw samples $t_m = \ln(1/rnd_m)/p_m(X(t_j))$ for all $m \in \{1, \ldots, M\}$.

Step 3: Calculate $\Delta = \min_m\{t_m\}$ and $l = \arg\min_m\{t_m\}$.

Step 4: Update the state as $X_{j+1} = X_j + s_m$ and the next time jump as $t_{j+1} = t_j + \Delta$

Step 5: If $t_{j+1} > t_f$ STOP; otherwise, set $j = j + 1$ and go to Step 1.

Output: The list of jump times and states (t_j, X_j) for $j = 0, 1, \ldots, (j + 1)$.

The Next Reaction Method[98, 116, 128] is particularly advantageous for systems with low reaction rates or when individual reactions have a huge influence on the system dynamics. It can handle systems with varying reaction rates, and adapt to changes in the reaction network. A modified version of the Next Reaction Method[128], introduced by Anderson et al., further enhances computational efficiency by reducing the number of propensity updates during simulation. Instead of recalculating the propensities of all reactions at each simulation step, only the propensities of the reactions involving the reactants that have changed since the previous reaction are updated. As a result, only one independent random variable needs to be generated at each jump time.

modified Next Reaction Method

Given: Initial time t_0, Final time t_f, Initial state $X(t_0) = x_0 \in \mathbb{Z}^N_{\geq 0}$.

Step 0: Set the jump counter $j = 0$, the initial time $t_0 = 0$, and the initial state $X(t_0) = x_0 \in \mathbb{Z}^N_{\geq 0}$.

For each $m \in \{1, \ldots, M\}$, internal time $T_m = 0$ and the first jump time of Y_m (unit Poisson process) as $S_m = \ln(1/rnd_{m_0})$.

Step 1: Calculate the time-step $\Delta t_m = \frac{S_m - T_m}{p_m(X_j)}$ for each $m \in \{1, \ldots, M\}$.

Step 2: Calculate $\Delta = \min_m\{\Delta t_m\}$ and $r = \arg\min_m\{\Delta t_m\}$.

Step 3: Update the state as $X_{j+1} = X_j + s_m$ and the next jump time as $t_{j+1} = t_j + \Delta$

Update the internal times as $T_m = T_m + p_m(X_j\Delta)$ for each $m \in \{1, \ldots, M\}$.

Set the new jump time for the firing reaction as $S_m = S_m + \ln(1/rnd_j)$.

Step 4: If $t_{j+1} > t_f$ STOP; otherwise, set $j = j + 1$ and go to Step 1.

Output: The list of jump times and states (t_j, X_j) for $j = 0, 1, \ldots, (j + 1)$.

The most common stochastic simulation algorithm to approximate the dynamics of chemical systems is called the tau-leaping method[95, 116, 117, 129]. It is quite advantageous for systems with fast reactions and high molecular populations, where simulating each individual reaction event would be computationally unfeasible. In the algorithm, the simulation time is divided into discrete intervals, or “leaps" of fixed size, represented as τ, and the system state is updated in larger increments instead of simulating each individual reaction event. The method shares some similarities with the Euler method used for solving ordinary differential equations, as it supposes that the propensity is approximately constant between t and $t + \tau$. However, an approximation error is introduced due to the discreteness of reaction counts and neglecting the inherent stochasticity of individual reaction events. The accuracy of the method can be increased by selecting an appropriate time step size that balances the simulation accuracy and the computational efficiency.

Tau-leaping method

Given: Initial time t_0, Final time t_f, Initial state $X(t_0) = x_0 \in \mathbb{Z}^N_{\geq 0}$.
Step 0: Set the jump counter $j = 0$, the initial time $t_0 = 0$, and the initial state $X(t_0) = x_0 \in \mathbb{Z}^N_{\geq 0}$.
Step 1: Calculate $p_m(X(t_j))$ for each $m \in \{1, \ldots, M\}$ and choose a time-step τ_j.
Step 2: Draw independent samples $\Lambda_m = \mathbb{E}[P(p_m(X(t))\tau)]$ from the Poisson distribution for each $m \in \{1, \ldots, M\}$.
Step 3: Update the state as $X_{j+1} = X_j + \sum_{m=1}^{M} s_m \Lambda_m$ and the next jump time as $t_{j+1} = t_j + \tau_j$.
Step 4: If $t_{j+1} > t_f$ STOP; otherwise, set $j = j + 1$ and go to Step 1.
Output: The list of jump times and states (t_j, X_j) for $j = 0, 1, \ldots, (j + 1)$. The generated negative populations due to an unbounded Poisson random variable can be a huge problem, and in order to prevent it, some modifications can be found in the literature, such as applying postleap checks[130], which are highly effective in preventing the occurrence of unrealistic states. In some other cases, the accuracy of the method can be increased by using binomial distribution[131].

The R-leaping is an alternative simulation method to accelerate the Stochastic Simulation Algorithm (SSA). In this approach, the propensities are approximately the same during each simulation step as in the previous method, however, instead of using a fixed time step, the leap parameter is determined by the number of firing reactions (L) [117, 132]. The necessary time step for those L reactions to happen is governed by the gamma distribution, whereas the number of firings for each reaction can be sampled effectively using the correlated binomial distribution which follows a multinomial distribution. This sampling technique turns out to be a great way to reduce the possibility of decreasing the appearance of negative species. In R-leaping, at least $M-1$ degree of random variable needs to be generated. The exact version of R-leaping was obtained by utilizing the upper and lower bounds on the probabilities of multiple reactions sampled by the Gillespie algorithm. This method is combined with rejection sampling and adaptive multiplicity for reactions[133]. It is worth noting that considering the conditions for both the tau-leaping and the R-leaping leads to the outperforming S-leaping[134]. Despite some drawbacks of R-leaping, the S-leaping method is still efficient in cases like large and stiff systems.
R-leaping method
Given: Initial time t_0, Final time t_f, Initial state $X(t_0) = x_0 \in \mathbb{Z}^N_{\geq 0}$.
Step 0: Set the jump counter $j = 0$, the initial time $t_0 = 0$, and the initial state $X(t_0) = x_0 \in \mathbb{Z}^N_{\geq 0}$.
Step 1: Calculate the propensity function $p_m(X(t_j))$ for each reaction $m \in 1, 2, \ldots, M$.
Step 2: Determine the number of reaction steps L by summing the individual re-

action counts b_m. The b_m values are randomly generated based on a multinomial distribution with individual probabilities $\frac{p_m(X(t_j))}{\sum_{m=1}^{M} p_m(X(t_j))}$.
Step 3: Generate a gamma-distributed random variable with shape parameter L and rate to obtain the time step τ_j.
Step 4: Update the state as $X_{j+1} = X_j + \sum_{m=1}^{M} s_m b_m$, where s_m is the stoichiometry of species m in the reaction.
Step 5: Update the next jump time as $t_{j+1} = t_j + \tau_j$.
Step 6: If $t_{j+1} > t_f$, STOP; otherwise, set $j = j + 1$ and go to Step 1.
Output: The list of jump times and states (t_j, X_j) for $j = 0, 1, \ldots, (j + 1)$.

3 Research objectives

The formation of nanoparticles, from a kinetic point of view, has been elucidated by various models. However, the adaptation of existing models to accurately describe nanoparticle formation is still an ongoing challenge[66, 72, 135]. It is now evident that particle size plays a crucial role in their potential applications, as it greatly influences their catalytic properties and toxicity. Moreover, the average size and distribution of nanoparticles are determined by kinetic factors[77] and are thermodynamically unstable compared to the bulk solid phase. Therefore, controlling their size requires careful consideration of kinetics.

Previous research on nanoparticle formation has employed deterministic models, which yielded approximate solutions. These solutions not only align with stochastic simulations for cases involving small particle numbers but are also applicable for calculating the temporal evolution of nanoparticle concentration under the same synthesis conditions.

One key objective of this research is to explore and compare various kernel functions, such as mass, surface, Brownian, and diffusion kernels, to identify the most appropriate approximation for the final nanoparticle size distribution. These kernels serve as mathematical representations of the underlying mechanisms driving nanoparticle formation, enabling us to gain deeper insights into the role of different kinetic factors in determining nanoparticle size and distribution.

Additionally, this thesis aims to develop a robust methodology for interpreting experimental data on nanoparticle size distributions. By comparing advanced modeling techniques with experimental results, we can validate and refine the theoretical predictions, leading to a more comprehensive understanding of the complex kinetics involved in nanoparticle formation.

The outcomes of this research will not only contribute to the fundamental understanding of nanoparticle synthesis but also have practical implications for various

fields, including catalysis, nanomedicine, sensing, and renewable energy. By unraveling the intricate relationship between kinetic factors and nanoparticle size, we can pave the way for enhanced control over nanoparticle properties, opening up new possibilities for designing and optimizing nanomaterials for specific applications.

In conclusion, this thesis endeavors to advance our knowledge of nanoparticle kinetics by integrating stochastic modeling techniques, experimental data analysis, and theoretical insights. By overcoming the limitations of traditional deterministic models, this research aims to provide a comprehensive framework for understanding and predicting nanoparticle size distributions, thus contributing to the broader field of nanoscience and enabling the rational design of nanomaterials with tailored properties.

4

Assumptions and methods

4.1 The nucleation-growth type model

Kinetic models of nanoparticle synthesis can be complex due to the large number of concentration variables involved. To simplify the model, a technique called lumping is often employed. Lumping involves grouping together chemical species with similar kinetic properties into a single "lumped" species, reducing the number of independent variables in the system of ordinary differential equations. One such model is the mechanism-enabled population balance modeling developed by Handwerk et al.[79, 81]. However, the model discussed in this chapter is a non-lumped version, specifically a generalized nucleation-growth model that incorporates two types of steps with mass action kinetics.

The first step in this model is nucleation, where monomer units form kinetically effective nuclei[39]. The second step involves second-order particle growth, which occurs through the stepwise addition of monomer units. Notably, this model excludes the possibility of aggregation, which is the reaction between different nanoparticles. The chemical reactions and their rate equations[121] can be described as follows:

$$\begin{aligned} &n\mathrm{M} \xrightarrow{k_\mathrm{M}} \mathrm{C}_n && n \in \mathbb{Z}^+ && \upsilon_\mathrm{M} = k_\mathrm{M}[\mathrm{M}]^n \\ &\mathrm{C}_i + \mathrm{M} \xrightarrow{K(i)k_\mathrm{g}} \mathrm{C}_{i+1} && i \geq n && \upsilon_{\mathrm{g},i} = K(i)k_\mathrm{g}[\mathrm{M}][\mathrm{C}_i] \end{aligned} \tag{4.1}$$

The simple notation in the above equation actually reflects a large number of possible steps. Here M denotes a single monomer unit of a nanoparticle, whereas C_i stands for a nanoparticle containing exactly i (which is a positive integer) monomer units. The other positive integer n gives the lowest number of monomer units that form a kinetically effective nucleus. υ_M is the rate of nucleation, k_M is nth order rate constant, [M] is the concentration of the monomer unit M. Analogously, $\upsilon_{\mathrm{g},i}$ the rate of the growth step, k_g is the growth rate constant and $[\mathrm{C}_i]$ means the concentration

of C_i. The function $K(i)$ denotes the kernel function, which describes how the growth rate constant of a nanoparticle depends on its size. The fundamental role and the exact physical meaning of $K(i)$ will be explained in much more detail in an upcoming subsection. It is seen that the seemingly simple formulation used here actually comprises a large number of different kinetic models using the kernel functions and n values.

It is important to note that reversible reactions cannot be considered in this model, as their inclusion would yield the final state without the need for kinetic calculations, solely determined by the equilibrium constant. Under typical thermodynamic conditions of nanoparticle formation, the final state would be the bulk solid phase[72].

The system of simultaneous ordinary differential equations describing this generalized model can be written as:

$$\begin{aligned}
\frac{\mathrm{d}[\mathrm{M}]}{\mathrm{d}t} &= -n\upsilon_{\mathrm{M}} - \sum_{j=n}^{\infty} \upsilon_{\mathrm{g},j} = -nk_{\mathrm{M}}[\mathrm{M}]^n - \sum_{j=n}^{\infty} K(j)k_{\mathrm{g}}[\mathrm{M}][\mathrm{C}_i] \\
\frac{\mathrm{d}[\mathrm{C}_n]}{\mathrm{d}t} &= \upsilon_{\mathrm{M}} - \upsilon_{\mathrm{g},n} = k_{\mathrm{M}}[\mathrm{M}]^n - K(n)k_{\mathrm{g}}[\mathrm{M}][\mathrm{C}_n] \\
\frac{\mathrm{d}[\mathrm{C}_i]}{\mathrm{d}t} &= \upsilon_{\mathrm{g},i-1} - \upsilon_{\mathrm{g},i} = K(i-1)k_{\mathrm{g}}[\mathrm{M}][\mathrm{C}_{i-1}] - K(i)k_{\mathrm{g}}[\mathrm{M}][\mathrm{C}_i] \qquad i > n
\end{aligned} \tag{4.2}$$

As written, these equations feature an infinitely large number of dependent variables. The first equation contains all the dependent variables of the system, while [M] appears on the right-hand side of all the other equations. Consequently, this type of model cannot be solved using the conventional methods developed for the numerical integration of kinetic differential equations. For this system, typical initial conditions assume that all the mass of the system is present in the monomer units:

$$\begin{aligned}
&[\mathrm{M}](t=0) = [\mathrm{M}]_0 \\
&[\mathrm{C}_n](t=0) = 0 \\
&[\mathrm{C}_i](t=0) = 0 \qquad i > n
\end{aligned} \tag{4.3}$$

These initial conditions reflect the state of the system at the beginning of the synthesis process, where all the material is in the form of monomer units, and no nanoparticles of size n or greater are present.

Another significant point to consider in this model is that Equations 4.1 and 4.2 use the common formulation of isothermal solution-phase kinetics. In an isothermal reactor, the temperature does not change and cannot appear as a parameter in the differential equations. Otherwise, the temperature would modify the rate constants

of the two steps. The model here also assumes a unidirectional, irreversible reaction for the growth of a nanoparticle using concentrations, which originally implies that the nanoparticles are considered to be part of the homogeneous system. However, this is by no means a necessary condition: if the differential equations can capture the time-dependent changes, this method can be applied to other cases as well.

Reversible steps and possible reactions of two nanoparticles (aggregation) are not included in the model at all. The reason for this omission is that both kinds of processes would lead a kinetically viable way to the thermodynamically stable final state of the system, which is the bulk solid instead of a collection of nanoparticles. In such a model, nanoparticles in reasonable concentrations could only appear as intermediates.

In chemical kinetics, approximations such as the method of flooding, the pre-equilibrium approach, or steady-state approximation are often employed to simplify the solution procedure. These approximations typically aim to provide a symbolic solution with an error smaller than the typical error of experimental concentration determination. The considerations in obtaining solutions of the deterministic approach in this work will occasionally rely on such approximations, but these will be more sophisticated than the two common techniques mentioned. The approximations developed in this work will be validated against exact stochastic simulations.

4.1.1 Kernel functions

As previously discussed, the kernel functions play a crucial role in determining the particle size dependence of the growth rate constant in this model[136]. In this section, we introduce four commonly used kernels, which are summarized in Table 4.1.

Table 4.1: Different kernel functions used in this model

Name	kernel function
mass kernel	$K(i) = i$
surface kernel	$K(i) = i^{2/3}$
Brownian kernel	$K(i) = i^{1/3}$
diffusion kernel	$K(i) = 1$

The first kernel is the mass kernel, which assumes that the reactivity of a nanoparticle is directly proportional to its mass. This implies that larger particles will grow more rapidly than smaller particles, as they contain a greater number of monomer units (i). The mass kernel is given by the function $K(i) = i$, which is a simple linear relationship between the growth rate constant and the particle mass.

The second kernel is the surface kernel, which assumes that the reactivity of a nanoparticle is proportional to its surface area. As nanoparticles are assumed to be roughly spherical as the first approach, the surface area is proportional to the 2/3th power of the particle mass. Therefore, the surface kernel is given by the function $K(i) = i^{2/3}$. With this kernel, larger ones still grow more rapidly than smaller ones. As the surface area-to-volume ratio decreases with increasing size, this enhancement of reactivity is less steep than in the case of the mass kernel.

The third kernel is the Brownian kernel[26, 137], which assumes that the reactivity of a nanoparticle is proportional to its linear size. As the radius or diameter of a spherical nanoparticle is proportional to the 1/3th power of its mass, the Brownian kernel is given by the function $K(i) = i^{1/3}$. This still gives an enhanced relative reactivity for larger particles, but the increase is even less steep than for the surface kernel.

The fourth and final kernel is the diffusion kernel, which assumes that the reactivity of a nanoparticle is independent of its size. This is analogous to the size independence of the diffusion-controlled rate constant, as the lower mobility of larger particles is compensated by their larger reactive cross-section [119, 120]. Therefore, the diffusion kernel is given by the constant function $K(i) = 1$. This kernel implies that all particles will grow at the same rate, regardless of their size.

The choice of kernel function is an important consideration in modeling nanoparticle growth. The mass, surface, and Brownian kernels all introduce size dependence in the growth rate constant, while the diffusion kernel assumes size independence. Researchers should carefully select the kernel function that best fits their experimental system, taking into account the underlying physical processes that govern nanoparticle growth.

Some further discussion is appropriate here to reflect on the possibility of extending this model to nanoparticles whose shapes are significantly non-spherical. Kernel functions themselves do not assume anything about the shape of a particle. The precise mathematical condition of using this approach is that if two nanoparticles contain the same number of monomer units, then the reactivity must be the same. This is a condition that is often met in actual synthesis processes as the particle shapes are seldom entirely random (inability to distinguish between growth directions would give spherical shapes anyway) but are governed by the inherent properties of the particles. Overall, this means that the model and the concept of kernel functions are still valid in these cases, although the actual mathematical form of the kernel function might be different from those given in Table 4.1.

4.2 Dimensionless quantities

In order to simplify the solution procedure and address issues related to the physical dimensions of the variables (concentration, time, rate constants), it is useful to introduce scaled variables [89, 120, 136]. These new variables are defined as follows:

$$m = \frac{[\mathrm{M}]}{[\mathrm{M}]_0}, \qquad c_i = \frac{[\mathrm{C}_i]}{[\mathrm{M}]_0}, \qquad \tau = k_\mathrm{g}[\mathrm{M}]_0 t, \qquad \alpha = \frac{k_\mathrm{M}([\mathrm{M}]_0)^{n-2}}{k_\mathrm{g}} \tag{4.4}$$

Here, m represents the dimensionless concentration of the monomer units, $[\mathrm{M}]_0$ is the initial concentration of the monomer units, c_i denotes the dimensionless concentration of nanoparticles containing i monomer units, τ represents the dimensionless time, and α is the dimensionless ratio of the nucleation and growth rate constants. It is important to note that these variables are non-negative real numbers due to their physical interpretation.

Using these scaled variables, the system of ordinary differential equations describing the model can be simplified as follows:

$$\begin{aligned} \frac{\mathrm{d}m}{\mathrm{d}\tau} &= -n\alpha m^n - \sum_{j=n}^{\infty} K(j) m c_j \\ \frac{\mathrm{d}c_n}{\mathrm{d}\tau} &= \alpha m^n - K(n) m c_n \\ \frac{\mathrm{d}c_i}{\mathrm{d}\tau} &= K(i-1) m c_{i-1} - K(i) m c_i \qquad i > n \end{aligned} \tag{4.5}$$

These equations represent the time evolution of the dimensionless concentrations. The initial conditions when the dimensionless time is zero are typically given as:

$$\begin{aligned} &m(\tau = 0) = 1 \\ &c_i(\tau = 0) = 0 \qquad i > n \qquad n \in \mathbb{Z}^+ \end{aligned} \tag{4.6}$$

In the following calculations and results, we will use these scaled variables.

Forming meaningful nanoparticles typically requires small values of alpha ($\alpha \ll 1$). This condition implies that the growth step must be much faster than the seed formation step.

4.3 Moments

In the mathematical description of the model outlined in the previous subsections, it is convenient to introduce the qth moment of the dimensionless concentration c_i

[54, 86, 136, 138], which is defined as:

$$\mu_q = \sum_{j=n}^{\infty} j^q c_j \tag{4.7}$$

Here, q can be any real number, it is not necessarily positive or integer. The initial conditions are such that all dimensionless nanoparticle concentrations (c_i values) are zero at $\tau = 0$, so the initial value of every moment is zero independently of q:

$$\mu_q(\tau = 0) = 1 \tag{4.8}$$

The time dependence of the moments can be easily calculated by multiplying the ith term of the system of differential equations (Equation 4.5) with i^q and summing up all resulting equations. This yields the following expression:

$$\begin{aligned} n^q \frac{\mathrm{d}c_n}{\mathrm{d}\tau} + \sum_{i=n+1}^{\infty} i^q \frac{\mathrm{d}c_i}{\mathrm{d}\tau} &= n^q \alpha m^n - n^q K(n) m c_n \\ + \sum_{i=n+1}^{\infty} i^q K(i-1) m c_{i-1} - \sum_{i=n+1}^{\infty} i^q K(i) m c_i & \end{aligned} \tag{4.9}$$

The above equation can be stated in a somewhat more concise form:

$$\sum_{i=n}^{\infty} i^q \frac{\mathrm{d}c_i}{\mathrm{d}\tau} = n^q \alpha m^n + \sum_{i=n}^{\infty} [(i+1)^q - i^q] K(i) m c_i \tag{4.10}$$

The first moment, μ_1, has a clear physical meaning as it represents the total number of monomer units present in the nanoparticles:

$$\mu_1 = \sum_{i=n}^{\infty} i^1 c_i = \sum_{i=n}^{\infty} i c_i \tag{4.11}$$

The time derivative of the first moment can be expressed as:

$$\frac{\mathrm{d}\mu_1}{\mathrm{d}\tau} = \sum_{i=n}^{\infty} i \frac{\mathrm{d}c_i}{\mathrm{d}\tau} = n\alpha m^n + \sum_{i=n}^{\infty} K(i) m c_i \tag{4.12}$$

Notably, the derivative of the first moment is the negation of the differential equation for the monomer units in Equation 4.5. Therefore, the following expression holds:

$$\frac{\mathrm{d}\mu_1}{\mathrm{d}\tau} + \frac{\mathrm{d}m}{\mathrm{d}\tau} = 0 \tag{4.13}$$

Since the initial condition at $\tau = 0$ is known (all c_i values are zero and $m = 1$ due to scaling introduced earlier), this equation can be easily integrated into the following, highly useful form:

$$\mu_1 + m = 1 \tag{4.14}$$

Given the fact that the time derivative of the first moment is always positive, it must be a monotonically increasing function, whereas the function of m (scaled concentration of the monomer units) is a monotonically decreasing function of the dimensionless time (τ).

The physical meaning of the zeroth moment is also known: it represents the sum of the concentrations of the nanoparticles of different size. Similarly to the first moment, it is a monotonically increasing function. Furthermore, it is easily seen from the definitions that the first moment is always greater than the zeroth moment as c_i values are non-negative at all times. The zeroth moment can be expressed by comparing Equation 4.11 with the following definition equation:

$$\mu_0 = \sum_{i=n}^{\infty} i^0 c_i = \sum_{i=n}^{\infty} c_i \tag{4.15}$$

The differential equation for the zeroth moment can be obtained by summing all the differential equations in the model (Equation 4.5) and is written as:

$$\frac{\mathrm{d}\mu_0}{\mathrm{d}\tau} = \alpha m^n \tag{4.16}$$

Clearly, μ_0 is an increasing function of time as its first derivative is non-negative. The analytical solutions for the zeroth moment will be explored in each kernel function in the following subsections.

For the Brownian kernel, a new concept needs to be introduced, which is the 1/3rd moment. In the later parts of this work, it will be shown that it is very advantageous to approximate it by the weighted geometric mean of the zeroth and first moments:

$$\mu_{1/3} = \sum_{i=n}^{\infty} i^{1/3} c_i \cong \mu_0^{2/3} \mu_1^{1/3} \tag{4.17}$$

Similarly, for the surface kernel, the 2/3rd moment is very favorably approximated as the weighted geometric mean of the first and zeroth moments:

$$\mu_{2/3} = \sum_{i=n}^{\infty} i^{2/3} c_i \cong \mu_0^{1/3} \mu_1^{2/3} \tag{4.18}$$

These moments provide additional information about the distribution of nanopar-

ticles and can be used to analyze the system dynamics. Also, their introduction facilitates finding analytical and approximated solutions of Equation 4.5.

4.4 Average sizes and polydispersity

The model studied here was initially expanded to interpret the time dependence of the average particle size in a quantitative manner. The size of a nanoparticle population can be described using several properties. Assuming that a particle is approximately spherical, its radius or diameter must be proportional to the cube root of the number of monomer units in it. Various approaches exist to define the average sizes for the nanoparticle population, including the cube-root number-average size (r_{C}), the number-average size (r_{A}), the mass-average size (r_{W}), and the Z-average size (r_{Z}).

The cube-root number-average size (r_{C}) can be characterized analytically in the easiest way and helps characterize the typical size of the nanoparticles in terms of the number of monomer units they contain assuming spherical shapes for the particles.

The number-average size (r_{A}) represents the average size of individual nanoparticles in the population, weighted by the number of particles of each size. It is useful for understanding the typical size of the particles in the population, but it does not consider the relative abundance of particles of different sizes. Typically, it is used in combination with another measure, such as the mass-average size or the polydispersity, to fully characterize the size distribution of a nanoparticle population.

The mass-average size (r_W) is based on the weight of the particles in a given sample. It assigns more weight to larger particles and is often used in applications where particle mass is important, such as in catalysis.

Another important measure is the Z-average size (r_{Z}), which can be directly determined from dynamic light scattering methods. It is calculated by measuring the intensity of scattered light from the nanoparticles as a function of time and analyzing the fluctuations in this intensity. The Z-average size represents the hydrodynamic diameter of the nanoparticles, taking into account their shape, size, and surface charge. This measure is particularly useful for characterizing nanoparticles in solution, where they may undergo Brownian motion and other dynamic effects.

The average sizes can be approximated using the following equations:

$$\begin{aligned} r_{\mathrm{C}} &= r_0 \sqrt[3]{\frac{\sum_{i=n}^{\infty} i c_i}{\sum_{i=n}^{\infty} c_i}} & r_{\mathrm{A}} &= r_0 \frac{\sum_{i=n}^{\infty} i^{1/3} c_i}{\sum_{i=n}^{\infty} c_i} \\ r_{\mathrm{W}} &= r_0 \frac{\sum_{i=n}^{\infty} i^{4/3} c_i}{\sum_{i=n}^{\infty} i c_i} & r_{\mathrm{Z}} &= r_0 \frac{\sum_{i=n}^{\infty} i^{2} c_i}{\sum_{i=n}^{\infty} i^{5/3} c_i} \end{aligned} \tag{4.19}$$

Here, r_0 represents the reference size, which is the radius of the hypothetical nanoparticle containing a single monomer unit only. Typically, this reference r_0 falls within the range of 0.1 and 0.2 nm. The four types of average sizes are usually quite close to each other, for which the mathematical condition is that the distribution needs to be relatively narrow and unimodal. Throughout this work, the cube-root average number will be employed because it can usually be calculated with fewer approximations than all the others.

The moments have particular significance in relation to the calculation of average size. First of all, the average number of monomer units in a nanoparticle can be determined by dividing the total number of monomer units by the number of nanoparticles:

$$\bar{M} = \frac{\mu_1}{\mu_0} = \frac{1-m}{\mu_0} \tag{4.20}$$

Here, $\bar{M}$ represents the average number of monomer units. However, in most experimental studies, this variable is examined at the end of the process, so it is advisable to calculate its limiting value at infinite time:

$$\bar{M}_{\infty} = \frac{1}{\lim_{m \to 0} \mu_0} \tag{4.21}$$

The different average sizes (Equation 4.19) can also be expressed in terms of moments:

$$\begin{aligned} r_{\mathrm{C}} &= r_0 \sqrt[3]{\frac{\mu_1}{\mu_0}} & r_{\mathrm{A}} &= r_0 \frac{\mu_{1/3}}{\mu_0} \\ r_{\mathrm{W}} &= r_0 \frac{\mu_{4/3}}{\mu_1} & r_{\mathrm{Z}} &= r_0 \frac{\mu_2}{\mu_{5/3}} \end{aligned} \tag{4.22}$$

Another measure used to characterize the size distribution is polydispersity, which provides information about the variability of particle sizes. It is calculated as

follows:

$$\mathrm{PD}^* = \sqrt[3]{\frac{\mu_2\mu_0}{\mu_1^2}} - 1 \tag{4.23}$$

Polydispersity is a measure of the width of the particle size distribution, reflecting the degree of variation in particle sizes within the population.

In summary, these measures provide insights into different aspects of the size distribution and are useful for characterizing nanoparticles in various applications and conditions. Additionally, the moments and polydispersity are important parameters that help quantify the size distribution and variability within the nanoparticle population.

4.5 Stochastic approach

A few years ago, the lumped kinetic model of Finke and coworkers was criticized by J. Martin[139–141], who highlighted a problem that got our attention: the importance of a nucleation rate constant for a single nucleated particle scenario is unknown. Classical chemical kinetics works with concentrations as continuous variables, whereas in reality, stochastic kinetics refers to the study of chemical reactions and processes at the molecular level, taking into account the inherent randomness and fluctuations associated with such systems. In this context, the molecule numbers represent the number of specific molecular species involved in the system.

In the context of stochastic kinetics, instead of continuous concentrations, the number of molecules is applied, and it can be considered as a continuous time Markov chain model ($X(\tau) = (X_0(\tau), X_1(\tau), \ldots, X_N(\tau))$. The sum of all the monomer units and all the nanoparticles present gives the total molecule number as can be seen:

$$x_0(\tau) + \sum_{i=n}^{\infty} i x_i(\tau) = N \tag{4.24}$$

The determination of the number of all possible states can be obtained by counting the number of solutions for this equation. Each state can be uniquely identified by summing the numbers of all particle types. Consequently, counting the feasible states implies a so-called combinatorial problem, which involves determining the number of solutions for a set of simultaneous Diophantine equations. The number of solutions for these equations is often referred to as a partition function, symbolized by $p(N)$. Unfortunately, there does not exist any closed-form expression for calculating this function. In particular, the most significant known prime number among $p(N)$ is $p(1289844341)$, which consists of almost 40000 digits[142], which makes it impossible

to handle all potential states by solely improving computational power, leading to situations when it becomes unfeasible to deal with every possible state.

The stoichiometric matrix can also be defined for this model in the given way:

$$\mathbf{S}((N-n+2)\times M) = \begin{bmatrix} -n & -1 & -1 & \cdots & -1 & -1 \\ +1 & -1 & 0 & \cdots & 0 & 0 \\ 0 & +1 & -1 & \cdots & 0 & 0 \\ \vdots & \vdots & \vdots & \ddots & \vdots & \vdots \\ 0 & 0 & 0 & \cdots & 1 & -1 \\ 0 & 0 & 0 & \cdots & 0 & 1 \end{bmatrix} \begin{matrix} \rightarrow & x_0 \\ \rightarrow & x_n \\ \rightarrow & x_{n+1} \\ \vdots & \\ \rightarrow & x_{N-1} \\ \rightarrow & x_N \end{matrix} \tag{4.25}$$

The propensities $p_i(\tau)$ determine the likelihood of different molecular events occurring at a given time τ. In this case, there are three possible types of events: nucleation, growth, and no event (i.e., when $i = 0$). The propensities are defined as follows:

$$p_i(\tau) = \begin{cases} \alpha \binom{x_0(\tau)}{n} & \text{if} \quad i = 0 \\ 0 \quad \text{if} \quad n > i \geq 1 \\ K(i)x_0(\tau)x_i(\tau) & \text{if} \quad i \geq n \end{cases} \tag{4.26}$$

The Gillespie algorithm is a stochastic simulation algorithm used to model the time evolution of the system. It generates a series of stochastic events that simulate individual molecular events. The algorithm follows the steps outlined below:

1. Initialize the system with the given initial conditions.
2. Enter a loop that iterates until a specified endpoint is reached or a termination condition is met.
3. Calculate the total propensity $\sum_{j=1}^{N} p_j(\tau^{\text{old}})$, which represents the sum of all propensities at the current time point τ^{old}.
4. Generate two random numbers rnd_1 and rnd_2.
5. Update the time to the next event τ^{new} using the equation:

$$\tau^{\text{new}} = \tau^{\text{old}} - \frac{\ln rnd_1}{\sum_{j=1}^{N} p_j(\tau^{\text{old}})} \tag{4.27}$$

6. Determine the index i of the event that occurs using the inequality:

$$\frac{\sum_{j=1}^{i-1} p_j(\tau^{\text{old}})}{\sum_{j=1}^{N} p_j(\tau^{\text{old}})} \leq rnd_2 < \frac{\sum_{j=1}^{i} p_j(\tau^{\text{old}})}{\sum_{j=1}^{N} p_j(\tau^{\text{old}})} \tag{4.28}$$

   This step randomly selects the event type based on the relative propensities. rnd_2 is a random number between 0 and 1.

7. Update the system state based on the selected event:

$$\begin{aligned} &x_0(\tau^{\text{new}}) = x_0(\tau^{\text{old}}) - n; x_n(\tau^{\text{new}}) = x_n(\tau^{\text{old}}) + 1, && \text{if} \quad i = 1 \\ &x_0(\tau^{\text{new}}) = x_0(\tau^{\text{old}}) - 1; x_i(\tau^{\text{new}}) = x_i(\tau^{\text{old}}) - 1; && \\ &x_{i+1}(\tau^{\text{new}}) = x_{i+1}(\tau^{\text{old}}) + 1, && \text{if} \quad i > n \end{aligned} \tag{4.29}$$

These equations update the molecular numbers after each event. If $i = 1$, it represents the nucleation event, so the number of monomers decreases by n while the number of nanoparticles with size n increases by 1. For $i > n$, it represents a growth event, so the number of monomers and nanoparticles with size i decreases by 1, and the number of nanoparticles with size $i + 1$ increases by 1.

The Gillespie algorithm repeats steps 3 to 7 until a specified endpoint is reached or a termination condition is met. At each iteration, the algorithm outputs several variables that provide information about the system's dynamics at that particular time point. These variables can be further analyzed to understand the behavior of the system over time. All the necessary simulations were implemented in Matlab, the sample codes for each of the kernel functions can be found in the Appendices.

5 Results and discussions

Exact analytical solutions are obtained for the time-dependent concentrations of all different types of nanoparticles in three scenarios. For all other combinations of kernel function and minimum seed sizes, feasible approximations are employed which then are compared with simulation results using the Stochastic Simulation Algorithm (SSA), which is applied for different kernels as well.

5.1 Exact analytical solutions

5.1.1 Diffusion kernel with first-order nucleation

When the diffusion kernel is applied, the reactivities of the particles are considered to be independent of the size, i.e. $K(i) = 1$. The infinite sum presented in the time derivative of m in the first line becomes equivalent to the zeroth moment:

$$\begin{aligned} \frac{\mathrm{d}m}{\mathrm{d}\tau} &= -n\alpha m^n - \sum_{j=n}^{\infty} mc_j \\ \frac{\mathrm{d}\mu_0}{\mathrm{d}\tau} &= \alpha m^n \end{aligned} \tag{5.1}$$

As already noted, the zeroth moment is always a monotonically increasing function. Therefore, the dependent variable m can be regarded as a function of the zeroth moment (μ_0) rather than the dimensionless time (τ):

$$\frac{\mathrm{d}m}{\mu_0} = -n - \frac{\mu_0}{\alpha} m^{1-n} \tag{5.2}$$

This transformation is useful because it decreases the number of variables. At the same time, the initial and final values of μ_0 are both known, so the equation will still be useful in predicting the final distribution. Also, if all variables are known as a

function of μ_0, then the time dependence can also be handled through this selected variable. The ordinary differential equation in Equation (5.2) looks challenging to solve for general values of n. However, it has a particularly favorable form when the minimum size seed is one monomer unit ($n = 1$):

$$\frac{\mathrm{d}m}{\mathrm{d}\mu_0} = -1 - \frac{\mu_0}{\alpha} \tag{5.3}$$

This case is straightforward because the right-hand side is independent of m, allowing for a simple integration to solve the equation taking into consideration the initial condition ($\mu_0 = 0$ when $m = 1$):

$$m = -\frac{1}{2\alpha}\mu_0^2 - \mu_0 + 1 \tag{5.4}$$

Since all the monomer units are consumed in the final state ($\tau = \infty$), the final value of the zeroth moment can be determined by substituting $m = 0$ into Equation 5.4, which yields the following result:

$$\lim_{\tau\to\infty} \mu_0 = \sqrt{\alpha^2 + 2\alpha} - \alpha \tag{5.5}$$

Upon substituting the solution for m into Equation 5.1, the following separable ordinary differential equation can be obtained:

$$\frac{\mathrm{d}\mu_0}{\mathrm{d}\tau} = -\frac{\mu_0^2}{2} - \alpha\mu_0 + \alpha \tag{5.6}$$

Standard but extensive calculations lead to the analytical solution of the zeroth moment:

$$\mu_0 = -\alpha + \sqrt{\alpha(2+\alpha)}\,\mathrm{th}\left(\frac{\tau\sqrt{\alpha(2+\alpha)}}{2} + \mathrm{arth}\left(\sqrt{\frac{\alpha}{2+\alpha}}\right)\right) \tag{5.7}$$

Here the notation th stands for the hyperbolic tangent function, arth for the inverse hyperbolic tangent function. After finding this solution of the zeroth moment, the same technique can be used for other dependent variables as well, c_i is regarded as the function of μ_0 instead of τ, which leads to a system of linear, first-order ordinary differential equations:

$$\begin{aligned} \frac{\mathrm{d}c_1}{\mathrm{d}\mu_0} &= 1 - \frac{c_1}{\alpha} \\ \frac{\mathrm{d}c_i}{\mathrm{d}\mu_0} &= \frac{c_{i-1}}{\alpha} - \frac{c_i}{\alpha} \qquad i > 1 \end{aligned} \tag{5.8}$$

The exact solution of this equation for c_i is the following:

$$c_i = \alpha - \alpha \mathrm{e}^{-\mu_0/\alpha} \sum_{j=0}^{i-1} \frac{1}{j!} \left(\frac{\mu_0}{\alpha}\right)^j \tag{5.9}$$

Eventually, the non-scaled variables are determined for later uses. The concentration of the monomer units takes this form:

$$[\mathrm{M}] = \frac{2[\mathrm{M}]_0 k_\mathrm{g} + k_\mathrm{M}}{[\mathrm{M}]_0 k_\mathrm{g} + [\mathrm{M}]_0 \mathrm{ch}\left(2\mathrm{arth}\left(\sqrt{\frac{k_\mathrm{M}}{2[\mathrm{M}]_0 k_\mathrm{g} + k_\mathrm{M}}}\right) + [\mathrm{M}]_0 k_\mathrm{g} t \sqrt{\frac{k_\mathrm{M}(2[\mathrm{M}]_0 k_\mathrm{g} + k_\mathrm{g})}{[\mathrm{M}]_0^2 k_\mathrm{g}^2}}\right) k_\mathrm{g}} \tag{5.10}$$

For the nanoparticle concentrations, the following form is obtained:

$$[\mathrm{C}_i] = -\frac{1}{[\mathrm{M}]_0 k_\mathrm{g}} \left(\mathrm{e}^{\frac{k_\mathrm{M}\left(k_\mathrm{M} - [\mathrm{M}]_0 k_\mathrm{g} \sqrt{\frac{k_\mathrm{M}(2[\mathrm{M}]_0 k_\mathrm{g} + k_\mathrm{M})}{[\mathrm{M}]_0^2 k_\mathrm{g}^2}}\right) \mathrm{th}\left(\mathrm{arth}\left[\sqrt{\frac{k_\mathrm{M}}{2[\mathrm{M}]_0 k_\mathrm{g} + k_\mathrm{M}}}\right] + \frac{1}{2}[\mathrm{M}]_0 t k_\mathrm{g} \sqrt{\frac{k_\mathrm{M}(2[\mathrm{M}]_0 k_\mathrm{g} + k_\mathrm{M})}{[\mathrm{M}]_0^2 k_\mathrm{g}^2}}\right]}{[\mathrm{M}]_0^2 k_\mathrm{g}^2}} - 1 \right)$$
$$k_\mathrm{M} \sum_{j=0}^{i-1} \frac{1}{j!} \left(\frac{[\mathrm{M}]_0 k_\mathrm{g} \sqrt{\frac{k_\mathrm{M}(2[\mathrm{M}]_0 k_\mathrm{g} + k_\mathrm{M})}{[\mathrm{M}]_0^2 k_\mathrm{g}^2}} \mathrm{th}\left(\frac{1}{2}[\mathrm{M}]_0 t k_\mathrm{g} \sqrt{\frac{k_\mathrm{M}(2[\mathrm{M}]_0 k_\mathrm{g} + k_\mathrm{M})}{[\mathrm{M}]_0^2 k_\mathrm{g}^2}} + \mathrm{arth}\left(\sqrt{\frac{k_\mathrm{M}}{2[\mathrm{M}]_0 k_\mathrm{g} + k_\mathrm{M}}}\right)\right)}{k_\mathrm{M}} - 1 \right) \tag{5.11}$$

And at last, the average size of the nanoparticles and the cube-root number-average size can be formed in the following ways:

$$\bar{M}_\infty = \sqrt{\frac{[\mathrm{M}]_0^3 k_\mathrm{g}^3}{2k_\mathrm{M}^3 - [\mathrm{M}]_0^2 k_\mathrm{g}^2}} \tag{5.12a}$$

$$r_\mathrm{C} = \frac{r_0}{\sqrt[6]{\frac{2k_\mathrm{M}^3 - k_\mathrm{g}[\mathrm{M}]_0^2}{k_\mathrm{g}^3 [\mathrm{M}]_0^3}}} \tag{5.12b}$$

5.1.2 Diffusion kernel with second-order nucleation

Equation 5.2 can be given for the case of a second-order nucleation step (when $n = 2$):

$$\frac{\mathrm{d}m}{\mathrm{d}\mu_0} = -1 - \frac{\mu_0}{\alpha m} \tag{5.13}$$

For this ordinary differential equation, only an implicit solution can be derived:

$$\begin{aligned} &2\sqrt{\frac{\alpha}{4-\alpha}} \arctan\left(\sqrt{\frac{\alpha}{4-\alpha}} \frac{\mu_0 + 2m}{\mu_0}\right) \\ &= \pi \sqrt{\frac{\alpha}{4-\alpha}} + \ln\left(\frac{\mu_0^2}{\alpha} + m\mu_0 + m^2\right) \end{aligned} \tag{5.14}$$

It is noted that this implicit form cannot be directly applied at $m = 1$, where the initial conditions directly give $\mu_0 = 0$. In addition, the above equation is somewhat

constrained by the condition $\alpha \neq 4$, but this limitation has no significance as $\alpha << 1$ is true in all practically important cases. The final value of the zeroth moment (i.e. at time infinity) can be given by substituting $m = 0$ into Equation 5.14:[1]

$$\lim_{\tau\to\infty} \mu_0 = \sqrt{\alpha} e^{\sqrt{\frac{\alpha}{4-\alpha}}} \left(\arctan\left(\sqrt{\frac{\alpha}{4-\alpha}} \right) - \frac{\pi}{2} \right) \tag{5.15}$$

General solutions could not be found for larger integer values of n.

However, a numerical solution can be easily depicted for this scenario. First, the ordinary differential equation system is considered again, which describes the time-dependence of the concentration of all species:

$$\begin{aligned} \frac{\mathrm{d}[\mathrm{M}]}{\mathrm{d}t} &= -2k_\mathrm{M}[\mathrm{M}]^2 - \sum_{j=2}^{\infty} k_\mathrm{g}[\mathrm{M}][\mathrm{C}_i] \\ \frac{\mathrm{d}[\mathrm{C}_2]}{\mathrm{d}t} &= k_\mathrm{M}[\mathrm{M}]^2 - k_\mathrm{g}[\mathrm{M}][\mathrm{C}_2] \\ \frac{\mathrm{d}[\mathrm{C}_i]}{\mathrm{d}t} &= k_\mathrm{g}[\mathrm{M}][\mathrm{C}_{i-1}] - k_\mathrm{g}[\mathrm{M}][\mathrm{C}_i] \qquad i > 2 \end{aligned} \tag{5.16}$$

All equations, except for the first one, are summed:

$$\sum_{j=2}^{\infty} \frac{\mathrm{d}[\mathrm{C}_j]}{\mathrm{d}t} = k_\mathrm{M}[\mathrm{M}]^2 \tag{5.17}$$

This equation and the first part of Equation 5.16 form a separate system that contains no other variables.

$$\begin{aligned} \frac{\mathrm{d}[\mathrm{M}]}{\mathrm{d}t} &= -2k_\mathrm{M}[\mathrm{M}]^2 - k_\mathrm{g}[\mathrm{M}] \sum_{j=2}^{\infty} [\mathrm{C}_j] \\ \frac{\mathrm{d}}{\mathrm{d}t} \sum_{j=2}^{\infty} [\mathrm{C}_j] &= k_\mathrm{M}[\mathrm{M}]^2 \end{aligned} \tag{5.18}$$

This method is suitable for calculating the time dependence of the concentration of the monomer unit ([M]).

It is important to note that this technique, most unfortunately, cannot determine the final value of the infinite sum, nor can it determine the individual concentrations of C_i. One possible solution is to consider the infinite sums as a function of the

[1] Equations 5.14 and 5.15 appear as Equations 23 and 24 in the original paper connected to the thesis (Journal of Mathematical Chemistry, Vol. 59 p. 1808) with some unfortunate typos. The forms shown in this dissertation are the correct ones.

concentration of M:

$$\frac{\mathrm{d}}{\mathrm{d}t}\sum_{j=2}^{\infty}[\mathrm{C}_j] = \frac{-k_\mathrm{M}[\mathrm{M}]^2}{2k_\mathrm{M}[\mathrm{M}]^2 + k_\mathrm{g}[\mathrm{M}]\sum\limits_{j=2}^{\infty}[\mathrm{C}_j]} \tag{5.19}$$

Numerical integration can accurately determine the sum value down to $[\mathrm{M}] = 0$ as the initial conditions are known (the sum is zero when $[\mathrm{M}] = [\mathrm{M}]_0$). Once the value of the sum is calculated, $[\mathrm{C}_2]$ has to be taken as a function of [M] as well.

$$\frac{\mathrm{d}[\mathrm{C}_2]}{\mathrm{d}[\mathrm{M}]} = \frac{k_\mathrm{g}[\mathrm{M}][\mathrm{C}_2] - k_\mathrm{M}[\mathrm{M}]^2}{2k_\mathrm{M}[\mathrm{M}]^2 + k_\mathrm{g}[\mathrm{M}]\sum\limits_{j=2}^{\infty}[\mathrm{C}_j]} \tag{5.20}$$

The numerical values of the infinite sum in the denominator are already known as a function of [M]. Therefore, by using numerical integration, we can find the value of $[\mathrm{C}_2]$ at $[\mathrm{M}] = 0$, which will be the final result. To obtain additional $[\mathrm{C}_i]$ functions, we can numerically integrate the following equations one after another:

$$\frac{\mathrm{d}[\mathrm{C}_i]}{\mathrm{d}[\mathrm{M}]} = \frac{k_\mathrm{g}[\mathrm{M}][\mathrm{C}_i] - k_\mathrm{M}[\mathrm{M}]^2[\mathrm{C}_{i-1}]}{2k_\mathrm{M}[\mathrm{M}]^2 + k_\mathrm{g}[\mathrm{M}]\sum\limits_{j=2}^{\infty}[\mathrm{C}_j]} \qquad i > 2 \tag{5.21}$$

Numerical results up to $i = 100,000$ can be obtained in a reasonable computation time. These are suitable for comparison with Gillespie simulation results.

First, the half-lives of the concentration of the monomer units are determined from 100 individual stochastic simulation results and the numerical calculations, and this is presented in Figure 5.1. The final nanoparticle size distribution is also illustrated in Figure 5.2 and proves that the predictions of the two approaches are in great agreement. Finally, the same distribution for the mass of the particles rather than the size is displayed in Figure 5.3.

5.1.3 Mass kernel with first-order nucleation

This is a specific case of the mass kernel (when $K(i) = i$) since the kinetically effective nucleus can be formed using only one single monomer unit. The infinite sum present in the first part of Equation 4.5 (representing the time dependence of m) is identical to the solution of the first moment (Equation 4.14). Accordingly, the aforementioned equation can be transformed into a separable ordinary differential equation determining the dependence of the scaled concentration of the monomer

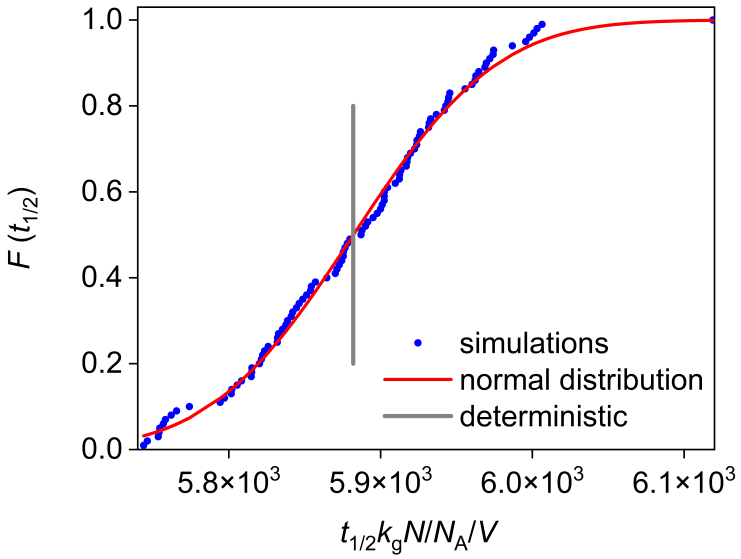

Figure 5.1: The cumulative distribution function of the half-lives for the dimensionless concentration of the monomer units. Parameters: $N = 10^7$, $\alpha = 5 \times 10^{-8}$

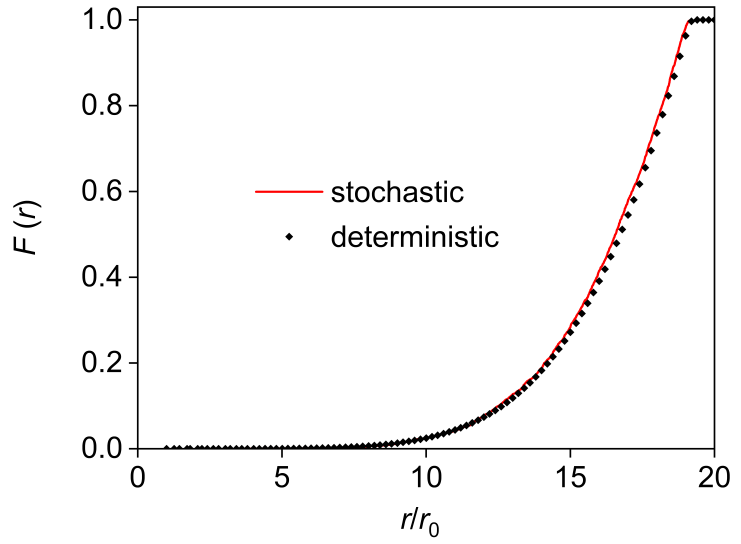

Figure 5.2: The final particle size distribution in stochastic simulation runs in comparison with the deterministic prediction for diffusion kernel, $n = 2$ with the following parameters: $N = 10^7$, $\alpha = 5 \times 10^{-8}$.

units on the scaled time:

$$\frac{\mathrm{d}m}{\mathrm{d}\tau} = -n\alpha m^n - m(1-m) \tag{5.22}$$

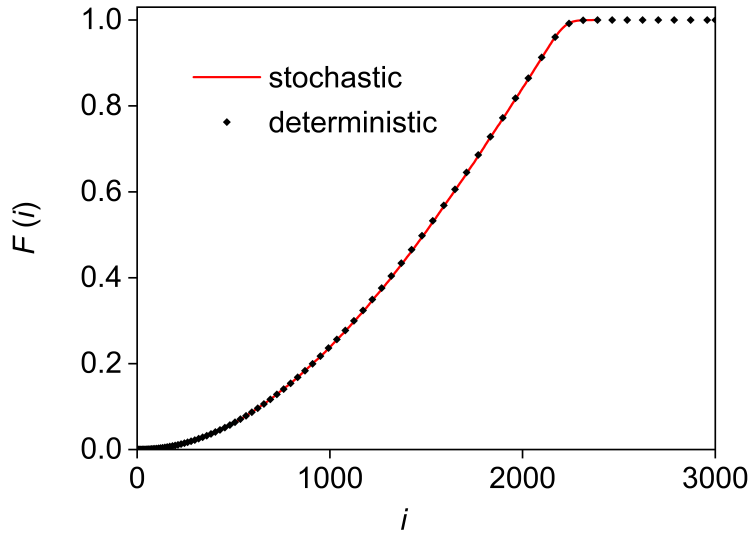

Figure 5.3: The final particle mass distribution (using the number of monomer units, i, as an independent variable) in stochastic simulation runs in comparison with the deterministic prediction for diffusion kernel, $n = 2$ with the following parameters: $N = 10^7$, $\alpha = 5 \times 10^{-8}$.

A general solution to this equation (for all values of n) seems to be very challenging to find. For this particular scenario ($n = 1$), this ordinary differential equation converts to the following form:

$$\frac{\mathrm{d}m}{\mathrm{d}\tau} = -\alpha m - m(1-m) \tag{5.23}$$

The solution can be deduced quite easily:

$$m = \frac{\alpha + 1}{\alpha \mathrm{e}^{(\alpha+1)\tau} + 1} \tag{5.24}$$

Our study revealed that it is more suitable to represent the c_i concentrations as a function of the dimensionless concentration of the monomer unit (m) rather than the dimensionless time (τ). With this change in the independent variable, which is made possible by the fact that m is a strictly monotonic function of τ, the ordinary differential equation describing c_n takes the following form:

$$\frac{\mathrm{d}c_n}{\mathrm{d}m} = \frac{nc_n - \alpha m^{n-1}}{n\alpha m^{n-1} + (1-m)} \tag{5.25}$$

For the case specifically dealt with in this subsection ($n = 1$), this differential equa-

tion simplifies to the following one:

$$\frac{\mathrm{d}c_1}{\mathrm{d}m} = \frac{c_1 - \alpha}{\alpha + (1 - m)} \tag{5.26}$$

Once more, a general solution for Equation 5.25 could not be found despite our extensive efforts. For the particular form in Equation 5.26, however, a specific formula could be given:

$$c_1 = \frac{\alpha - \alpha m}{1 + \alpha - m} \tag{5.27}$$

With the same change of independent variable, so considering the scaled concentrations of the nanoparticles as a function of m rather than τ, the part of Equation 4.5 describing c_i can be stated as:

$$\frac{\mathrm{d}c_i}{\mathrm{d}m} = \frac{ic_i - (i-1)c_{i-1}}{n\alpha m^{n-1} + 1 - m} \quad i > n \tag{5.28}$$

The particular equation for the case $n = 1$ is the following then:

$$\frac{\mathrm{d}c_i}{\mathrm{d}m} = \frac{ic_i - (i-1)c_{i-1}}{\alpha + 1 - m} \tag{5.29}$$

Once the solution of the first one is known (i.e. c_n is known), the equation enables the straight calculation of variables c_i, and so thus the general solution is obtained, as well:

$$c_i = \frac{\alpha}{i}\left(\frac{1-m}{\alpha + 1 - m}\right) \tag{5.30}$$

In the context of the mass kernel, the zeroth moment is only important for calculating the average particle size. This feature can be derived by integrating the proper form of the Equation 4.16:

$$\frac{\mathrm{d}\mu_0}{\mathrm{d}\tau} = \alpha m \tag{5.31}$$

On the other hand, merging Equation 4.16 and 5.22 can help to determine the zeroth moment as the function of the m, and additionally, for the first-order nucleation, the following differential equation is defined as the second part:

$$\frac{\mathrm{d}\mu_0}{\mathrm{d}m} = -\frac{\alpha}{n\alpha + (1-m)m^{1-n}} \tag{5.32}$$

For the particular case of $n = 1$, the equation is:

$$\frac{\mathrm{d}\mu_0}{\mathrm{d}m} = -\frac{\alpha}{\alpha + 1 - m} \tag{5.33}$$

Equation 5.33 is a separable differential equation, for which the solution is relatively easily given for the initial condition $\mu_0(\tau = 0) = 0$ or $\mu_0(m = 1) = 0$:

$$\mu_0 = \alpha(\alpha+1)\tau + \alpha \ln\left(\frac{1+\alpha}{1+\alpha \mathrm{e}^{(\alpha+1)\tau}}\right) = \alpha \ln\left(1 + \frac{1}{\alpha} - \frac{m}{\alpha}\right) \tag{5.34}$$

Since the final size distribution of nanoparticles is usually obtained by experimental studies, the concentration of nanoparticles at the final state has to be determined for this purpose:

$$\lim_{\tau\to\infty} c_i = \frac{\alpha}{i}\left(\frac{1}{\alpha+1}\right)^i \tag{5.35}$$

In order to simplify future comparisons with experimental data sets, it is inevitable to convert, at the very least, the final results into the non-scaled, original parameter set. The concentration of the monomer unit is sought to have this formula:

$$[\mathrm{M}] = \frac{[\mathrm{M}]_0 k_\mathrm{g} + k_\mathrm{M}}{[\mathrm{M}]_0 k_\mathrm{g} + \mathrm{e}^{\frac{t([\mathrm{M}]_0 k_\mathrm{g} + k_\mathrm{M})}{[\mathrm{M}]_0^2}} k_\mathrm{M}} \tag{5.36}$$

The concentration of the nanoparticles takes the following form:

$$[\mathrm{C}_i] = \frac{\left(1 - \mathrm{e}^{-\frac{t([\mathrm{M}]_0 k_\mathrm{g} + k_\mathrm{M})}{[\mathrm{M}]_0^2}}\right) k_\mathrm{M}}{i\left([\mathrm{M}]_0 k_\mathrm{g} + k_\mathrm{M}\right)} \tag{5.37}$$

The final average number of monomer units in a nanoparticle and the cube-root number-average size can be calculated in these ways:

$$\bar{M}_\infty = \frac{[\mathrm{M}]_0 k_\mathrm{g}}{\ln\left(1 + \frac{[\mathrm{M}]_0 k_\mathrm{g}}{k_\mathrm{M}}\right) k_\mathrm{M}} \tag{5.38a}$$

$$r_\mathrm{C} = r_0 \frac{[\mathrm{M}]_0 k_\mathrm{g}}{\ln\left(1 + \frac{[\mathrm{M}]_0 k_\mathrm{g}}{k_\mathrm{M}}\right) k_\mathrm{M}} \tag{5.38b}$$

Many experimental studies track the time dependence of the concentration of monomer units[86]. The graph in Figure 5.4 illustrates the dimensionless concentration of monomer units as a function of dimensionless time for the mass and diffusion kernel with first-order nucleation steps. The graph suggests that the time dependence has some similarities with the induction behavior[143, 144] observed in certain experimental results[72–74, 145].

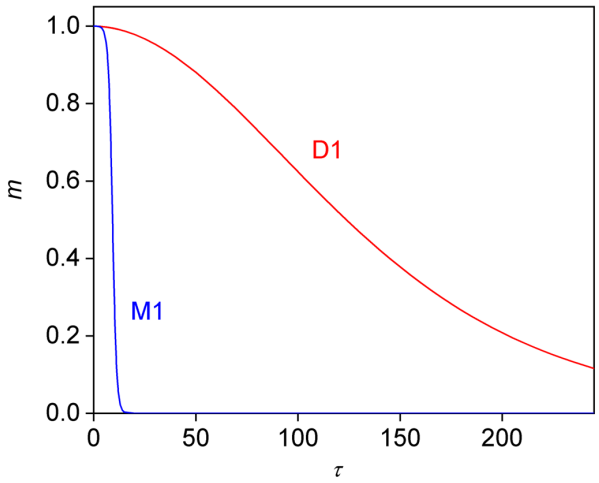

Figure 5.4: m (dimensionless concentration of the monomer units) as a function of the dimensionless time (τ) in the case of the mass kernel(M1) and the diffusion kernel(D1), both with $n = 1$ and $\alpha = 10^{-4}$.

5.1.4 Mass kernel with second-order nucleation

In this scenario, the nucleation step is bimolecular similarly to the later growth steps, and Equation 5.22, which gives the dependence of the dimensionless concentration of the monomer unit (m) on dimensionless time, can be expressed in the given form ($n = 2$ in Equation 5.22):

$$\frac{\mathrm{d}m}{\mathrm{d}\tau} = -2\alpha m^2 - m(1-m) \tag{5.39}$$

Finding the solution to this equation does not require special efforts. It must be kept in mind that the initial condition is $m(\tau = 0) = 1$. However, the case of $\alpha = 0.5$ is a special one, which must be dealt with separately. The main coefficient of the quadratic term on the right-hand side of Equation 5.39 becomes zero, hence the equation shortens to the description of a first-order process. The general solution (including the case of $\alpha = 0.5$) is given in the following equation:

$$\begin{aligned} m &= \frac{1}{1 - 2\alpha + 2\alpha \mathrm{e}^{\tau}} \qquad \text{if} \quad \alpha \neq 0.5 \\ m &= \mathrm{e}^{-\tau} \qquad \text{if} \quad \alpha = 0.5 \end{aligned} \tag{5.40}$$

Figure 5.5 presents the solutions given in Equation 5.40 for various α values. In this figure, it is evident that the loss of the monomer units at high values of α exhibits an "ordinary" kinetic curve. Nevertheless, at low α values, the shape

has similarities with that of the clock reactions or autocatalytic reactions[143–145]. This behavior is comprehensible since in this scheme, a very small amount of initially formed nanoparticles reacts with the monomer units in a fast reaction.

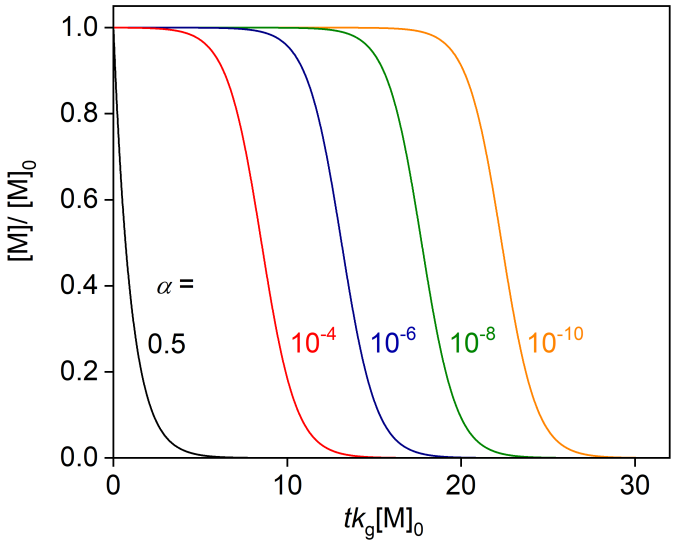

Figure 5.5: The scaled concentration of the monomer units as a function of scaled time for some different values of the ratio of the nucleation and growth rate constants in the case of the mass kernel with $n = 2$.

Since the concentration of the monomer units is considered to be a monotonically decreasing function, all the concentrations of the nanoparticles can be examined as a function of the m rather than the dimensionless time. This approach makes it possible to find the analytical solution without sacrificing any information, as the time dependence of the monomer units can already be derived in Equation 5.40. So converting m to be the independent variable, the rate equation takes this form:

$$\begin{aligned} \frac{\mathrm{d}c_2}{\mathrm{d}m} &= \frac{2c_2 - \alpha m}{2\alpha m + (1-m)} \\ \frac{\mathrm{d}c_i}{\mathrm{d}m} &= \frac{(i-1)c_{i-1} - ic_i}{(1-2\alpha)m - 1} \qquad i \geq 3 \end{aligned} \tag{5.41}$$

The above equation exhibits an interesting property, which facilitates the analytical solution of the entire infinite system of differential equations. The first line gives the derivative of c_2 only involving the m and c_2 variables on the right-hand side. Consequently, it can be solved without depending on the other functions. Actually, for the solution of the c_3 and c_4, the method is very similar, *e.g.* the equation for c_3 solely relies on the functions of c_2, c_3, and obviously on the m. Thus, it is noteworthy

that the analytical solutions of all these simultaneous differential equations can be obtained consecutively, as c_i only depends on itself, the c_{i-1}, and evidently on the independent variable, m. Additionally, all the individual equations are considered to be nonhomogeneous first-order linear differential equations, which have a solution using a general strategy, leading to the following formula:

$$\begin{aligned} c_i &= C[1-(1-2\alpha)m]^{i/(2\alpha-1)} \\ &- [1-(1-2\alpha)m]^{i/(2\alpha-1)}(i-1)\int [1-(1-2\alpha)m]^{-i/(2\alpha-1)-1}c_{i-1}\mathrm{d}m \end{aligned} \tag{5.42}$$

Applying the above formula yields the solution of c_2:

$$c_2 = -\frac{\alpha}{4\alpha-6}(1+2m) + \frac{3\alpha}{4\alpha-6}\left(\frac{1}{2\alpha}-\frac{m}{2\alpha}+m\right)^{2/(2\alpha-1)} \tag{5.43}$$

And with this, the function for c_3 can be found without difficulties:

$$\begin{aligned} c_3 &= -\frac{\alpha(-3+\alpha-3m)}{3(\alpha-2)(\alpha-2)} + \frac{3\alpha}{2\alpha-3}\left(\frac{1-m}{2\alpha}+m\right)^{2/(2\alpha-1)} \\ &- \frac{4\alpha}{3(\alpha-2)}\left(\frac{1-m}{2\alpha}+m\right)^{3/(2\alpha-1)} \end{aligned} \tag{5.44}$$

The same technique leads us to the function of c_4:

$$\begin{aligned} c_4 &= \frac{\alpha\,(-18+11\alpha-2\alpha^2-12m)}{4(2\alpha-5)(2\alpha-3)(\alpha-2)} + \frac{9\alpha}{2(2\alpha-3)}\left(\frac{1-m}{2\alpha}+m\right)^{2/(2\alpha-1)} \\ &- \frac{4\alpha}{\alpha-2}\left(\frac{1-m}{2\alpha}+m\right)^{3/(2\alpha-1)} + \frac{15\alpha}{4(2\alpha-5)}\left(\frac{1-m}{2\alpha}+m\right)^{4/(2\alpha-1)} \end{aligned} \tag{5.45}$$

The previous three formulas (Equations 5.43, 5.44, 5.45) enable it to find the general solution of the c_i function. Obviously, the special case ($\alpha = 0.5$) has a simpler solution:

$$\begin{aligned} c_i &= \frac{\alpha(i+1)!(-1)^{i-1}(m-1)}{\prod_{j=2}^{i}(2\alpha-j-1)} \\ &+ \sum_{j=2}^{i}\frac{\alpha(j^2-1)}{j(2\alpha-j-1)}\binom{i-1}{j-1}(-1)^j\left[\left(\frac{1-m}{2\alpha}+m\right)^{j/(2\alpha-1)}-1\right] \end{aligned} \tag{5.46}$$

$$\text{if} \quad i \geq 2, \alpha \neq 0.5$$

$$c_i = \frac{1}{i}(m-1) + \sum_{j=2}^{i}\frac{j^2-1}{j^2}(-1)^{j-1}\binom{i-1}{j-1}[\mathrm{e}^{j(m-1)}-1] \quad \text{if} \quad \alpha = 0.5$$

The proof of this solution can also be accomplished by mathematical induction (see Proofs and derivations). Since the final distribution of the nanoparticle population is of great importance in most cases, which can be interpreted as the limit of the c_i functions at infinite time (when $m = 0$ and $\alpha \neq 0.5$):

$$\lim_{\tau\to\infty} c_i = \frac{\alpha(i-1)!(-1)^i}{\prod_{j=2}^{i}(2\alpha - j - 1)} + \sum_{j=2}^{i} \frac{\alpha(j^2-1)}{j(2\alpha-j-1)} \binom{i-1}{j-1} (-1)^j \left[\left(\frac{1}{2\alpha} \right)^{j/(2\alpha-1)} - 1 \right] \tag{5.47}$$

As already stated before, the condition for the formation of large nanoparticles is equivalent to the very small values of α. Thus Equation 5.47 can be simplified to the following form in these practically meaningful cases:

$$\lim_{\tau\to\infty} c_i \cong \alpha \frac{i-1}{i(i+1)} \qquad \text{if} \quad \alpha << 1 \tag{5.48}$$

Figure 5.6 illustrates the final distribution as a function of i as defined by Equations 5.47 and 5.48. This figure clearly shows that there is a significant difference in the results of Equation 5.48 in the case where α is above 0.01. The observed deviation does not appear for smaller values of α. Basically, Equation 5.48 can be used as an approximate form in most practical cases in nanoparticle synthesis. It should be emphasized that direct numerical use of the complete formula (Equation 5.48) for performing computations with values $i > 40$ requires special treatments because the calculations of sums involving binomial terms with alternating signs become complicated. These problems originate from the necessity to handle small differences between very large numbers for precise calculations, which can be highly challenging from the point of view of computational number representation. It is usually desirable to rely on some further analytical formulas on binomial coefficients to enhance the efficiency of such calculations.

The zeroth moment (given in Equation 5.32) has the following form in this specific case:

$$\frac{\mathrm{d}\mu_0}{\mathrm{d}m} = -\frac{\alpha m}{1 + (2\alpha - 1)m} \tag{5.49}$$

Since the right-hand side does not even contain the zeroth moment, this differential equation can be solved simply by integrating the function on the right-hand side. Taking into consideration the initial condition (when $m = 1$, then $\mu_0 = 0$), the

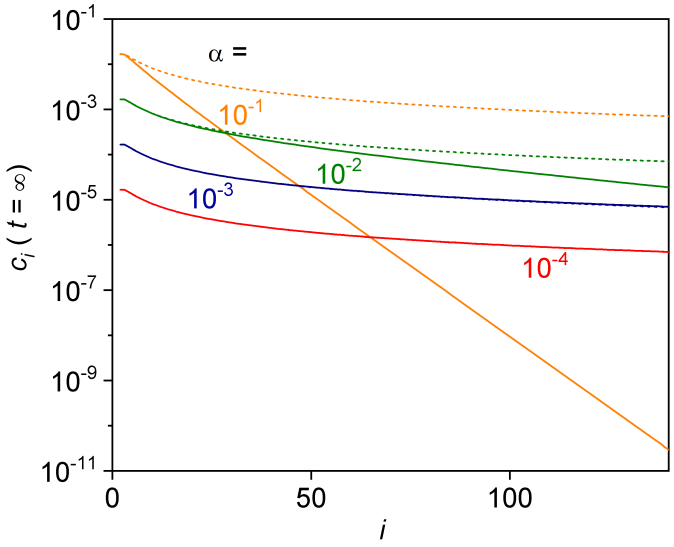

Figure 5.6: The limiting values of the dimensionless concentrations of nanoparticles C_i at infinity time as a function of i in the case of the mass kernel with $n = 2$. Different colors mean different values of the ratio of the nucleation and growth rate constant (α) as given in the figure. Solid lines were calculated by the full formula, whereas the dashed lines show the simplified formula for $\alpha << 1$.

general form of the solution is as follows:

$$\mu_0 = \frac{\alpha}{(1-2\alpha)(1-2\alpha+2\alpha e^{\tau})} + \frac{\alpha\tau - \alpha + 2\alpha^2}{(1-2\alpha)^2} - \frac{\alpha \ln(1-2\alpha+2\alpha e^{\tau})}{(1-2\alpha)^2} =$$
$$= \frac{\alpha m - \alpha}{1-2\alpha} + \frac{\alpha \ln(\frac{1}{2\alpha} - \frac{m}{2\alpha} + m)}{(1-2\alpha)^2} \quad \text{if} \quad \alpha \neq 0.5 \tag{5.50}$$
$$\mu_0 = -\frac{1}{4}m^2 + m + \frac{1}{4} \quad \text{if} \quad \alpha = 0.5$$

The average number of monomer units (average size of nanoparticles) is expressed in Equation 4.21 and Figure 5.7 shows this value as a function of the ratio of the two rate constants.

The requirement of forming large nanoparticles is the small value of α which is just verified by Figure 5.7. Actually, particles containing fewer than 100 monomer units are typically not regarded as nanoparticles, so it seems that restricting the analysis of similar models to the case where $\alpha << 1$ is entirely acceptable in practice since the larger values would imply the absence of meaningful nanoparticle formation.

Finding the analytical solution for larger integer values of n has been attempted but remained unsuccessful. Some limited progress was made for $n = 3$, where the

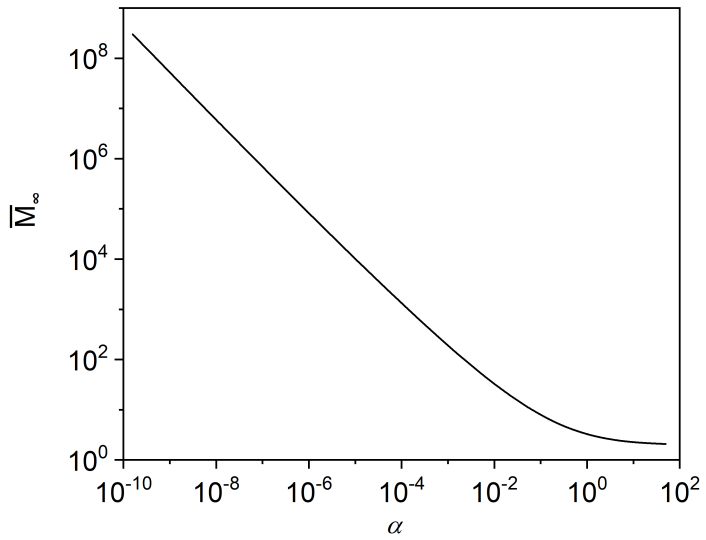

Figure 5.7: The average size of the nanoparticles in the final state as the function of the ratio of the nucleation and growth rate constants (α) in the case of the mass kernel with $n = 2$.

separable differential equation for the time dependence of m (Equation 5.22) takes the following form:

$$\frac{\mathrm{d}m}{\mathrm{d}\tau} = -3\alpha m^3 - m(1-m) \tag{5.51}$$

In this case, the integration after the separation of variables can be accomplished, but it yields an overall formula that remains implicit for m:

$$\begin{aligned}\tau = &\frac{1}{\sqrt{1-12\alpha}}\left[\operatorname{arth}\left(\frac{6\alpha m-1}{\sqrt{1-12\alpha}}\right) - \operatorname{arth}\left(\frac{6\alpha-1}{\sqrt{1-12\alpha}}\right)\right] \\ &+ \frac{1}{2}\ln\left(1 - \frac{1}{3\alpha m} + \frac{1}{3\alpha m^2}\right)\end{aligned} \tag{5.52}$$

This formula could be still useful in a scenario where the role of the variables is reversed, so all of the other concentrations are given as a function of m and time is calculated by the above equation for the specific m values. However, analytical formulas giving the c_i concentrations as a function of m could not be found for $n = 3$. Returning to the case of $n = 2$, Equation 5.32 for the zeroth moment has the following specific form:

$$\frac{\mathrm{d}\mu_0}{\mathrm{d}m} = -\frac{\alpha m^2}{1 + m(3\alpha m - 1)} \tag{5.53}$$

As seen, this differential equation can again be solved by simply integrating the

right-hand side. The analytical solution is:

$$\mu_0 = \frac{1-m}{3} + \frac{(1-6\alpha)}{9\alpha\sqrt{1-12\alpha}}\mathrm{arth}\left(\frac{(1-m)\sqrt{1-12\alpha}}{1+6\alpha m-m}\right) - \frac{1}{18\alpha}\ln\left(\frac{1}{3\alpha} - \frac{m}{3\alpha} = m^2\right) \tag{5.54}$$

For higher values of n (*i.e.* $n \geq 4$), no analytical formulas have been found for the dependence of the zeroth moment on m.

Transforming the final results into the primary, non-dimensionless forms is often important for analyzing actual experimental results. This is done here for $n = 2$. First, the concentration of the monomer units displays the following time dependence:

$$[\mathrm{M}] = \frac{[\mathrm{M}]_0 k_\mathrm{g} \mathrm{e}^{-[\mathrm{M}]_0 k_\mathrm{g} t}}{2k_\mathrm{M} + (k_\mathrm{g} - 2k_\mathrm{M})\mathrm{e}^{-[\mathrm{M}]_0 k_\mathrm{g} t}} \tag{5.55}$$

Then, the concentration of the nanoparticles can be gained, as well:

$$[\mathrm{C}_i] = \frac{[\mathrm{M}]_0 2k_\mathrm{g}^{i-2} k_\mathrm{M}^2 (i-1)}{(2k_\mathrm{M} + (k_\mathrm{g} - 2k_\mathrm{M})\mathrm{e}^{-[\mathrm{M}]_0 k_\mathrm{g} t})} \prod_{j=2}^{i} (2k_\mathrm{M} - k_\mathrm{g} j - k_g) + [\mathrm{M}]_0 \sum_{j=2}^{i} \frac{k_\mathrm{M}\,(j^2-1)}{(2k_\mathrm{M} - k_\mathrm{g} j - k_\mathrm{g})\,j} \binom{i-1}{j-1} (-1)^j \left[\left(\frac{k_\mathrm{g}}{2k_\mathrm{M} + (k_\mathrm{g} - 2k_\mathrm{M})\mathrm{e}^{-[\mathrm{M}]_0 k_\mathrm{g} t}}\right)^{k_\mathrm{g}/(2k_\mathrm{M}-k_\mathrm{g})} - 1\right] \tag{5.56}$$

Finally, the average size of the nanoparticles at the end of the process and the cube-root number-average size assembled into these forms:

$$\bar{M}_\infty = \frac{-(k_\mathrm{g}-2k_\mathrm{M})^2}{k_\mathrm{M}(k_\mathrm{g}-2k_\mathrm{M}) + k_\mathrm{g} k_\mathrm{M} \ln\left(\frac{2k_\mathrm{M}}{k_\mathrm{g}}\right)} \tag{5.57a}$$

$$r_C = r_0 \sqrt[3]{\frac{4k_\mathrm{M}^2 - 4k_\mathrm{M}k_\mathrm{g} + k_\mathrm{g}^2}{k_\mathrm{M}(k_\mathrm{g}-2k_\mathrm{M}) + k_\mathrm{g} k_\mathrm{M} \ln\left(\frac{2k_\mathrm{M}}{k_\mathrm{g}}\right)}} \tag{5.57b}$$

The Gillespie algorithm, as introduced in the previous section, is initially applied for this type of model, and compared with the exact analytical solution. These simulations are implemented using MATLAB. Figure 5.8 illustrates the dependence on the different initial numbers of monomer units.

Comparing the stochastic simulation results of the dimensionless concentration of the monomer units with the analogous deterministic calculations is shown in Figure 5.9 under fixed parameter values of $\alpha = 10^{-6}$ and $N = 10^6$. The results

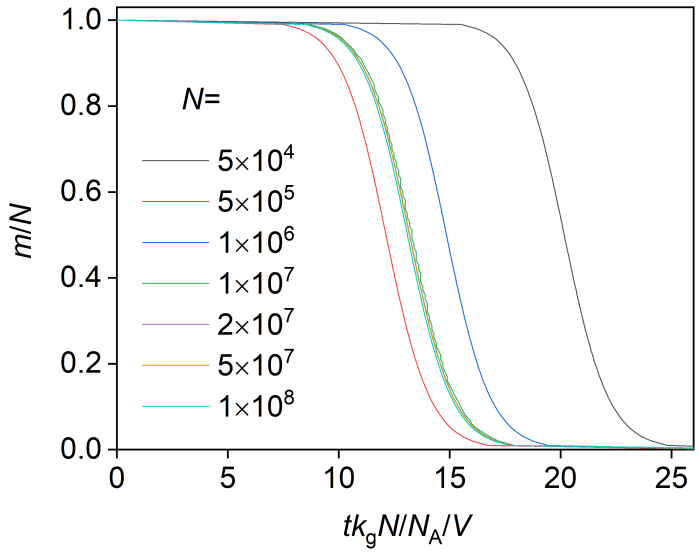

Figure 5.8: The effect of different initial numbers of monomer units in simulation runs with $\alpha = 10^{-6}$.

of the five separate Gillespie simulations clearly exhibit differences, which are very similar to the autocatalytic reactions. Moreover, it is also observable that some of them proceed at a faster rate than others.

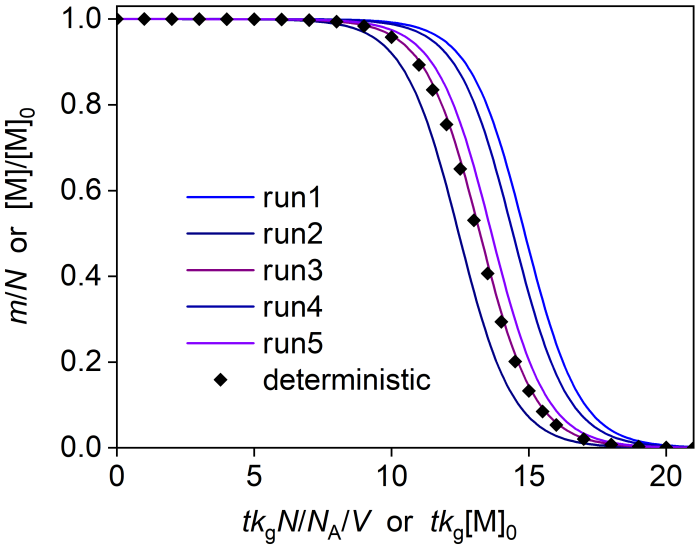

Figure 5.9: The scaled concentration of the monomer unit as a function of the (scaled) time in five repetitive simulation runs with the parameters: $N = 10^6$, $\alpha = 10^{-6}$. The deterministic results for the same process are shown by the black diamond-shaped markers.

Figure 5.10 demonstrates the impact of the different ratios of the rate constants on the scaled concentration of the monomer units as a function of the dimensionless time.

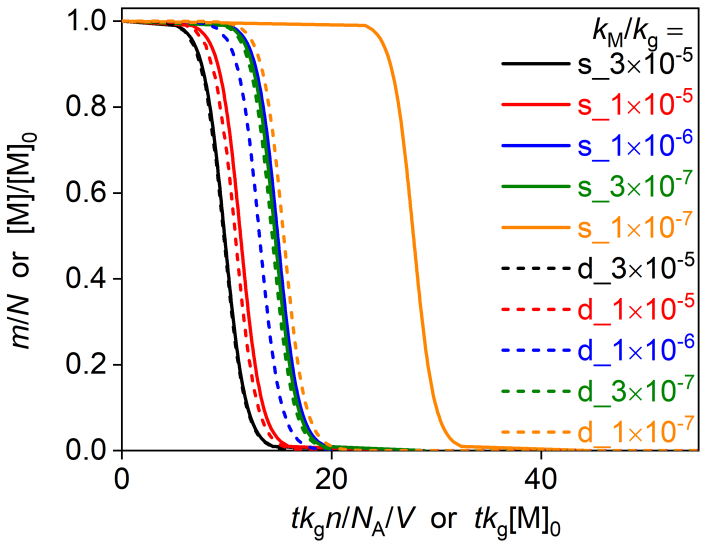

Figure 5.10: The effect of the rate constant ratio as a function of the scaled concentration of the monomer unit in a simulation run at $N = 10^6$. The stochastic simulation results are shown by solid line, while the deterministic calculations are represented by dashed lines.

The scaled average sizes of the two approaches are also presented from the same five simulations, which are already used in Figure 5.11, along with the deterministic calculation. In the stochastic results, the curves are not strictly monotonic. Despite the overall general increase in the average size, short regions of decline can sometimes be observed in small time intervals. Obviously, this phenomenon can be attributed to single nucleation events: when a new seed is formed whose size is tiny, the average size is reduced because the other particles do not grow in this step.

In order to illustrate the extent of the deviations generated by stochastic fluctuations, the simulation runs were launched with the same set of parameters 100 times. From each of the simulation results, the half-life values ($t_{1/2}$) were collected as characteristic time descriptors. The half-life is the time in which the initial concentration of the monomer unit is reduced to half of the original value. It must be emphasized that this half-life is not similar to the half-life of first-order reactions in that it depends on the initial concentration.

When it comes to representing such data, displaying the cumulative distribution functions is much more useful than showing histograms. This is because histograms

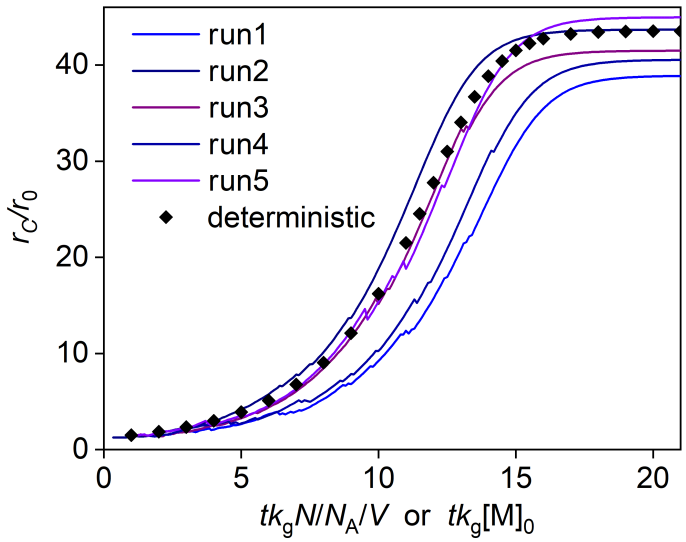

Figure 5.11: The scaled average size in five repetitive simulations runs as a function of the (scaled) time with the following parameters: $N = 10^6$, $\alpha = 10^{-6}$

categorize events in an arbitrary way, which can significantly affect the final outcome. The use of cumulative distribution functions completely avoids these issues. In Figure 5.12, the ordinate defines the cumulative distribution function, indicating the probability of obtaining a half-life shorter than $t_{1/2}$ in a simulation run. In deterministic kinetics, the initial condition uniquely determines the kinetic curves, resulting in a single half-life value without any distribution, which is represented by a single grey vertical line and this is very close to the time of 50% probability. Moreover, a red continuous curve displays the best fitting normal distribution to the curve, which fits the simulation points well. The small fluctuations from stochastic kinetics follow a normal distribution due to the central limit theorem of probability theory[117]. This adherence of the half-life distribution to normal distribution suggests that the relative fluctuations should be smaller as the initial number of monomer units increases. It is also noteworthy that even at a low particle number of 10^8, no significant deviations from the normal distribution are observed. In many cases, where stochastic effects are present in macroscopic systems, significant deviations can be observed at small molecule numbers.

Figures 5.13 and 5.14 demonstrate the analogous results for two different α values (10^{-6} and 10^{-8}). The distributions of the half-lives are different in both cases, but the overall pattern and the strict adherence to the normal distribution remain consistent.

As stated before, the size distribution obtained from a nanoparticle synthesis

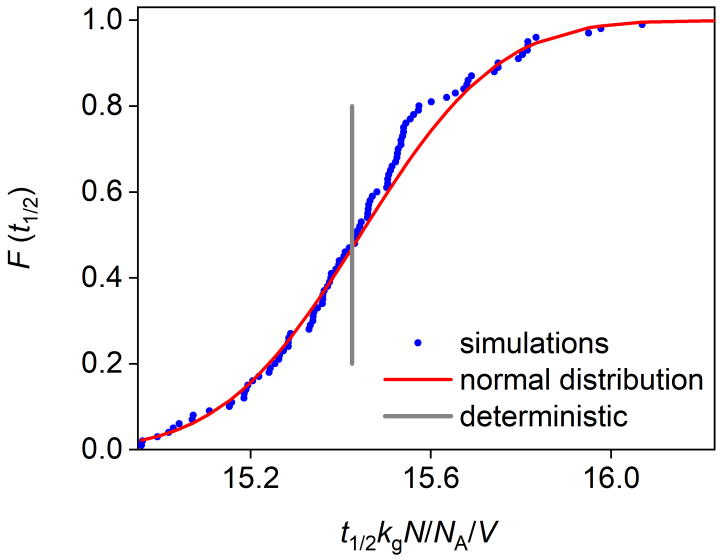

Figure 5.12: The cumulative distribution function of the half-lives for the dimensionless concentration of the monomer units. Parameters: $N = 10^8$, $\alpha = 10^{-7}$

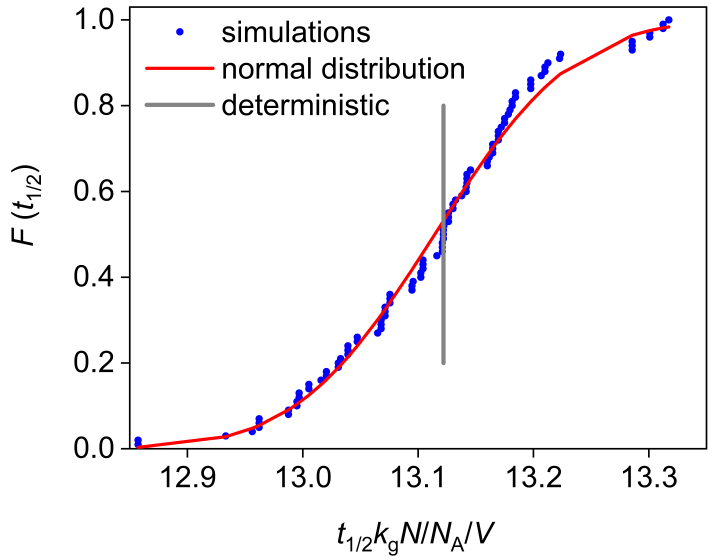

Figure 5.13: The cumulative distribution function of the half-lives for the dimensionless concentration of the monomer units. Parameters: $N = 10^8$, $\alpha = 10^{-6}$

method is a crucial descriptor. The size distribution can be calculated for the final state by both stochastic simulations and deterministic formulas. Figure 5.15 compares both methods, using the cumulative distribution function instead of the probability density function, as explained in Figure 5.12. The ordinate of Figure 5.15 shows $F(r)$, which is the probability that the size of a randomly selected particle

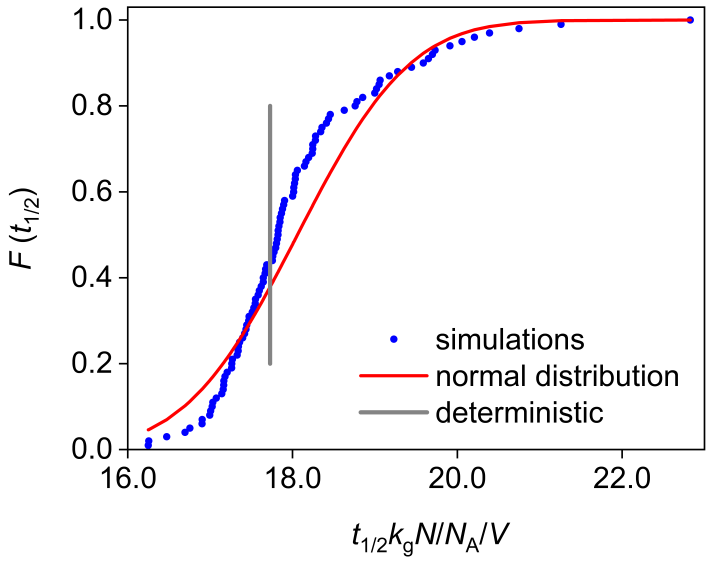

Figure 5.14: The cumulative distribution function of the half-lives for the dimensionless concentration of the monomer units. Parameters: $N = 10^8$, $\alpha = 10^{-8}$

in the final mixture is smaller than r. The graph highlights only three simulations as they are very similar to each other. However, a larger number of simulations were performed, and the same unique distribution was always reached as the final result. Moreover, the distribution obtained in the stochastic run is almost identical to the one predicted by the deterministic approach. Although some deviations can be observed above the scaled particle size of 60, these are minor artifacts that might be associated with number representation issues in calculating the alternately signed sum of large binomial coefficients in Equation 5.56.

It is important to note that the original calculation for Figure 5.15 was based only on 10^8 monomer units which is still considered to be a very small amount of substance in chemical synthesis methods. However, even with this small sample size, the stochastic runs produce results that closely match the deterministic prediction. This definitely demonstrates the Kurtz theorem[122] for the nucleation-growth mechanism with autocatalytic phenomena is valid, as it provides a practical agreement between the two approaches.

The results also show some detectable fluctuations in reaction time, which are similar to those seen in simple autocatalytic reactions [109] and are not specific to nanoparticle formation. The results also prove that even with an initial number of monomer units as low as 10^7, the stochastic and deterministic approaches predict nearly identical particle size distribution. This comparison validates the deterministic kinetic approach and calculations for the size distribution in such systems.

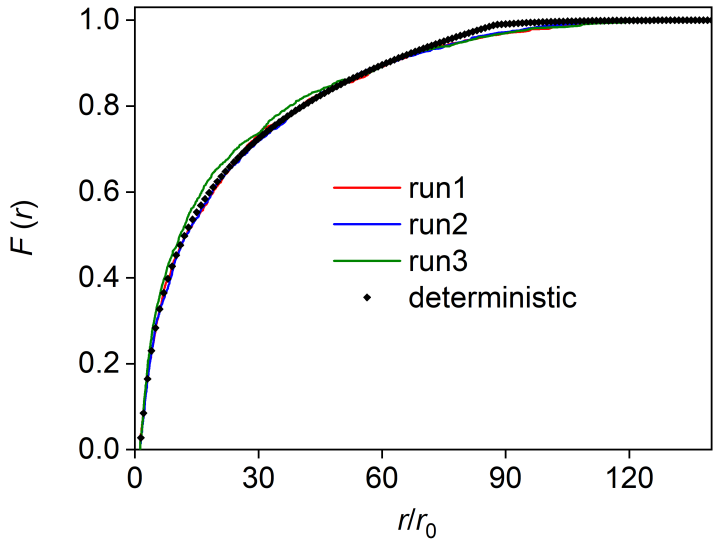

Figure 5.15: The final particle size distribution in stochastic simulation runs is compared with the deterministic prediction for the system with the same parameters: $N = 10^8$, $\alpha = 10^{-6}$

5.2 Approximated solutions of the zeroth moment

The possibilities of finding the analytical solution of the simultaneous system of differential equations have probably been exhausted in the previous subsections. A full solution was given for the diffusion kernel with $n = 1$, as well as for the mass kernel with $n = 1$ and $n = 2$. Some partial results were reported for other cases. Nothing could be derived for the Brownian and surface kernels, the fact that kernel function involves non-integer powers of i in Table 4.1 seems to preclude any such attempts. However, as usual in chemical kinetics, some plausible approximations might facilitate finding formulas that are not precise but are still useful for practical purposes as they are so close to the exact solutions that the difference is experimentally undetectable.

Taking the dimensionless concentration of the monomer units as a function of the zeroth moment rather than τ is considered to be a kind of simplification (and it is not yet an approximation). With this idea in mind, the general formula (without specifying the kernel function) that describes the dependence of the dimensionless monomer unit concentration (m) on the zeroth moment (μ_0) can be given in the following form:

$$\frac{\mathrm{d}m}{\mathrm{d}\mu_0} = -n - \frac{m \sum_{j=n}^{\infty} K(j) c_j}{\alpha m^n} \tag{5.58}$$

It is important to highlight that the final distribution of the total concentration of the particles can be derived by examining the state when all the monomer units are used up. Furthermore, the nanoparticles can reach a meaningful size if the growth step is much faster than the nucleation step. This condition can be expressed mathematically as the following inequality:

$$n << \frac{m \sum_{j=n}^{\infty} K(j)c_j}{\alpha m^n} \tag{5.59}$$

With this criterion in mind, the first additive term from the right-hand side of Equation 5.58 can be dropped and the following general approximation yields:

$$\frac{\mathrm{d}m}{\mathrm{d}\mu_0} \cong -\frac{m \sum_{j=n}^{\infty} K(j)c_j}{\alpha m^n} \tag{5.60}$$

The further kernel-specific derivations start from this differential equation. These will be presented in separate subsections.

5.2.1 Diffusion kernel

The conditions of the diffusion kernel function entail the size independence of the particles, so the infinite sum in Equation 5.60 is identical to the zeroth moment, so this differential equation can be written in the following specific form now:

$$\frac{\mathrm{d}m}{\mathrm{d}\mu_0} = -\frac{\mu_0}{\alpha m^{n-1}} \tag{5.61}$$

Finding the solution to this equation is quite straightforward considering the initial condition ($\mu_0 = 0$ if $m = 1$):

$$\frac{\alpha}{n} m^n - \frac{\alpha}{n} = -\frac{1}{2}\mu_0^2 \tag{5.62}$$

Obviously, the function of m can be easily derived from the above solution:

$$\mu_0 = \sqrt{\frac{2\alpha}{n}\left(1 - m^n\right)} \tag{5.63}$$

The final value of the zeroth moment can be determined from the above equation readily by setting $m = 0$ in it:

$$\lim_{m\to 0} \mu_0 = \sqrt{\frac{2\alpha}{n}} \tag{5.64}$$

From this, the average number of monomer units in the nanoparticles (as in Equation 4.21) and the cube-root number-average size (defined in Equation 4.19) in the final state can be directly obtained as follows:

$$\bar{M}_\infty = \sqrt{\frac{nk_\mathrm{g}}{2[\mathrm{M}]_0^{n-2}k_\mathrm{M}}} \tag{5.65a}$$

$$r_\mathrm{C} = r_0 \sqrt[6]{\frac{nk_\mathrm{g}}{2[\mathrm{M}]_0^{n-2}k_\mathrm{M}}} \tag{5.65b}$$

The latter result can be compared to stochastic Gillespie simulations which are already presented in Figure 5.16 for this kernel function. In the present dissertation, this testing was carried out for five different values of n ($n = 1, 2, 3, 4, 5$). Figure

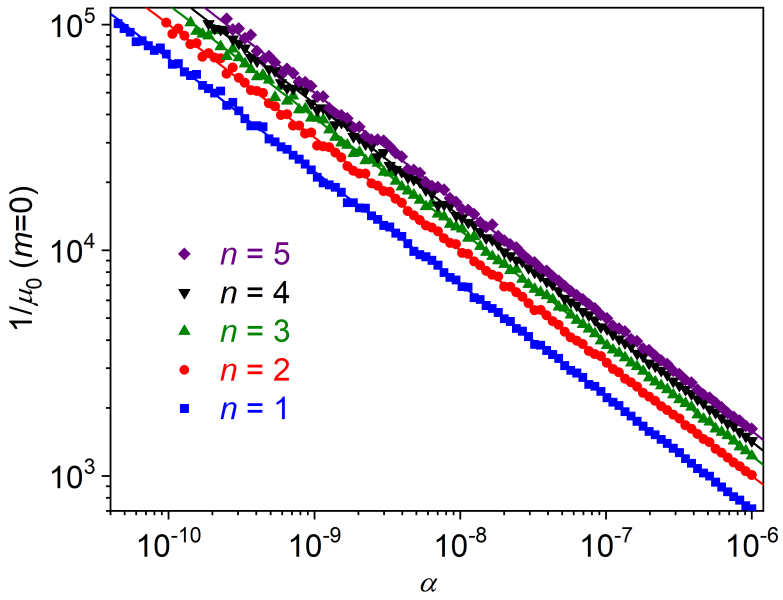

Figure 5.16: Average final particle size as a function of the ratio of the nucleation and growth rate constants for the diffusion kernel, $n = 1, 2, 3, 4, 5$. Markers represent the stochastic simulation results, whereas the lines show the deterministic approximation formula.

5.16 proves that the two approaches are in excellent agreement with each other. The previous sections already showed that the exact solutions of the deterministic model match the stochastic simulations nicely, which means that no problems arise from the assumption that the concentrations are continuous functions of time. The

agreement seen in Figure 5.16 underlines the fact that no major error is caused by simplifying the assumption of the inequality stated in Equation 5.59.

It should be mentioned that the α values were selected in a way that ensured the formation of at least 100 nanoparticles in each simulation run (and with each n value of the kernel function) entailing the fact that the largest average size of the nanoparticles can be 10^5. This kind of restriction is inevitable to avoid a great amount of significant intrinsic noise. Actually, these fluctuations can already be seen in Figure 5.16, meaning that as the values of α reduce, the relative difference of the mean from a consistent trend rises. Nevertheless, the extremely low overall number of particles present in the system for cases of very low α values would also impose serious problems on the accuracy of any deterministic computations. This effect is demonstrated by Figure 5.17, which shows how the average particle size depends on the total number of particles generated in stochastic Gillespie simulations.

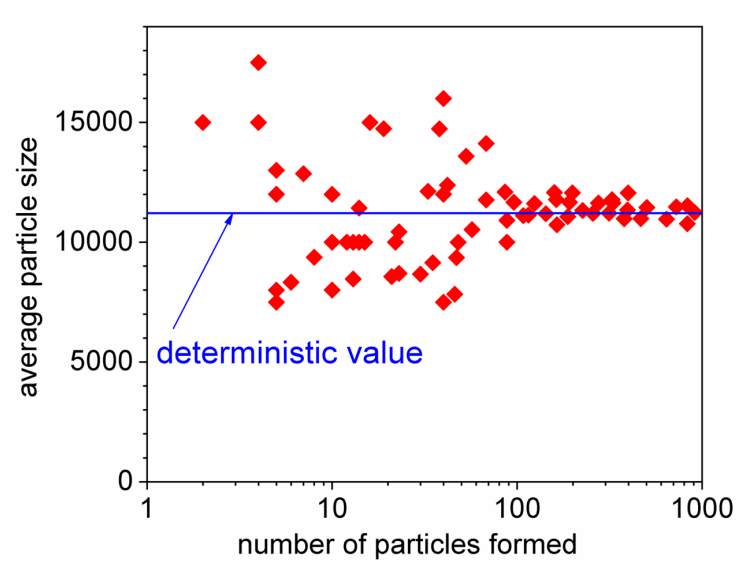

Figure 5.17: The dependence of the average particle size on the total number of nanoparticles formed in stochastic Gillespie simulations.

Because of the implications of Figure 5.17, the requirement calling for the formation of at least 100 nanoparticles in the final state was applied in forthcoming simulations with the other kernel functions as well. This selection is necessary because when the total number of nanoparticles is lower, stochastic fluctuations become the dominant factor in determining the average size, making it difficult to calculate reasonably accurate expectations from a limited number of single simulation runs.

The 1/3th moment ($\mu_{1/3}$), which is significant for calculating one of the average sizes, can be calculated with an additional approximation already introduced in Equation 4.17 in an earlier section. The 1/3th moment is given as the function of

m as follows:

$$\mu_{1/3} = \mu_0^{2/3}\mu_1^{1/3} = \sqrt[3]{(1-m)(1-m^n)\frac{2\alpha}{n}} \tag{5.66}$$

The final value of this moment for the case, when time tends to infinity (and $m = 0$ holds), is therefore:

$$\lim_{m\to 0}\mu_{1/3} = \sqrt[3]{\frac{2\alpha}{n}} \tag{5.67}$$

These results deduced above can be used to give the formula for the number-average size of the population of nanoparticles (r_A), which can be expressed in the following form:

$$r_\mathrm{A} = r_0\frac{\mu_{1/3}}{\mu_0} = r_0\sqrt[6]{\frac{n}{2\alpha}} = r_0\sqrt[6]{\frac{nk_\mathrm{g}}{2k_\mathrm{M}[\mathrm{M}]_0^{n-2}}} \tag{5.68}$$

The 2/3th moment is less important from a practical point of view, but its value can be determined using analogous ways of thought. The formula for m-dependence is given as follows:

$$\mu_{2/3} = \mu_0^{1/3}\mu_1^{2/3} = (1-m)^{2/3}\sqrt[6]{\frac{2\alpha}{n}(1-m^n)} \tag{5.69}$$

The final value can be obtained by substituting $m = 0$ into the above equation, which yields:

$$\lim_{m\to 0}\mu_{2/3} = \sqrt[6]{\frac{2\alpha}{n}} \tag{5.70}$$

5.2.2 Surface kernel

For this kind of kernel function, as was stated in Section 4.3, a separate approximation needs to be considered for calculating the value of the 2/3th moment as the weighted geometrical mean of the zeroth and first moments (Equation 4.18). With this additional assumption, the differential equation giving the dependence of m on μ_0 takes the following simplified form:

$$\frac{\mathrm{d}m}{\mathrm{d}\mu_0} = -\frac{\mu_0^{1/3}(1-m)^{2/3}}{\alpha m^{n-1}} \tag{5.71}$$

This ordinary differential equation can be rearranged into a form where the variables are separated:

$$\frac{\alpha m^{n-1}\mathrm{d}m}{(1-m)^{2/3}} = -\mu_0^{1/3}\mathrm{d}\mu_0 \tag{5.72}$$

Integrating the right-hand side is straightforward, which yields the following equation:

$$\int \frac{\alpha m^{n-1}}{(1-m)^{2/3}} \mathrm{d}m = -\frac{3}{4}\mu_0^{4/3} \tag{5.73}$$

A general integral of the left-hand side is not easy to find. In order to obtain the solution, a useful strategy is to solve the equation for individual, low values of n first. When these solutions are obtained, some patterns can be observed within them, which imply a regularity with increasing n values. In this way, the form of the general solution can be conjectured and then proved by simply substituting it into Equation 5.71. The general solution found with this strategy is the following:

$$\mu_0 = \alpha^{3/4}(1-m)^{1/4}\left(\sum_{i=0}^{n-1}\left(\frac{4}{3n}\prod_{j=i+1}^{n}\frac{3j}{3j-2}\right)m^i\right)^{3/4} \tag{5.74}$$

The final value of the zeroth moment can be found by substituting $m = 0$ into the above equation. This will yield a very simple formula, as only the zeroth order term of the summation remains in it:

$$\lim_{m\to 0}\mu_0 = \left(\frac{4\alpha}{3n}\prod_{j=1}^{n}\frac{3j}{3j-2}\right)^{3/4} \tag{5.75}$$

Employing the formulas derived above, the average number of monomer units and the cube-root number-average size take the following forms:

$$\bar{M}_\infty = \sqrt[4]{\tfrac{27}{64}}\left(\frac{[\mathrm{M}]_0^{n-2}k_\mathrm{M}}{nk_\mathrm{g}}\prod_{j=1}^{n}\tfrac{3j}{3j-2}\right)^{-3/4} \tag{5.76a}$$

$$r_C = r_0\sqrt[4]{\tfrac{3}{4}}\left(\frac{[\mathrm{M}]_0^{n-2}k_\mathrm{M}}{nk_\mathrm{g}}\prod_{j=1}^{n}\tfrac{3j}{3j-2}\right)^{-1/4} \tag{5.76b}$$

Figure 5.18 shows the validity of the solution tested by comparing them to the exact Gillespie simulation results.

In the case of the selection of the values of α, two main factors must be taken into consideration: first, as mentioned earlier, more than 100 nanoparticles need to be formed in each run. Second, the Gillespie simulations are excessively time-consuming here probably because the 2/3th powers of many numbers are calculated during the process. This decelerates the computations very significantly and only makes it possible to calculate fewer full simulations.

Here, computing the further approximation, the $\mu_{2/3}$, can be used to demonstrate

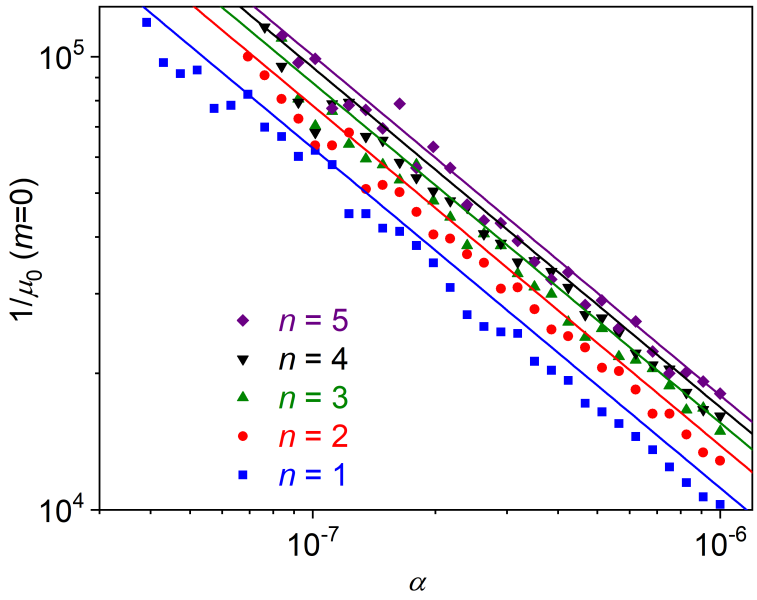

Figure 5.18: Average final particle size as a function of the ratio of the nucleation and growth rate constants for the surface kernel, $n = 1, 2, 3, 4, 5$. Markers represent the stochastic simulation results, whereas the lines show the deterministic approximation formula.

the validity of the deterministic results compared to the stochastic ones. The full form of the 2/3th moment is given as:

$$\mu_{2/3} = \alpha^{1/4} \left(\sum_{i=0}^{n-1} \left(\frac{4}{3n} \prod_{j=i+1}^{n} \frac{3j}{3j-2} \right) m^i \right)^{1/4} (1-m)^{3/4} \tag{5.77}$$

Similarly to the zeroth moment, giving the final value (*i.e.* the one when time tends to infinity) of this 2/3th moment is possible with a less complicated formula:

$$\lim_{m \to 0} \mu_{2/3} = \alpha^{1/4} \left(\frac{4}{3n} \prod_{j=1}^{n} \frac{3j}{3j-2} \right)^{1/4} \tag{5.78}$$

Using these formulas, Figure 5.19 presents the agreement between the approximation-dependent deterministic and the exact stochastic simulation approaches with two different α values for the case $n = 1$ (a viable seed consisting of a single monomer unit). The general agreement is acceptable. What is emphasized by the figure is the agreement is better when a lower value of α is used (i.e. the average size of the nanoparticles in the final state is larger). Also, it is revealed that with the higher value of α shown in the figure, the agreement gets slightly worse when m approaches 0, which means the end of the process.

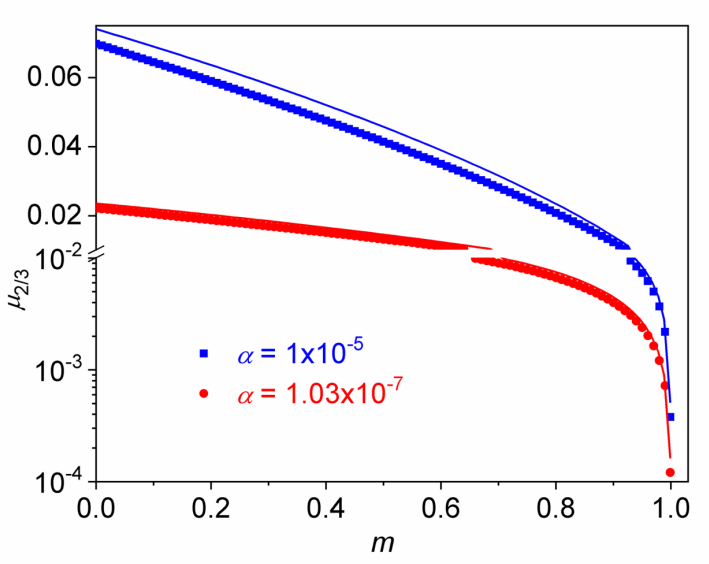

Figure 5.19: The 2/3th moment as a function of the scaled concentrations of the monomer units with two different α values for the surface kernel $n = 1$. Markers represent the stochastic simulation results, whereas the lines show the deterministic approximation formula.

Similarly to the diffusion kernel, the 1/3th moment is also of interest here as it gives a way to calculate one of the possible average sizes (r_{A}) that characterize the population of nanoparticles. Similarly to the diffusion kernel, the approximation introduced in Equation 4.17 is used. The 1/3th moment is given as the function of m as follows:

$$\mu_{1/3} = \mu_0^{2/3}\mu_1^{1/3} = (1-m)^{1/2}\left(\sum_{i=0}^{n-1}\left(\frac{4\alpha}{3n}\prod_{j=i+1}^{n}\frac{3j}{3j-2}\right)m^i\right)^{1/2} \tag{5.79}$$

The final value is again obtained by setting $m = 0$ in the above equation:

$$\lim_{m\to 0}\mu_{1/3} = \left(\frac{4\alpha}{3n}\prod_{j=1}^{n}\frac{3j}{3j-2}\right)^{1/2} \tag{5.80}$$

The average size r_{A} after the end of the synthesis process can be calculated using the following formula:

$$r_{\mathrm{A}} = r_0\left(\frac{4\alpha}{3n}\prod_{j=1}^{n}\frac{3j}{3j-2}\right)^{-1/4} \tag{5.81}$$

5.2.3 Brownian kernel

Applying the Brownian kernel also necessitates the use of a further approximation for calculating the 1/3th moment (introduced in Section 4.3 as Equation 4.17). The ordinary differential equation giving m as the function of the zeroth moment has the following form in this case:

$$\frac{\mathrm{d}m}{\mathrm{d}\mu_0} = -\frac{\mu_0^{2/3}(1-m)^{1/3}}{\alpha m^{n-1}} \tag{5.82}$$

This is a separable ordinary differential equation that can be re-arranged into the following form:

$$\frac{\alpha m^{n-1}\mathrm{d}m}{(1-m)^{1/3}} = -\mu_0^{2/3}\mathrm{d}\mu_0 \tag{5.83}$$

The right-hand side can be integrated readily:

$$\int \frac{\alpha m^{n-1}}{(1-m)^{1/3}}\mathrm{d}m = -\frac{3}{5}\mu_0^{5/3} \tag{5.84}$$

To find the general solution for this, the same technique needs to be employed here as for the surface kernel (solving for small individual values of n, conjecturing the general formula, and then proving it by substituting into the original differential equation). The general solution is the following:

$$\mu_0 = \alpha^{3/5}(1-m)^{2/5}\left(\sum_{i=0}^{n-1}\left(\frac{5}{3n}\prod_{j=i+1}^{n}\frac{3j}{3j-1}\right)m^i\right)^{3/5} \tag{5.85}$$

The final value of the zeroth moment (μ_0 as time tends to infinity) can be given in this way:

$$\lim_{m\to 0}\mu_0 = \alpha^{3/5}\left(\frac{5}{3n}\prod_{j=1}^{n}\frac{3j}{3j-1}\right)^{3/5} \tag{5.86}$$

With this approximation, a formula giving the value of the 1/3th moment ($\mu_{1/3}$) as a function of m can be provided as follows:

$$\mu_{1/3} = \alpha^{2/5}\left(\sum_{i=0}^{n-1}\left(\frac{5}{3n}\prod_{j=i+1}^{n}\frac{3j}{3j-1}\right)m^i\right)^{2/5}(1-m)^{3/5} \tag{5.87}$$

The final value of this 1/3th moment at time infinity is again deduced by setting

$m = 0$ in the previous equation:

$$\lim_{m\to 0} \mu_{1/3} = \alpha^{2/5} \left(\frac{5}{3n} \prod_{j=1}^{n} \frac{3j}{3j-1} \right)^{2/5} \tag{5.88}$$

Since the solution of the $\mu_{1/3}$ is also known, in this specific case, the number-average size of the population of nanoparticles (r_A) can also be determined. The non-scaled equation of the two average sizes of the nanoparticles and the cube-root number-average size for this scheme are rewritten to these forms:

$$\bar{M}_\infty = \left(\tfrac{3}{5}\right)^{3/5} \left(\frac{[\mathrm{M}]_0^{n-2} k_\mathrm{M}}{n k_\mathrm{g}} \prod_{j=1}^{n} \frac{3j}{3j-1} \right)^{-3/5} \tag{5.89a}$$

$$r_\mathrm{C} = r_0 \left(\tfrac{3}{5}\right)^{1/5} \left(\frac{[\mathrm{M}]_0^{n-2} k_\mathrm{M}}{n k_\mathrm{g}} \prod_{j=1}^{n} \frac{3j}{3j-1} \right)^{-1/5} \tag{5.89b}$$

$$r_\mathrm{A} = r_0 \left(\tfrac{3}{5}\right)^{1/5} \left(\tfrac{\alpha}{n}\right)^{2/5} \left(\frac{[\mathrm{M}]_0^{n-2} k_\mathrm{M}}{n k_\mathrm{g}} \right)^{-3/5} \left(\prod_{j=1}^{n} \frac{3j}{3j-1} \right)^{-1/5} \tag{5.89c}$$

The practical validity of these deterministic results is demonstrated in the same way as it was done for the surface kernel. Figure 5.20 shows the comparison between deterministic formulas and stochastic simulations for the final value of the average number of monomer units as a function of the α. The same conditions are used for the selection of the α values, as in the previous two cases.

For this specific kernel, comparing the values of the 1/3th moment calculated from the deterministic form with the stochastic can also be used to test the agreement between the two methods. The result of this comparison is displayed in Figure 5.21.

Similarly to the previous two cases, the 2/3th moment can also given using the results obtained thus far. The m-dependence of $\mu_{2/3}$ takes the following form:

$$\mu_{2/3} = \mu_0^{1/3} \mu_1^{2/3} = (1-m)^{4/5} \left(\sum_{i=0}^{n-1} \left(\frac{5\alpha}{3n} \prod_{j=i+1}^{n} \frac{3j}{3j-1} \right) m^i \right)^{1/5} \tag{5.90}$$

The value in the final state is:

$$\lim_{m\to 0} \mu_{2/3} = \left(\frac{5\alpha}{3n} \prod_{j=1}^{n} \frac{3j}{3j-1} \right)^{1/5} \tag{5.91}$$

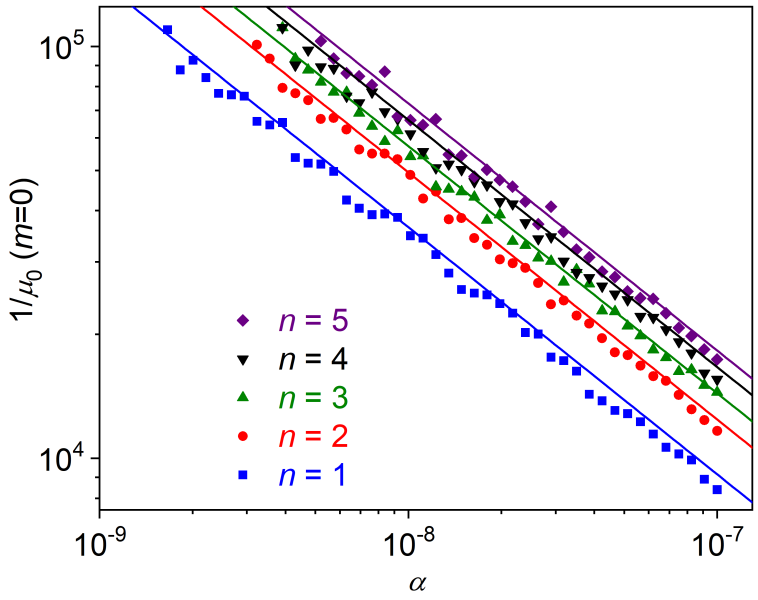

Figure 5.20: Average final particle size as a function of the ratio of the nucleation and growth rate constants for the Brownian kernel, $n = 1, 2, 3, 4, 5$. Markers represent the stochastic simulation results, whereas the lines show the deterministic approximation formula.

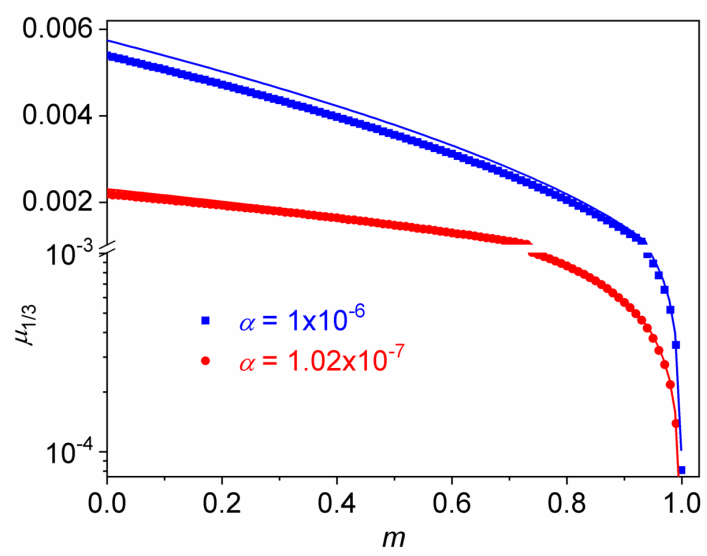

Figure 5.21: The 1/3th moment as a function of the scaled concentration of the monomer unit with two different α values for the Brownian kernel with $n = 2$. Markers represent the stochastic simulation results, whereas the lines show the deterministic approximation formula.

5.2.4 Mass kernel

The mass kernel shows some differences from the previous kernels. The infinite sum in Equation 5.60 is exactly equal to the result of the first moment ($\mu_1 = 1-m$) in this

case, which seems a simpler case than the previous kernel dealt with. Even though this would seem contradictory at first sight, employing fewer approximations than for the previous cases proved to be a better strategy for the mass kernel. Instead of neglecting the entire term of nucleation in Equation 5.58, it is only the exponent in the first terms that changed from n to 1. The logic behind this change is that nucleation is only important at the beginning of the process, where m hardly changes from its initial value of 1, so it only causes a minor error if the exponent is changed. In this way, the following approximation differential equation yields instead of the one analogous to Equation 5.59:

$$\frac{\mathrm{d}m}{\mathrm{d}\mu_0} \cong -\frac{\alpha n + 1 - m}{\alpha m^{n-1}} \tag{5.92}$$

The analytical solution is quite simple when the nucleation is first-order ($n = 1$):

$$\mu_0 = \alpha \ln\left(\frac{\alpha + 1 - m}{\alpha}\right) \qquad \text{for} \quad n = 1 \tag{5.93}$$

The cases when $n > 1$ are considerably more difficult. Using the same strategy as for the surface and Brownian kernels (*i.e.* solving for small individual values of n at first, conjecturing the general formula and then proving it by substituting into Equation 5.92), the full form of the solution can be determined as follows:

$$\mu_0 = \alpha(1+\alpha n)^{n-1} \ln\left(\frac{\alpha n + 1 - m}{\alpha n}\right) + \alpha \sum_{i=1}^{n-1} \frac{1}{i}(1+\alpha n)^{n-1-i}\left(m^i - 1\right) \tag{5.94}$$

The final value of the zeroth moment μ_0 can once again be obtained by substituting $m = 0$ into the above equation. The results are as follows:

$$\begin{aligned} &\lim_{m\to 0} \mu_0 = \alpha \ln\left(\frac{\alpha + 1}{\alpha}\right) \qquad \text{for} \quad n = 1 \\ &\lim_{m\to 0} \mu_0 = \alpha(1+\alpha n)^{n-1} \ln\left(\frac{\alpha n + 1}{\alpha n}\right) - \alpha \sum_{i=1}^{n-1} \frac{1}{i}(1+\alpha n)^{n-1-i} \quad \text{for} \quad n > 1 \end{aligned} \tag{5.95}$$

At last, the average number of monomer units in the particles needs to be obtained. This gives the same formula as the exact solution for $n = 1$ (Equation 5.38), which is understandable as no approximation is actually used in Equation 5.92. For larger

values of n, the following equation can be given:

$$\bar{M}_\infty = \frac{[\mathrm{M}]_0^{-n}\left([\mathrm{M}]_0^2 + [\mathrm{M}]_0^n n k_\mathrm{M}\right)\left(1+\frac{[\mathrm{M}]_0^{n-2} n k_\mathrm{M}}{k_\mathrm{g}}\right)^{-n}}{\ln\left(1+\frac{[\mathrm{M}]_0^{2-n}k_\mathrm{g}}{n k_\mathrm{M}}\right)k_\mathrm{M}} \\ \sum_{i=1}^{n-1}\frac{1}{i}\frac{[\mathrm{M}]_0^{2-n}k_\mathrm{g}\left(1+\frac{[\mathrm{M}]_0^{n-2}k_\mathrm{M}}{k_\mathrm{g}}\right)^{1+i-n}}{k_\mathrm{M}} \qquad \text{if} \quad n>1 \tag{5.96}$$

The cube-root number-average size can be directly given from the above equation and takes the following form:

$$r_\mathrm{C} = r_0 \sqrt[3]{\frac{[\mathrm{M}]_0^{-n}\left([\mathrm{M}]_0^2 + [\mathrm{M}]_0^n n k_\mathrm{M}\right)\left(1+\frac{[\mathrm{M}]_0^{n-2} n k_\mathrm{M}}{k_\mathrm{g}}\right)^{-n}}{\ln\left(1+\frac{[\mathrm{M}]_0^{2-n}k_\mathrm{g}}{n k_\mathrm{M}}\right)k_\mathrm{M}}} \\ \times \sum_{i=1}^{n-1}\frac{1}{i}\frac{[\mathrm{M}]_0^{2-n}k_\mathrm{g}\left(1+\frac{[\mathrm{M}]_0^{n-2}k_\mathrm{M}}{k_\mathrm{g}}\right)^{1+i-n}}{k_\mathrm{M}} \qquad \text{if } n>1 \tag{5.97}$$

The validity of these deterministic formulas is proved again by the comparison of the average nanoparticle size as a function of the dimensionless rate constant ratio calculated by the result with the corresponding Gillespie simulation results.

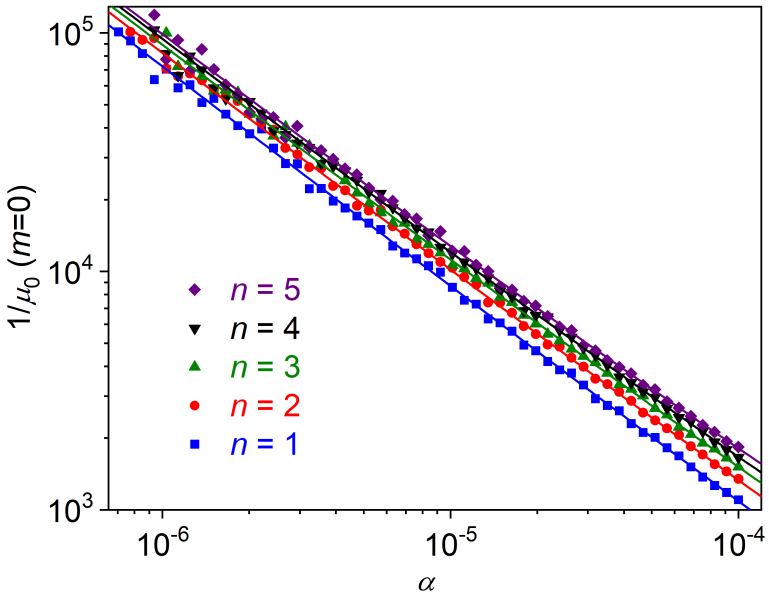

Figure 5.22: Average final particle size as a function of the ratio of the nucleation and growth rate constants for the mass kernel, $n = 1, 2, 3, 4, 5$. Markers represent the stochastic simulation results, whereas the lines show the deterministic approximation formula.

For the mass kernel, the 1/3th and 2/3th moment can also be given as a function of m using sequences of thought very similar to the previous kernels. The 2/3th moment is approximated as follows:

$$\mu_{2/3} = \mu_0^{1/3}\mu_1^{2/3} = (1-m)^{2/3}\left(\alpha\,(1+\alpha n)^{n-1}\ln\left(\frac{1+(\alpha-1)n}{\alpha n}\right)\right)^{1/3} + (1-m)^{2/3}\left(\alpha\sum_{i=1}^{n-1}\frac{1}{i}\,(1+\alpha n)^{n-1-i}\left(m^i-1\right)\right)^{1/3} \tag{5.98}$$

The 2/3th moment in the final state is given by the usual method of substituting $m = 0$ into the above formula:

$$\lim_{m\to 0}\mu_{2/3} = \sqrt[3]{\alpha(1+\alpha n)^{n-1}\ln\left(\frac{1+(\alpha-1)n}{\alpha n}\right) + \alpha\sum_{i=1}^{n-1}\frac{1}{i}\,(1+\alpha n)^{n-1-i}} \tag{5.99}$$

Along very similar lines, the m-dependence of the 1/3th moment ($\mu_{1/3}$) can be given as follows:

$$\mu_{1/3} = \mu_0^{2/3}\mu_1^{1/3} = (1-m)^{1/3}\left(\alpha\,(1+\alpha n)^{n-1}\ln\left(\frac{1+(\alpha-1)n}{\alpha n}\right)\right)^{2/3} + (1-m)^{1/3}\left(\alpha\sum_{i=1}^{n-1}\frac{1}{i}\,(1+\alpha n)^{n-1-i}\left(m^i-1\right)\right)^{2/3} \tag{5.100}$$

The final value of the 1/3th moment is again obtainable by substituting $m = 0$ in the previous equation:

$$\lim_{m\to 0}\mu_{1/3} = \left(\alpha(1+\alpha n)^{n-1}\ln\left(\frac{1+(\alpha-1)n}{\alpha n}\right) + \alpha\sum_{i=1}^{n-1}\frac{1}{i}\,(1+\alpha n)^{n-1-i}\right)^{2/3} \tag{5.101}$$

Using the 1/3th moment, the final value of the average size r_A can be given similarly to the previous kernels:

$$r_\mathrm{A} = r_0\left(\alpha(1+\alpha n)^{n-1}\ln\left(\frac{1+(\alpha-1)n}{\alpha n}\right) + \alpha\sum_{i=1}^{n-1}\frac{1}{i}\,(1+\alpha n)^{n-1-i}\right)^{-1/3} \tag{5.102}$$

5.2.5 Time dependence and numerical calculation of the concentration

In most measurements of nanoparticle synthesis, the final size distribution is measured, although the time dependence of the average size is occasionally monitored

as well. The availability of this kind of measurement data provides a further opportunity to demonstrate the usefulness of the previously presented theoretical results. To achieve this, it is crucial to express the time dependence of the variables. This can be managed through the differential equation governing the time evolution of the concentration of monomer units. This equation has the following general form, which is now stated using the moments defined earlier:

$$\frac{\mathrm{d}m}{\mathrm{d}\tau} = -n\alpha m^n - m\mu_q \tag{5.103}$$

In the above equation, q has the same role as the different kernel functions such as the diffusion kernel ($q = 0$), the surface kernel ($q = 2/3$), the Brownian kernel ($q = 1/3$), and the mass kernel ($q = 1$). The following integration enables the calculation of the time required to reach a specific value of m, which is denoted m_{target} here to distinguish it from the general notation of the variable m:

$$\tau = -\int_1^{m_{\mathrm{target}}} \frac{1}{n\alpha m^n + m\mu_q(m)} \mathrm{d}m \tag{5.104}$$

The concept of calculating the time it takes to reach a set of concentrations is not a very common one in chemical kinetics, one of the rare previous examples was published by Du and Espenson in their experimental description of some classical redox processes[146]. The functional form of $\mu_q(m)$ does not permit the analytical evaluation of the integral for the cases handled here. However, numerical integration can be easily performed to compute the necessary time values. For the diffusion kernel, Equation 5.104 is converted into the following form:

$$\tau = -\int_1^{m_{\mathrm{target}}} \frac{1}{n\alpha m^n + m\sqrt{\frac{2\alpha}{n}\left(1 - m^n\right)}} \mathrm{d}m \tag{5.105}$$

The specific form of Equation 5.104 for the surface kernel can stated using the results in earlier subsections as follows:

$$\tau = -\int_1^{m_{\mathrm{target}}} \frac{1}{n\alpha m^n + m\left(\sum_{i=0}^{n-1}\left(\frac{4\alpha}{3n}\prod_{j=i+1}^{n}\frac{3j}{3j-2}\right)m^i\right)^{1/4}(1-m)^{3/4}} \mathrm{d}m \tag{5.106}$$

A similar process for the Brownian kernel yields an analogous integral expression for τ:

$$\tau = -\int_1^{m_{\text{target}}} \frac{1}{n\alpha m^n + m\alpha^{2/5}\left(\sum_{i=0}^{n-1}\left(\frac{5}{3n}\prod_{j=i+1}^{n}\frac{3j}{3j-1}\right)m^i\right)^{2/5}(1-m)^{3/5}}\mathrm{d}m \quad (5.107)$$

Finally, a less demanding formula results from the use of the mass kernel, which is given as:

$$\tau = -\int_1^{m_{\text{target}}} \frac{1}{n\alpha m^n + m(1-m)}\mathrm{d}m \quad (5.108)$$

The calculations with the method were employed to make a comparison with some measured data published in the literature. In the first example (displayed in Figure 5.23), the average sizes of individual nanoparticles in the population were calculated as a function of time assuming the Brownian kernel. It is worth mentioning that the solid lines in Figure 5.23 denote the model predictions based on intuitive parameter sets that could be obtained through trial and error. These parameter sets are found to represent reasonable agreement with the experimental data[84, 86] and demonstrate the usefulness of the model in interpreting various other observed results. Most unfortunately, proper non-linear least square fitting with the standard algorithm is not possible due to the reversal of the role of dependent and independent variables stated in Equation 5.104. In Figure 5.23, the experimental results from the formation of amino-PEG-covered gold nanoparticles can be seen. The model calculations are made for the Brownian kernel with five various values of n (1, 2, 3, 4, and 5). It is interesting to see that a difference in the size of the viable seed (n) does not cause any crucial distinction in the comparison of measured and predicted data, perhaps the measured data would be needed on a longer time scale for the clear distinction between n values. Figure 5.24 shows experimental data from the process of titania nanoparticle formation observed during basic hydrolysis of titanium(IV)-bis(ammonium-lactato)-dihydroxide [86] compared with model predictions for the mass kernel with $n = 4$. It should kept in mind that calculating the theoretical prediction in this graph needed the value of $\mu_{1/3}$, which was obtained from Equation 5.100. The results in the graph show that the simple nucleation-growth model can be successfully used to explain even the time dependence observed in experimental procedures.

At this stage, it seems to be noteworthy that the introduced approximations (Equations 5.63, 5.74, 5.85, 5.94) also offer a numerical approach for computing the time-dependent c_i variables, which method is analogous to the one employed to

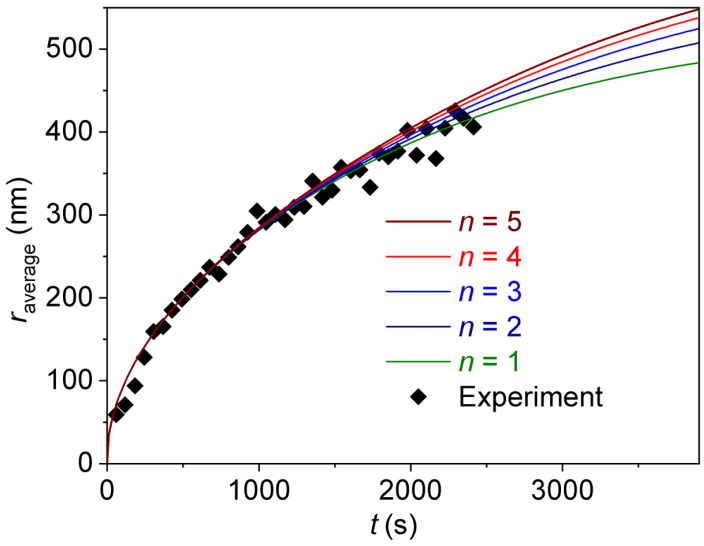

Figure 5.23: Number-average particle size as a function of time: a comparison of model calculations with experimental data. Data from reference[84]. Model predictions: Brownian kernel with different n values displayed in the graph itself, $\alpha = 1 \times 10^{-19}, k_g[\mathrm{M}]_0 = 0.002\,\mathrm{s}^{-1}, r_0 = 0.1\,\mathrm{nm}$.

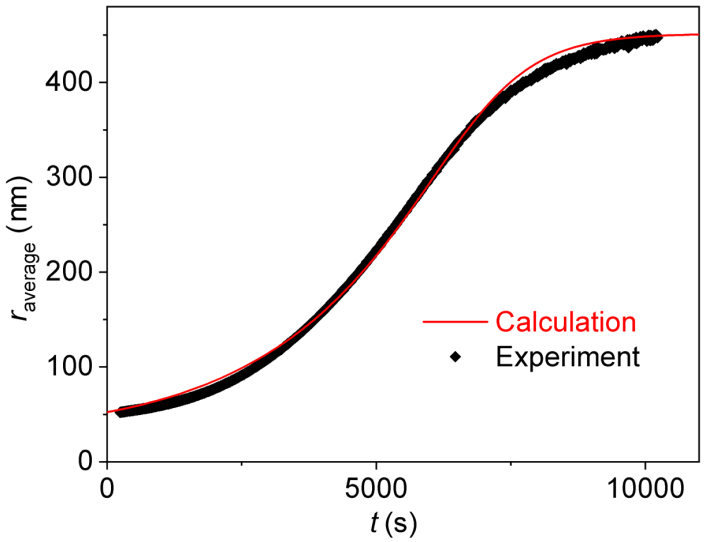

Figure 5.24: Number-average particle size as a function of time: a comparison of model calculations with experimental data. Data from reference[86]. Model predictions: Mass kernel with with $n = 4, \alpha = 6 \times 10^{-5}, k_g[\mathrm{M}]_0 = 0.0012\,\mathrm{s}^{-1}, r_0 = 33\,\mathrm{nm}$.

calculate the time necessary for a given m value. The mentioned equations provide the zeroth moment as a function of m, and by using the Equations 4.17 and 4.18, the variable μ_q, which is essential for the chosen kernel, can be expressed as a function of the monomer unit concentration. This allows the formulation of a differential

equation for c_n and the computation of its dependence on m:

$$\frac{\mathrm{d}c_n}{\mathrm{d}m} = c_n \frac{K(n)}{n\alpha m^{n-1} + \mu_q(m)} - \frac{\alpha m^{n-1}}{n\alpha m^{n-1} + \mu_q(m)} \tag{5.109}$$

It should be noticed in the equation that all the variables but $c_n(m)$ are known. Thus, a standard numerical integration technique, such as the Runge-Kutta or the Gear algorithm, is able to provide a solution for $c_n(m)$. After getting this one ascertained, the other nanoparticle concentrations ($c_i(m)$ for $i > n$) can be calculated iteratively in a recursive manner by numerically solving the differential equation given below:

$$\frac{\mathrm{d}c_i}{\mathrm{d}m} = c_i \frac{K(i)}{n\alpha m^{n-1} + \mu_q(m)} - c_{i-1} \frac{K(i-1)}{n\alpha m^{n-1} + \mu_q(m)} \qquad i > n \tag{5.110}$$

The use of this method is illustrated for the Brownian kernel ($n = 5$ and $\alpha = 10^{-3}$) in two different graphs. Figure 5.25 illustrates some arbitrarily chosen c_i values as a function of dimensionless time. Figure 5.26 displays the c_i values as a function of

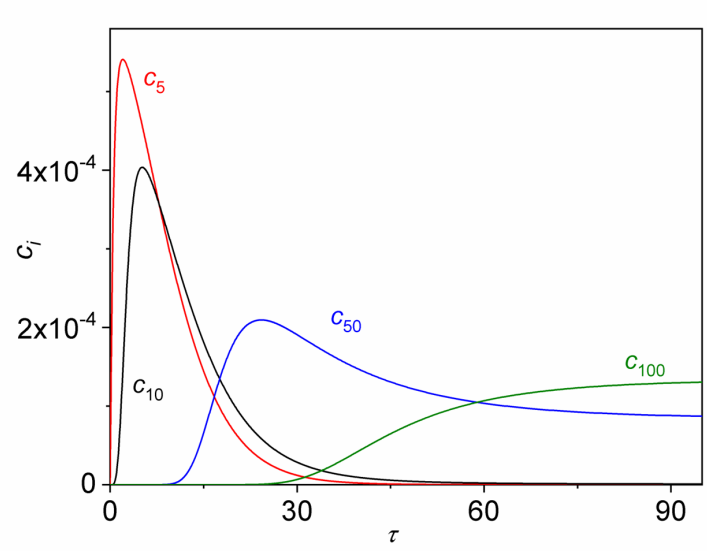

Figure 5.25: Kinetic traces (fixed c_i concentrations as a function τ) for the Brownian kernel, $n = 5, \alpha = 10^{-3}$.

i at chosen fixed values of m (and therefore τ, which can also be computed). This representation actually displays the final size distribution (where $m = 0$ and $\tau = \infty$), so it proves that prediction of the full final distribution is possible. However, this can only be done in viable computation time only if the chosen values of α are relatively high, which corresponds to small average particle sizes. In the case of the graphs shown in this section ($\alpha = 10^{-3}$), calculating up to i=150 is sufficient

to define the full distribution. Earlier examples in the chapter showed that for the most useful predictions (*e.g.* Figures 5.23 and 5.24) calculating up to $i = 10^7$ would be necessary.

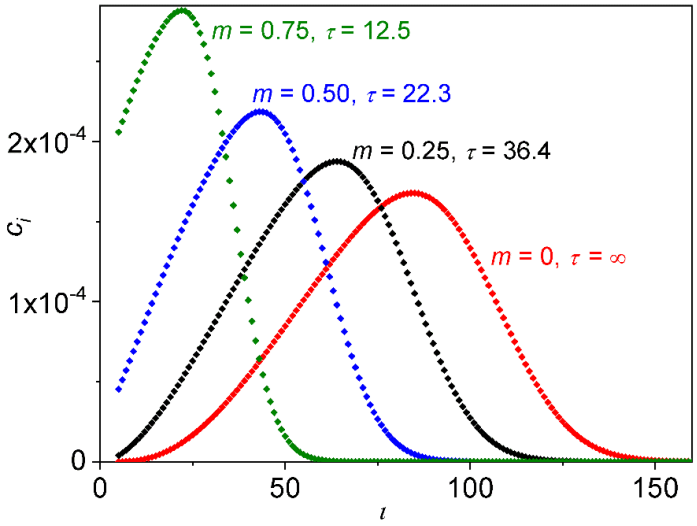

Figure 5.26: Selected c_i values as a function i at some fixed values of m for the Brownian kernel, $n = 5, \alpha = 10^{-3}$.

5.3 Some results on induced nucleation

For several experimental studies, a reagent, a so-called external inductor, is employed to help the formation of the first kinetically effective nuclei [1, 12, 84, 86] and using such a reagent is a prevalent practice in polymerization processes[147], as well. The nucleation-growth model studied in this dissertation can accommodate the presence of such an inductor. One possibility is to include a new reagent, P, in the nucleation step. The overall kinetic model can be given in the following form then:

$$\begin{aligned} &\mathrm{P} + n\mathrm{M} \xrightarrow{k_\mathrm{p}} \mathrm{C}_n && n, i \in \mathbb{Z}^+ && \upsilon_\mathrm{p} = k_\mathrm{p}[\mathrm{P}] \\ &\mathrm{C}_i + \mathrm{M} \xrightarrow{K(i)k_\mathrm{g}} \mathrm{C}_{i+1} && i \geq n && \upsilon_{\mathrm{g},i} = K(i)k_\mathrm{g}[\mathrm{M}][\mathrm{C}_i] \end{aligned} \tag{5.111}$$

The system of differential equations describing the time dependence of the particles can be obtained:

$$\begin{aligned}
\frac{\mathrm{d[M]}}{\mathrm{d}t} &= -n\upsilon_\mathrm{p} - \sum_{j=n}^{\infty} \upsilon_{\mathrm{g},j} = -nk_\mathrm{p}[\mathrm{P}] - \sum_{j=n}^{\infty} K(j)k_\mathrm{g}[\mathrm{M}][\mathrm{C}_i] \\
\frac{\mathrm{d[C}_n\mathrm{]}}{\mathrm{d}t} &= \upsilon_\mathrm{p} - \upsilon_{\mathrm{g},n} = k_\mathrm{p}[\mathrm{P}] - K(n)k_\mathrm{g}[\mathrm{M}][\mathrm{C}_n] \\
\frac{\mathrm{d[C}_i\mathrm{]}}{\mathrm{d}t} &= \upsilon_{\mathrm{g},i-1} - \upsilon_{\mathrm{g},i} = K(i-1)k_\mathrm{g}[\mathrm{M}][\mathrm{C}_{i-1}] - K(i)k_\mathrm{g}[\mathrm{M}][\mathrm{C}_i] \qquad i > n \\
\frac{\mathrm{d[P]}}{\mathrm{d}t} &= -\upsilon_\mathrm{p} = -k_\mathrm{p}[\mathrm{P}] \qquad [\mathrm{P}]_0 << [\mathrm{M}]_0
\end{aligned} \tag{5.112}$$

The condition given in the last line is not mathematically necessary but is a very natural one chemically: too much inductor would result in the formation of tiny particles only. In order to obtain the dimensionless version of the model (similarly to the spontaneous nucleation model), the already stated quantities (Equation 4.4) are needed and besides those, two new variables have to be introduced:

$$p = \frac{[\mathrm{P}]}{[\mathrm{M}]_0}, \qquad\qquad \beta = \frac{k_\mathrm{p}}{[\mathrm{M}]_0 k_\mathrm{g}} \tag{5.113}$$

Variable p is the dimensionless concentration of the external inductor (P), whereas β represents the dimensionless rate constant of induced nucleation. With the dimensionless variables introduced, the system of ordinary differential equations can be rewritten into the following form:

$$\begin{aligned}
\frac{\mathrm{d}m}{\mathrm{d}\tau} &= -n\beta p - \sum_{j=n}^{\infty} K(j)mc_j \\
\frac{\mathrm{d}c_n}{\mathrm{d}\tau} &= \beta p - K(n)mc_n \\
\frac{\mathrm{d}c_i}{\mathrm{d}\tau} &= K(i-1)mc_{i-1} - K(i)mc_i \\
\frac{\mathrm{d}p}{\mathrm{d}\tau} &= -\beta p
\end{aligned} \tag{5.114}$$

First of all, some considerations can be utilized regardless of the details of the model. The initial value of p is denoted p_0:

$$p_0 = [\mathrm{P}]_0/[\mathrm{M}]_0 << 1 \tag{5.115}$$

Then it can be noticed that the last line in Equation 5.114 is a first-order differential equation for p without the influence of any other variables. So the solution is the

usual exponential function for the time dependence of p.

$$p = p_0 \mathrm{e}^{-\beta\tau} \tag{5.116}$$

As a next step, the differential equation for the zeroth moment as a function of τ is written, which takes a simple form:

$$\frac{\mathrm{d}\mu_0}{\mathrm{d}\tau} = \beta p \tag{5.117}$$

Once more, it is crucial to emphasize that the zeroth moment is a monotonically increasing function, and it can be noticed that μ_0 is not dependent on the choice of the kernel function, either. Consequently, the time dependence of the total concentration of the nanoparticles can be found as given below:

$$\mu_0 = p_0 \left(1 - \mathrm{e}^{-\beta\tau}\right) \tag{5.118}$$

The final value of the zeroth moment (*i.e.* at $\tau = \infty$) is useful to state at this point:

$$\lim_{\tau\to\infty} \mu_0 = p_0 \tag{5.119}$$

The model featuring induced nucleation can be investigated for each of the investigated kernel functions. Considering the diffusion kernel, the differential equation describing m as a function of the dimensionless time assumes the following form under the given conditions:

$$\frac{\mathrm{d}m}{\mathrm{d}\tau} = -n\beta p_0 \mathrm{e}^{-\beta\tau} - m p_0 \left(1 - \mathrm{e}^{-\beta\tau}\right) \tag{5.120}$$

Some progress toward the analytical solution is possible in this case, but an integration without a closed-form result remains in the formula:

$$\begin{aligned} m = {} & \mathrm{e}^{p_0/\beta - p_0 \mathrm{e}^{-\beta\tau}/\beta - p_0\tau} \\ & - n\beta p_0 \mathrm{e}^{-p_0 \mathrm{e}^{-\beta\tau}/\beta - p_0\tau} \int_0^\tau \mathrm{e}^{p_0 \mathrm{e}^{-\beta\xi}/\beta + p_0\xi - \beta\xi} \mathrm{d}\xi \end{aligned} \tag{5.121}$$

Moving on to the mass kernel, the differential equation describing the time dependence of the monomer units is represented as follows:

$$\frac{\mathrm{d}m}{\mathrm{d}\tau} = -n\beta p_0 \mathrm{e}^{-\beta\tau} - m(1 - m) \tag{5.122}$$

The software Mathematica ascertained the existence of a closed-form analytical so-

lution for this differential equation involving gamma and confluent hypergeometric functions (see Proofs and derivations), but, most unfortunately, this solution is exceedingly complex and its use would be impractical for in a real application. Other than the mentioned two cases, no plausible hints at obtaining an analytical solution have been uncovered for induced nucleation. If necessary, suitable approximations could be developed for these cases, but meeting that challenge awaits future attempts in chemical kinetics.

6 Conclusion

In summary, this dissertation presents a comprehensive nucleation-growth model that elucidates nanoparticle formation processes through two key reactions: seed formation from n monomers and subsequent growth via monomer addition. The kernel functions determine the dependence of the growth step on the particle size, and for practical reasons, four distinct kernels are considered here: the mass kernel (direct relationship with the number of monomers), the Brownian kernel (directly related to the radius of the particle), the surface kernel (directly proportional to the surface area of the particle), and finally the diffusion kernel (independent of the nanoparticle size). To simplify the set of ordinary differential equations describing this kinetic model, dimensionless quantities were introduced. The mathematical framework for this population necessitates the application of moments, where the first moment characterizes the overall count of monomer units within the particles, while the zeroth moment represents the sum of the concentration of the nanoparticles. Exploring additional types of moments could be beneficial in deriving general solutions for the average sizes.

Furthermore, the research goes beyond deterministic computations by incorporating stochastic kinetics via Gillespie simulations. Utilizing a Monte Carlo simulation method, the Stochastic Simulation Algorithm offers a robust framework for exploring molecular-level dynamics.

Exact analytical solutions could only be found for the diffusion kernel with first-order nucleation, and the mass kernel with first- and second-order nucleation. The results of the latter were validated by stochastic simulations. These can also give the time dependence of the concentration of the nanoparticles.

In all other scenarios (all four kernel functions and regardless of n), approximation methods were necessary, leading us to focus on solving the zeroth moment. Once more, this approach was validated against Gillespie simulation outcomes.

7 Összefoglalás

Összefoglalva, ez a disszertáció egy általános gócképződési-növekedési modellt tárgyal, amely bemutatja a nanorészecskék képződési folyamatait két kulcsfontosságú reakción keresztül: gócképződés n monomeregységből és a későbbi növekedés monomeregységek hozzáadásával. A kernel függvények meghatározzák a növekedési lépésnek a részecske méretétől való függését, és gyakorlati okokból itt négy különböző kernelt veszünk figyelembe: a tömegkernel (közvetlen kapcsolat a monomerek számával), a Brown-kernel (közvetlenül összefügg a részecske sugarával), a felületkernel (közvetlen arányosság a részecske felületével), és végül a diffúziós kernel (független a nanorészecske méretétől). A kinetikai modellt leíró közönséges differenciálegyenletek egyszerűsítése érdekében dimenziómentes mennyiségek kerültek bevezetésre. Ennek a populációnak a matematikai kerete a momentumok alkalmazását igényli, ahol az első momentum jellemzi a részecskékben található monomeregységek számát, míg a nulladik momentum a részecskék összkoncentrációját reprezentálja. További momentumok bevezetése hasznos lehet az átlagos méretek általános megoldásainak meghatározásához.

Továbbá, a kutatás meghaladja a determinisztikus számításokat a Gillespie-szimulációk révén beépített sztochasztikus kinetika integrálásával. A Monte Carlo-szimulációs módszer felhasználása, különösen a Sztochasztikus Szimulációs Algoritmus, erős keretet biztosít a molekuláris szintű dinamika vizsgálatához.

Pontos analitikai megoldások csak az elsőrendű gócképződéssel járó diffúziós kernelre és az első- és másodrendű gócképződéssel rendelkező tömegkernel eseteiben található. Az utóbbi eredményeit sztochasztikus szimulációkkal is validáltuk. Ezek szintén adhatnak információt a nanorészecskék koncentrációjának időfüggéséről.

Minden más esetben (az összes kernel függvényre és n értékétől függetlenül) közelítő módszerek bevezetése szükséges volt, amelyek a nulladik momentum megoldására koncentráltak. Ezeket az eredményeket megint csak igazoltuk pontos Gillespie-

szimulációkkal szemben.

References

1. Zibareva, I. V., Ilina, L. Y. & Vedyagin, A. A. Catalysis by nanoparticles: the main features and trends. *Reaction Kinetics, Mechanisms and Catalysis* **127,** 19–24 (Feb. 2019).
2. Azouani, R. *et al.* TiO2 doping by hydroxyurea at the nucleation stage: towards a new photocatalyst in the visible spectral range. *Physical Chemistry Chemical Physics* **12,** 11325 (2010).
3. Ettlinger, R. *et al.* Toxicity of metal–organic framework nanoparticles: from essential analyses to potential applications. *Chemical Society Reviews* **51,** 464–484 (2022).
4. Chen, G., Roy, I., Yang, C. & Prasad, P. N. Nanochemistry and Nanomedicine for Nanoparticle-based Diagnostics and Therapy. *Chemical Reviews* **116,** 2826–2885 (Jan. 2016).
5. Kinnear, C., Moore, T. L., Rodriguez-Lorenzo, L., Rothen-Rutishauser, B. & Petri-Fink, A. Form Follows Function: Nanoparticle Shape and Its Implications for Nanomedicine. *Chemical Reviews* **117,** 11476–11521 (Sept. 2017).
6. Elahi, N., Kamali, M. & Baghersad, M. H. Recent biomedical applications of gold nanoparticles: A review. *Talanta* **184,** 537–556 (July 2018).
7. Rahman, M. M. *et al.* Recent advancements of nanoparticles application in cancer and neurodegenerative disorders: At a glance. *Biomedicin & Pharmacotherapy* **153,** 113305 (Sept. 2022).
8. Attia, N. F. *et al.* Iron oxide nanoparticles and their pharmaceutical applications. *Applied Surface Science Advances* **11,** 100284 (Oct. 2022).
9. Martínez, G. *et al.* Environmental Impact of Nanoparticles' Application as an Emerging Technology: A Review. *Materials* **14,** 166 (Dec. 2020).

10. Fatima, F., Hashim, A. & Anees, S. Efficacy of nanoparticles as nanofertilizer production: a review. *Environmental Science and Pollution Research* **28,** 1292–1303 (Oct. 2020).

11. Saravanan, A. *et al.* A review on biosynthesis of metal nanoparticles and its environmental applications. *Chemosphere* **264,** 128580 (Feb. 2021).

12. Xu, L., Liang, H.-W., Yang, Y. & Yu, S.-H. Stability and Reactivity: Positive and Negative Aspects for Nanoparticle Processing. *Chemical Reviews* **118,** 3209–3250 (Mar. 2018).

13. Jeevanandam, J., Barhoum, A., Chan, Y. S., Dufresne, A. & Danquah, M. K. Review on nanoparticles and nanostructured materials: history, sources, toxicity and regulations. *Beilstein Journal of Nanotechnology* **9,** 1050–1074 (Apr. 2018).

14. Maroušek, J. Review: Nanoparticles can change (bio)hydrogen competitiveness. *Fuel* **328,** 125318 (Nov. 2022).

15. Buchman, J. T., Hudson-Smith, N. V., Landy, K. M. & Haynes, C. L. Understanding Nanoparticle Toxicity Mechanisms To Inform Redesign Strategies To Reduce Environmental Impact. *Accounts of Chemical Research* **52,** 1632–1642 (June 2019).

16. Mohammadzadeh, V. *et al.* Applications of plant-based nanoparticles in nanomedicine: A review. *Sustainable Chemistry and Pharmacy* **25,** 100606 (Apr. 2022).

17. Gu, X. *et al.* Preparation and antibacterial properties of gold nanoparticles: a review. *Environmental Chemistry Letters* **19,** 167–187 (Aug. 2020).

18. Deshmukh, S., Patil, S., Mullani, S. & Delekar, S. Silver nanoparticles as an effective disinfectant: A review. *Materials Science and Engineering: C* **97,** 954–965 (Apr. 2019).

19. Ajdary, M. *et al.* Health Concerns of Various Nanoparticles: A Review of Their in Vitro and in Vivo Toxicity. *Nanomaterials* **8,** 634 (Aug. 2018).

20. Baranowska-Wójcik, E., Szwajgier, D., Oleszczuk, P. & Winiarska-Mieczan, A. Effects of Titanium Dioxide Nanoparticles Exposure on Human Health—a Review. *Biological Trace Element Research* **193,** 118–129 (Apr. 2019).

21. Lisovskii, A. F. On the Thermodynamics of Nanoparticle Formation. *Journal of Superhard Materials* **42,** 9–17 (Jan. 2020).

22. Wheeler, L. M., Kramer, N. J. & Kortshagen, U. R. Thermodynamic Driving Force in the Spontaneous Formation of Inorganic Nanoparticle Solutions. *Nano Letters* **18,** 1888–1895 (Feb. 2018).

23. Luo, W., Hu, W. & Xiao, S. Size Effect on the Thermodynamic Properties of Silver Nanoparticles. *The Journal of Physical Chemistry C* **112,** 2359–2369 (Jan. 2008).

24. Zhang, H., Huang, F., Gilbert, B. & Banfield, J. F. Molecular Dynamics Simulations, Thermodynamic Analysis, and Experimental Study of Phase Stability of Zinc Sulfide Nanoparticles. *The Journal of Physical Chemistry B* **107,** 13051–13060 (Nov. 2003).

25. Barnard, A. S. Direct Comparison of Kinetic and Thermodynamic Influences on Gold Nanomorphology. *Accounts of Chemical Research* **45,** 1688–1697 (June 2012).

26. Polte, J. Fundamental growth principles of colloidal metal nanoparticles – a new perspective. *CrystEngComm* **17,** 6809–6830 (2015).

27. Galina, H. & Lechowicz, J. B. in *Grafting/Characterization Techniques/Kinetic Modeling* 135–172 (Springer Berlin Heidelberg).

28. Woehl, T. J. *et al.* Direct Observation of Aggregative Nanoparticle Growth: Kinetic Modeling of the Size Distribution and Growth Rate. *Nano Letters* **14,** 373–378 (Dec. 2013).

29. Sun, H., Jiao, R., An, G., Xu, H. & Wang, D. Influence of particle size on the aggregation behavior of nanoparticles: Role of structural hydration layer. *Journal of Environmental Sciences* **103,** 33–42 (2021).

30. Mazo, R. M. in *Brownian Motion* 46–61 (Oxford University Press, Oct. 2008).

31. Chavanis, P.-H. The Generalized Stochastic Smoluchowski Equation. *Entropy* **21,** 1006 (Oct. 2019).

32. Szała-Mendyk, B., Drajkowska, A. & Molski, A. Modified Smoluchowski Rate Equations for Aggregation and Fragmentation in Finite Systems. *The Journal of Physical Chemistry B* **127,** 6154–6162 (2023).

33. Beltran-Villegas, D. J., Sehgal, R. M., Maroudas, D., Ford, D. M. & Bevan, M. A. Colloidal cluster crystallization dynamics. *The Journal of Chemical Physics* **137** (Oct. 2012).

34. Katzourakis, V. E. & Chrysikopoulos, C. V. Modeling the Transport of Aggregating Nanoparticles in Porous Media. *Water Resources Research* **57** (2021).

35. Provis, J. L. & Vlachos, D. G. Silica Nanoparticle Formation in the TPAOH-TEOS-Hsub2/subO System: A Population Balance Model. *The Journal of Physical Chemistry B* **110,** 3098–3108 (Feb. 2006).

36. Becker, R. & Döring, W. Kinetische Behandlung der Keimbildung in übersättigten Dämpfen. *Annalen der Physik* **416,** 719–752 (1935).

37. Kalikmanov, V. I. in *Nucleation Theory* 17–41 (Springer Netherlands, Nov. 2012).

38. Warren, D. R. & Seinfeld, J. H. Nucleation and Growth of Aerosol From a Continuously Reinforced Vapor. *Aerosol Science and Technology* **3,** 135–153 (Jan. 1984).

39. Privman, V. Mechanisms of Diffusional Nucleation of Nanocrystals and Their Self-Assembly into Uniform Colloids. *Annals of the New York Academy of Sciences* **1161,** 508–525 (Apr. 2009).

40. Penrose, O. Metastable states for the Becker-Dring cluster equations. *Communications in Mathematical Physics* **124,** 515–541 (Dec. 1989).

41. Hingant, E. & Yvinec, R. in *Stochastic Processes, Multiscale Modeling, and Numerical Methods for Computational Cellular Biology* 175–204 (Springer International Publishing, 2017).

42. Sahu, P. & Prasad, B. L. V. Time and Temperature Effects on the Digestive Ripening of Gold Nanoparticles: Is There a Crossover from Digestive Ripening to Ostwald Ripening? *Langmuir* **30,** 10143–10150 (Aug. 2014).

43. Laurençot, P. & Mischler, S. From the Becker–Döring to the Lifshitz–Slyozov–Wagner Equations. *Journal of Statistical Physics* **106,** 957–991 (Mar. 2002).

44. Slemrod, M. in *Modeling in Applied Sciences* 149–171 (Birkhäuser Boston, 2000).

45. Filbet, F. & Laurençot, P. Numerical Approximation of the Lifshitz–Slyozov–Wagner Equation. *SIAM Journal on Numerical Analysis* **41,** 563–588 (Jan. 2003).

46. Damialis, A. The Lifshitz–Slyozov–Wagner equation for reaction-controlled kinetics. *Proceedings of the Royal Society of Edinburgh: Section A Mathematics* **140,** 273–289 (Mar. 2010).

47. Velázquez, J. On the Effect of Stochastic Fluctuations in the Dynamics of the Lifshitz–Slyozov–Wagner Model. *Journal of Statistical Physics* **99,** 57–113 (Apr. 2000).

48. Liu, Y., Kathan, K., Saad, W. & Prud'homme, R. K. Ostwald Ripening of β-Carotene Nanoparticles. *Physical Review Letters* **98,** 036102 (Jan. 2007).

49. Thanh, N. T. K., Maclean, N. & Mahiddine, S. Mechanisms of Nucleation and Growth of Nanoparticles in Solution. *Chemical Reviews* **114,** 7610–7630 (July 2014).

50. Desai, R. C. & Kapral, R. *Dynamics of Self-Organized and Self-Assembled Structures* (Cambridge University Press, Mar. 2009).

51. Oskam, G. & de Jesús Peet Poot, F. Synthesis of ZnO and TiO2 nanoparticles. *Journal of Sol-Gel Science and Technology* **37,** 157–160 (Feb. 2006).

52. Niethammer, B. A Scaling Limit of the Becker-Dring Equations in the Regime of Small Excess Density. *Journal of Nonlinear Science* **14,** 453–468 (Oct. 2004).

53. Gentry, S. T., Kendra, S. F. & Bezpalko, M. W. Ostwald Ripening in Metallic Nanoparticles: Stochastic Kinetics. *The Journal of Physical Chemistry C* **115,** 12736–12741 (June 2011).

54. Madras, G. & McCoy, B. J. Distribution kinetics theory of Ostwald ripening. *The Journal of Chemical Physics* **115,** 6699–6706 (Oct. 2001).

55. Marqusee, J. A. & Ross, J. Theory of Ostwald ripening: Competitive growth and its dependence on volume fraction. *The Journal of Chemical Physics* **80,** 536–543 (Jan. 1984).

56. Johnson, W. A. & Mehl, R. F. Reaction kinetics in processes of nucleation and growth. *Trans. Am. Inst. Min. Metall. Eng.* **135,** 416–442 (1939).

57. Todinov, M. On some limitations of the Johnson–Mehl–Avrami–Kolmogorov equation. *Acta Materialia* **48,** 4217–4224 (Nov. 2000).

58. Fanfoni, M. & Tomellini, M. The Johnson-Mehl- Avrami-Kohnogorov model: A brief review. *Il Nuovo Cimento D* **20,** 1171–1182 (July 1998).

59. Avrami, M. Kinetics of Phase Change. I General Theory. *The Journal of Chemical Physics* **7,** 1103–1112 (Dec. 1939).

60. Avrami, M. Kinetics of Phase Change. II Transformation-Time Relations for Random Distribution of Nuclei. *The Journal of Chemical Physics* **8,** 212–224 (Feb. 1940).

61. Avrami, M. Granulation, Phase Change, and Microstructure Kinetics of Phase Change. III. *The Journal of Chemical Physics* **9,** 177–184 (Feb. 1941).

62. Toda, A. Effect of a Nucleating Agent on Polymer Crystallization Analyzed Using the Original Avrami Model. *Macromolecules* **55,** 2202–2209 (Feb. 2022).

63. Zhdanov, V. P. & Kasemo, B. Kinetics of the formation of a new phase in nanoparticles. *Chemical Physics Letters* **460,** 158–161 (July 2008).

64. Jin, O. *et al.* Transformation Kinetics of LiBH4–MgH2 for Hydrogen Storage. *Molecules* **27,** 7005 (Oct. 2022).

65. Hömberg, D., Patacchini, F. S., Sakamoto, K. & Zimmer, J. A revisited Johnson–Mehl–Avrami–Kolmogorov model and the evolution of grain-size distributions in steel. *IMA Journal of Applied Mathematics* **82,** 763–780 (May 2017).

66. Kartseva, M. E., Shishmakova, E. M., Dement'eva, O. V. & Rudoy, V. M. The Growth of Phosphonium Gold Nanoparticles in Alkaline Media: Kinetics and Mechanism of the Process. *Colloid Journal* **83,** 707–712 (Nov. 2021).

67. Farjas, J. & Roura, P. Modification of the Kolmogorov–Johnson–Mehl–Avrami rate equation for non-isothermal experiments and its analytical solution. *Acta Materialia* **54,** 5573–5579 (Dec. 2006).

68. Shirzad, K. & Viney, C. A critical review on applications of the Avrami equation beyond materials science. *Journal of The Royal Society Interface* **20.** ISSN: 1742-5662 (June 2023).

69. LaMer, V. K. & Dinegar, R. H. Theory, Production and Mechanism of Formation of Monodispersed Hydrosols. *Journal of the American Chemical Society* **72,** 4847–4854 (Nov. 1950).

70. Mer, V. K. L. Nucleation in Phase Transitions. *Industrial & Engineering Chemistry* **44,** 1270–1277 (June 1952).

71. Whitehead, C. B., Watzky, M. A. & Finke, R. G. "Burst Nucleation" vs Autocatalytic, "Burst" Growth in Near-Monodisperse Particle-Formation Reactions. *The Journal of Physical Chemistry C* **124,** 24543–24554 (Oct. 2020).

72. Watzky, M. A. & Finke, R. G. Transition Metal Nanocluster Formation Kinetic and Mechanistic Studies. A New Mechanism When Hydrogen Is the Reductant: Slow, Continuous Nucleation and Fast Autocatalytic Surface Growth. *Journal of the American Chemical Society* **119,** 10382–10400 (Oct. 1997).

73. Bentea, L., Watzky, M. A. & Finke, R. G. Sigmoidal Nucleation and Growth Curves Across Nature Fit by the Finke–Watzky Model of Slow Continuous Nucleation and Autocatalytic Growth: Explicit Formulas for the Lag and Growth Times Plus Other Key Insights. *The Journal of Physical Chemistry C* **121,** 5302–5312 (Feb. 2017).

74. Watzky, M. A., Finney, E. E. & Finke, R. G. Transition-Metal Nanocluster Size vs Formation Time and the Catalytically Effective Nucleus Number: A Mechanism-Based Treatment. *Journal of the American Chemical Society* **130,** 11959–11969 (Aug. 2008).

75. Finney, E. E. & Finke, R. G. Is There a Minimal Chemical Mechanism Underlying Classical Avrami-Erofe'ev Treatments of Phase-Transformation Kinetic Data? *Chemistry of Materials* **21,** 4692–4705 (Sept. 2009).

76. Mondloch, J. E. & Finke, R. G. Kinetic Evidence for Bimolecular Nucleation in Supported-Transition-Metal-Nanoparticle Catalyst Formation in Contact with Solution: The Prototype Ir(1,5-*COD*)Cl/γ-Al_2O_3 to Ir(0)$\sim$900/γ-Al_2O_3 System. *ACS Catalysis* **2,** 298–305 (Jan. 2012).

77. Laxson, W. W. & Finke, R. G. Nucleation is Second Order: An Apparent Kinetically Effective Nucleus of Two for $Ir(0)_n$ Nanoparticle Formation from $[(1,5\text{-}COD)Ir^{I}\cdot P_2W_{15}Nb_3O_{62}]^{-}$ Plus Hydrogen. *Journal of the American Chemical Society* **136,** 17601–17615 (Dec. 2014).

78. Watzky, M. A. & Finke, R. G. Pseudoelementary Steps: A Key Concept and Tool for Studying the Kinetics and Mechanisms of Complex Chemical Systems. *The Journal of Physical Chemistry A* **125,** 10687–10705 (Dec. 2021).

79. Handwerk, D. R., Shipman, P. D., Whitehead, C. B., Özkar, S. & Finke, R. G. Mechanism-Enabled Population Balance Modeling of Particle Formation en Route to Particle Average Size and Size Distribution Understanding and Control. *Journal of the American Chemical Society* **141,** 15827–15839 (Sept. 2019).

80. Besson, C., Finney, E. E. & Finke, R. G. Nanocluster Nucleation, Growth, and Then Agglomeration Kinetic and Mechanistic Studies: A More General, Four-Step Mechanism Involving Double Autocatalysis. *Chemistry of Materials* **17,** 4925–4938 (Aug. 2005).

81. Handwerk, D. R., Shipman, P. D., Whitehead, C. B., Özkar, S. & Finke, R. G. Particle Size Distributions via Mechanism-Enabled Population Balance Modeling. *The Journal of Physical Chemistry C* **124,** 4852–4880 (Feb. 2020).

82. Long, D. K. *et al.* Estimating reaction parameters in mechanism-enabled population balance models of nanoparticle size distributions: A Bayesian inverse problem approach. *Journal of Computational Chemistry* **43,** 43–56 (Oct. 2021).

83. Azouani, R. *et al.* Stability and Growth of Titanium-oxo-alkoxy $Ti_xO_y(O^iPr)_z$ Clusters. *The Journal of Physical Chemistry C* **111,** 16243–16248 (Oct. 2007).

84. Zámbó, D., Pothorszky, S., Brougham, D. F. & Deák, A. Aggregation kinetics and cluster structure of amino-PEG covered gold nanoparticles. *RSC Advances* **6,** 27151–27157 (2016).

85. Soloviev, A., Tufeu, R., Sanchez, C. & Kanaev, A. V. Nucleation Stage in the $Ti(OPr)_4$ Sol-Gel Process. *The Journal of Physical Chemistry B* **105,** 4175–4180 (Apr. 2001).

86. Forgács, A. *et al.* Kinetic Model for Hydrolytic Nucleation and Growth of TiO_2 Nanoparticles. *The Journal of Physical Chemistry C* **122,** 19161–19170 (July 2018).

87. Labidi, S., Jia, Z., Amar, M. B., Chhor, K. & Kanaev, A. Nucleation and growth kinetics of zirconium-oxo-alkoxy nanoparticles. *Physical Chemistry Chemical Physics* **17,** 2651–2659 (2015).

88. Lazzari, S., Abolhasani, M. & Jensen, K. F. Modeling of the formation kinetics and size distribution evolution of II–VI quantum dots. *Reaction Chemistry and Engineering* **2,** 567–576 (2017).

89. Rempel, J. Y., Bawendi, M. G. & Jensen, K. F. Insights into the Kinetics of Semiconductor Nanocrystal Nucleation and Growth. *Journal of the American Chemical Society* **131,** 4479–4489 (Mar. 2009).

90. Kumar, S., Gandhi, K. S. & Kumar, R. Modeling of Formation of Gold Nanoparticles by Citrate Method. *Industrial & Engineering Chemistry Research* **46,** 3128–3136 (Oct. 2006).

91. McCoy, B. J. & Madras, G. Evolution to Similarity Solutions for Fragmentation and Aggregation. *Journal of Colloid and Interface Science* **201,** 200–209 (May 1998).

92. McCoy, B. J. Vapor Nucleation and Droplet Growth: Cluster Distribution Kinetics for Open and Closed Systems. *Journal of Colloid and Interface Science* **228,** 64–72 (Aug. 2000).

93. Rivallin, M., Benmami, M., Kanaev, A. & Gaunand, A. Sol–Gel Reactor With Rapid Micromixing. *Chemical Engineering Research and Design* **83,** 67–74 (Jan. 2005).

94. Santillán, M. *Chemical Kinetics, Stochastic Processes, and Irreversible Thermodynamics* (Springer International Publishing, 2014).

95. Anderson, D. F. & Kurtz, T. G. *Stochastic Analysis of Biochemical Systems* (Springer International Publishing, 2015).

96. Dóka, É. & Lente, G. Stochastic mapping of the Michaelis-Menten mechanism. *The Journal of Chemical Physics* **136,** 054111 (Feb. 2012).

97. Lente, G. A binomial stochastic kinetic approach to the Michaelis–Menten mechanism. *Chemical Physics Letters* **568-569,** 167–169 (May 2013).

98. Wilkinson, D. J. *Stochastic Modelling for Systems Biology* (Chapman and Hall/CRC, Apr. 2006).

99. Érdi, P. & Tóth, J. *Mathematical Models of Chemical Reactions: Theory and Applications of Deterministic and Stochastic Models* (Manchester University Press, 1989).

100. Lente, G. The Role of Stochastic Models in Interpreting the Origins of Biological Chirality. *Symmetry* **2,** 767–798 (Apr. 2010).

101. Dóka, É. & Lente, G. Mechanism-Based Chemical Understanding of Chiral Symmetry Breaking in the Soai Reaction. A Combined Probabilistic and Deterministic Description of Chemical Reactions. *Journal of the American Chemical Society* **133,** 17878–17881 (Oct. 2011).

102. Shao, J. & Liu, L. Stochastic Fluctuations and Chiral Symmetry Breaking: Exact Solution of Lente Model. *The Journal of Physical Chemistry A* **111,** 9570–9572 (Aug. 2007).

103. Lente, G. & Ditrói, T. Stochastic Kinetic Analysis of the Frank Model. Stochastic Approach to Flow-Through Reactors. *The Journal of Physical Chemistry B* **113,** 7237–7242 (Apr. 2009).

104. Frank, F. On spontaneous asymmetric synthesis. *Biochimica et Biophysica Acta* **11,** 459–463 (Jan. 1953).

105. Lente, G. Homogeneous Chiral Autocatalysis: A Simple, Purely Stochastic Kinetic Model. *The Journal of Physical Chemistry A* **108,** 9475–9478 (Oct. 2004).

106. Lente, G. Stochastic Kinetic Models of Chiral Autocatalysis: A General Tool for the Quantitative Interpretation of Total Asymmetric Synthesis. *The Journal of Physical Chemistry A* **109,** 11058–11063 (Nov. 2005).

107. Lente, G. Stochastic Analysis of the Parity-Violating Energy Differences between Enantiomers and Its Implications for the Origin of Biological Chirality. *The Journal of Physical Chemistry A* **110,** 12711–12713 (Nov. 2006).

108. Lente, G. The effect of parity violation on kinetic models of enantioselective autocatalysis. *Physical Chemistry Chemical Physics* **9,** 6134 (2007).

109. Lente, G. A novel method to compute the time dependence of state distributions in the stochastic kinetic description of an autocatalytic system. *Computers & Chemical Engineering* **125,** 587–593 (June 2019).

110. Einstein, A. Über die von der molekularkinetischen Theorie der Wärme geforderte Bewegung von in ruhenden Flüssigkeiten suspendierten Teilchen. *Annalen der Physik* **322,** 549–560 (1905).

111. Leontovich, M. Basic equations of the kinetic gas theory from the point of view of the theory of random processes. *Zhurnal Teoret. Ehksper. Fiziki.* 211–231 (1935).

112. Delbrück, M. Statistical Fluctuations in Autocatalytic Reactions. *The Journal of Chemical Physics* **8,** 120–124 (Jan. 1940).

113. Kramers, H. Brownian motion in a field of force and the diffusion model of chemical reactions. *Physica* **7,** 284–304 (Apr. 1940).

114. Rényi, A. Kémiai reakciók tárgyalása a sztochasztikus folyamatok elmélete segítségével(in Hungarian). (Treating chemical reactions using the theory of stochastic process.) *MTA AlkMat Int Közl.* 2:83–101 (1953).

115. Blomberg, C. Fluctuations for good and bad: The role of noise in living systems. *Physics of Life Reviews* **3,** 133–161 (Sept. 2006).

116. Tóth, J., Nagy, A. L. & Papp, D. *Reaction Kinetics: Exercises, Programs and Theorems* (Springer New York, 2018).

117. Érdi, P. & Lente, G. *Stochastic Chemical Kinetics* (Springer New York, 2014).

118. Horn, F. & Jackson, R. General mass action kinetics. *Archive for Rational Mechanics and Analysis* **47,** 81–116 (Jan. 1972).

119. Espenson, J. *Chemical Kinetics and Reaction Mechanisms* (McGraw-Hill, 1995).

120. Lente, G. *Deterministic Kinetics in Chemistry and Systems Biology* (Springer International Publishing, 2015).

121. Schmitz, G. & Lente, G. Fundamental concepts in chemical kinetics. *ChemTexts* **6,** . (Nov. 2019).

122. Kurtz, T. G. The Relationship between Stochastic and Deterministic Models for Chemical Reactions. *The Journal of Chemical Physics* **57,** 2976–2978 (Oct. 1972).

123. Gillespie, D. T. Deterministic Limit of Stochastic Chemical Kinetics. *The Journal of Physical Chemistry B* **113,** 1640–1644 (Jan. 2009).

124. Blount, D. Comparison of Stochastic and Deterministic Models of a Linear Chemical Reaction with Diffusion. *The Annals of Porbability* **19,** 1440–1462 (Oct. 1991).

125. Gillespie, D. T. A general method for numerically simulating the stochastic time evolution of coupled chemical reactions. *Journal of Computational Physics* **22,** 403–434 (Dec. 1976).

126. Gillespie, D. T. Exact stochastic simulation of coupled chemical reactions. *The Journal of Physical Chemistry* **81,** 2340–2361 (Dec. 1977).

127. Gillespie, D. T., Hellander, A. & Petzold, L. R. Perspective: Stochastic algorithms for chemical kinetics. *The Journal of Chemical Physics* **138,** 170901 (May 2013).

128. Anderson, D. F. A modified next reaction method for simulating chemical systems with time dependent propensities and delays. *The Journal of Chemical Physics* **127,** 214107 (Dec. 2007).

129. Gillespie, D. T. Approximate accelerated stochastic simulation of chemically reacting systems. *The Journal of Chemical Physics* **115,** 1716–1733 (July 2001).

130. Anderson, D. F. Incorporating postleap checks in tau-leaping. *The Journal of Chemical Physics* **128** (Feb. 2008).

131. Chatterjee, A., Vlachos, D. G. & Katsoulakis, M. A. Binomial distribution based -leap accelerated stochastic simulation. *The Journal of Chemical Physics* **122** (Dec. 2004).

132. Auger, A., Chatelain, P. & Koumoutsakos, P. R-leaping: Accelerating the stochastic simulation algorithm by reaction leaps. *The Journal of Chemical Physics* **125,** 084103 (Aug. 2006).

133. Mjolsness, E., Orendorff, D., Chatelain, P. & Koumoutsakos, P. An exact accelerated stochastic simulation algorithm. *The Journal of Chemical Physics* **130,** 144110 (Apr. 2009).

134. Lipková, J., Arampatzis, G., Chatelain, P., Menze, B. & Koumoutsakos, P. S-Leaping: An Adaptive, Accelerated Stochastic Simulation Algorithm, Bridging τ -Leaping and R-Leaping. *Bulletin of Mathematical Biology* **81,** 3074–3096 (July 2018).

135. Schaefer, D. W. *et al. Origin of porosity in synthetic materials* in *AIP Conference Proceedings* (AIP, 1987).

136. Matsoukas, T. & Gulari, E. Monomer-addition growth with a slow initiation step: A growth model for silica particles from alkoxides. *Journal of Colloid and Interface Science* **132,** 13–21 (Oct. 1989).

137. Kang, K., Redner, S., Meakin, P. & Leyvraz, F. Long-time crossover phenomena in coagulation kinetics. *Physical Review A* **33,** 1171–1182 (Feb. 1986).

138. McCoy, B. J. A population balance framework for nucleation, growth, and aggregation. *Chemical Engineering Science* **57,** 2279–2285 (June 2002).

139. Martin, J. D. Particle Size Is a Primary Determinant for Sigmoidal Kinetics of Nanoparticle Formation: A "Disproof" of the Finke–Watzky (F-W) Nanoparticle Nucleation and Growth Mechanism. *Chemistry of Materials* **32,** 3651–3656 (Feb. 2020).

140. Finke, R. G., Watzky, M. A. & Whitehead, C. B. Response to " Particle Size Is a Primary Determinant for Sigmoidal Kinetics of Nanoparticle Formation: A " Disproof" of the Finke–Watzky (F-W) Nanoparticle Nucleation and Growth Mechanism". *Chemistry of Materials* **32,** 3657–3672 (Apr. 2020).

141. Martin, J. D. Reply to "A Comparison of the Stochastic and Deterministic Approaches in a Nucleation–Growth Type Model of Nanoparticle Formation". *Chemistry of Materials* **33,** 5437–5445 (June 2021).

142. t5k.org. *Reginald McLean* `https://t5k.org/top20/page.php?id=54` (2023).

143. Lente, G., Bazsa, G. & Fábián, I. What is and what isn't a clock reaction? *New Journal of Chemistry* **31,** 1707–1707 (July 2007).

144. Horváth, A. K. & Nagypál, I. Classification of clock reactions. *ChemPhysChem* **16,** 588–594 (Feb. 2015).

145. Panzarasa, G., Osypova, A., Sicher, A., Bruinink, A. & Dufresne, E. R. Controlled formation of chitosan particles by a clock reaction. *Soft Matter* **14,** 6415–6418 (July 2018).

146. Du, G. & Espenson, J. H. Kinetics of the Reaction of Chromium(VI) with Tris(1,10-phenanthroline)iron(II) Ions in Acidic Solutions. Anion and Medium Effects: Perchlorate versus Triflate. *Inorganic Chemistry* **45,** 1053–1058 (Jan. 2006).

147. Kryven, I. Analytic results on the polymerisation random graph model. *Journal of Mathematical Chemistry* **56,** 140–157 (Jan. 2018).

Acknowledgement

I am deeply grateful to my supervisor, Prof. Gábor Lente, for his unwavering support and guidance throughout my Ph.D. journey. His patience, motivation, and vast knowledge have been invaluable assets to my research.

I extend my sincere appreciation to my colleagues at Politecnico di Torino for their professional assistance and support, which significantly enhanced the quality of my work.

I would also like to express my heartfelt thanks to my family and friends for their relentless support and encouragement during the writing of this thesis.

The research was funded by project no. RRF-2.3.1-21-2022-00009, titled National Laboratory for Renewable Energy, which has been implemented with the support provided by the Recovery and Resilience Facility of the European Union within the framework of Programme Széchenyi Plan Plus.

The work was also supported by the ÚNKP-23-4-I New National Excellence Program of the Ministry for Culture and Innovation from the source of the National Research, Development and Innovation Fund.

Proofs and derivations

Derivation of Equation 4.5

First, the dimensionless time has to be differentiated in the following way:

$$\frac{\mathrm{d}\tau}{\mathrm{d}t} = k_\mathrm{g}[\mathrm{M}]_0 \tag{1}$$

Then, the differential equations of Equation 4.2 are divided by $(k_\mathrm{g}[\mathrm{M}]_0^2)$:

$$\begin{aligned}
\frac{\mathrm{d}[\mathrm{M}]}{k_\mathrm{g}[\mathrm{M}]_0^2\mathrm{d}t} &= \frac{nk_\mathrm{M}[\mathrm{M}]^n}{k_\mathrm{g}[\mathrm{M}]_0^2} - \sum_{j=n}^{\infty} K(j)\frac{k_\mathrm{g}[\mathrm{M}][\mathrm{C}_i]}{k_\mathrm{g}[\mathrm{M}]_0^2} \\
\frac{\mathrm{d}[\mathrm{C}_n]}{k_\mathrm{g}[\mathrm{M}]_0^2\mathrm{d}t} &= \frac{k_\mathrm{M}[\mathrm{M}]^n}{k_\mathrm{g}[\mathrm{M}]_0^2} - K(n)\frac{k_\mathrm{g}[\mathrm{M}][\mathrm{C}_n]}{k_\mathrm{g}[\mathrm{M}]_0^2} \\
\frac{\mathrm{d}[\mathrm{C}_i]}{k_\mathrm{g}[\mathrm{M}]_0^2\mathrm{d}t} &= K(i-1)\frac{k_\mathrm{g}[\mathrm{M}][\mathrm{C}_{i-1}]}{k_\mathrm{g}[\mathrm{M}]_0^2} - K(i)\frac{k_\mathrm{g}[\mathrm{M}][\mathrm{C}_i]}{k_\mathrm{g}[\mathrm{M}]_0^2} \qquad i > n
\end{aligned} \tag{2}$$

With some simplification:

$$\begin{aligned}
\frac{\mathrm{d}\left(\frac{[\mathrm{M}]}{[\mathrm{M}]_0}\right)}{k_\mathrm{g}[\mathrm{M}]_0\mathrm{d}t} &= -n\frac{k_\mathrm{M}[\mathrm{M}]_0^{n-2}}{k_\mathrm{g}}\left(\frac{[\mathrm{M}]}{[\mathrm{M}]_0}\right)^n - \sum_{j=n}^{\infty} K(j)\frac{[\mathrm{M}]}{[\mathrm{M}]}\frac{[\mathrm{C}_i]}{[\mathrm{M}]} \\
\frac{\mathrm{d}\left(\frac{[\mathrm{C}_n]}{[\mathrm{C}_0]}\right)}{k_\mathrm{g}[\mathrm{M}]_0\mathrm{d}t} &= \frac{k_\mathrm{M}[\mathrm{M}]_0^{n-2}}{k_\mathrm{g}}\left(\frac{[\mathrm{M}]}{[\mathrm{M}]_0}\right)^n - K(n)\frac{[\mathrm{M}]}{[\mathrm{M}]}\frac{[\mathrm{C}_n]}{[\mathrm{M}]} \\
\frac{\mathrm{d}\left(\frac{[\mathrm{C}_i]}{[\mathrm{M}_0]}\right)}{k_\mathrm{g}[\mathrm{M}]_0\mathrm{d}t} &= K(i-1)\frac{[\mathrm{M}]}{[\mathrm{M}]}\frac{[\mathrm{C}_{i-1}]}{[\mathrm{M}]} - K(i)\frac{[\mathrm{M}]}{[\mathrm{M}]}\frac{[\mathrm{C}_i]}{[\mathrm{M}]} \qquad i > n
\end{aligned} \tag{3}$$

From these equations, the dimensionless quantities can be recognized.

Derivation of Equation 4.16

The time derivative can be obtained from the definition:

$$\frac{\mathrm{d}\mu_0}{\mathrm{d}\tau} = \sum_{i=n+1}^{\infty} \frac{\mathrm{d}c_i}{\mathrm{d}\tau} \tag{4}$$

All parts describing the time dependence of the nanoparticle concentration (c_i) in Equation 4.5 need to be summed:

$$\frac{\mathrm{d}c_n}{\mathrm{d}\tau} + \sum_{i=n+1}^{\infty} \frac{\mathrm{d}c_i}{\mathrm{d}\tau} = \alpha m^n - K(n)mc_n + \sum_{i=n+1}^{\infty} K(i-1)mc_{i-1} - \sum_{i=n+1}^{\infty} K(i)mc_i \tag{5}$$

After rearranging the indexes, the following form can be given:

$$\sum_{i=n}^{\infty} \frac{\mathrm{d}c_i}{\mathrm{d}\tau} = \alpha m^n + \sum_{i=n}^{\infty} K(i)mc_i - \sum_{i=n}^{\infty} K(i)mc_i \tag{6}$$

Dropping the last two parts of the right-hand side, the final form remains:

$$\sum_{i=n}^{\infty} \frac{\mathrm{d}c_i}{\mathrm{d}\tau} = \alpha m^n \tag{7}$$

Derivation of Equation 5.4

For $n = 1$, the differential equation changes:

$$\frac{\mathrm{d}m}{\mathrm{d}\mu_0} = -1 - \frac{\mu_0}{\alpha} \tag{8}$$

Since the m does not appear on the right-hand side, applying a simple integration leads to the solution:

$$m = -\frac{1}{2}\alpha {\mu_0}^2 - \mu_0 + C \tag{9}$$

The C represents the integration constant of which value can found by the initial conditons.

Derivation of Equation 5.5

The limiting value of the zeroth moment can be determined when all the monomer units are consumed ($m = 0$):

$$0 = -\frac{1}{2\alpha}{\mu_{0,\infty}}^2 - \mu_{0,\infty} + 1 \tag{10}$$

The solution of this simple equation can be found easily by the well-known quadratic equation:

$$\mu_{0,\infty} = \frac{1 \pm \sqrt{1 + 4\frac{1}{2\alpha}}}{-\frac{2}{2\alpha}} \tag{11}$$

Algebraic transformations and choosing the positive root gives the solution of Equation 5.5.

Proof of Equation 5.7

The equation is proved here by substituting the solution into the Equation5.6.
As a start, it is shown that the initial condition ($\mu_0 = 0$ when $\tau = 0$) is satisfied:

$$\begin{aligned}\mu_0(\tau=0) &= -\alpha + \sqrt{\alpha(2+\alpha)}\mathrm{th}\left(\mathrm{arth}\left(\sqrt{\frac{\alpha}{2+\alpha}}\right)\right) \\ &= \alpha + \sqrt{\alpha(2+\alpha)}\sqrt{\frac{\alpha}{2+\alpha}} = -\alpha + \sqrt{\alpha^2} = 0\end{aligned} \tag{12}$$

It is proven that it is satisfied.
The derivative of the tangent hyperbolic function is exactly the square of the secant hyperbolic secant function, which can be also interpreted as the square of the reciprocal of the hyperbolic cosine function:

$$\frac{\mathrm{dthz}}{\mathrm{dz}} = \mathrm{sech}^2\mathrm{z} = \frac{1}{\cosh^2\mathrm{z}} = \frac{4}{\left(\mathrm{e}^{\mathrm{z}}+\mathrm{e}^{-\mathrm{z}}\right)^2} \tag{13}$$

The derivative of the zeroth moment with respect to the dimensionless time can be given as:

$$\frac{\mathrm{d}\mu_0}{\mathrm{d}\tau} = \frac{\alpha(2+\alpha)}{2}\mathrm{sech}^2\left(\frac{\tau\sqrt{\alpha(2+\alpha)}}{2} + \mathrm{arth}\ \left(\sqrt{\frac{\alpha}{2+\alpha}}\right)\right) \tag{14}$$

Moreover, the hyperbolic secant function and the hyperbolic tangent function are connected by the given way:

$$\mathrm{sech}^2\mathrm{z} + \mathrm{th}^2\mathrm{z} - 1 = 0 \tag{15}$$

This can be tested by substituting the definitions:

$$\begin{aligned}&\frac{4}{\left(\mathrm{e}^{\mathrm{z}}+\mathrm{e}^{-\mathrm{z}}\right)^2} + \frac{\left(\mathrm{e}^{\mathrm{z}}-\mathrm{e}^{-\mathrm{z}}\right)^2}{\left(\mathrm{e}^{\mathrm{z}}+\mathrm{e}^{-\mathrm{z}}\right)^2} - 1 = \frac{4+\mathrm{e}^{2\mathrm{z}}-2+\mathrm{e}^{-2\mathrm{z}}}{\left(\mathrm{e}^{\mathrm{z}}+\mathrm{e}^{-\mathrm{z}}\right)^2} - 1 \\ &= \frac{\mathrm{e}^{2\mathrm{z}}+2+\mathrm{e}^{-2\mathrm{z}}}{\left(\mathrm{e}^{\mathrm{z}}+\mathrm{e}^{-\mathrm{z}}\right)^2} - 1 = \frac{\left(\mathrm{e}^{\mathrm{z}}+\mathrm{e}^{-\mathrm{z}}\right)^2}{\left(\mathrm{e}^{\mathrm{z}}+\mathrm{e}^{-\mathrm{z}}\right)^2} - 1 = 0\end{aligned} \tag{16}$$

Then the right-hand side of Equation 5.6 turns out to be:

$$
\begin{aligned}
&-\frac{{\mu_0}^2}{2}-\alpha\mu_0+\alpha \\
&=-\frac{1}{2}\left(-\alpha+\sqrt{\alpha\,(2+\alpha)}\mathrm{th}\left(\frac{\tau\sqrt{\alpha\,(2+\alpha)}}{2}+\mathrm{arth}\,\left(\sqrt{\frac{\alpha}{2+\alpha}}\right)\right)\right)^2 \\
&-\alpha\left(-\alpha+\sqrt{\alpha\,(2+\alpha)}\mathrm{th}\left(\frac{\tau\sqrt{\alpha\,(2+\alpha)}}{2}+\mathrm{arth}\,\left(\sqrt{\frac{\alpha}{2+\alpha}}\right)\right)\right)+\alpha \\
&=-\frac{1}{2}\alpha^2+\alpha\sqrt{\alpha\,(2+\alpha)}\mathrm{th}\left(\frac{\tau\sqrt{\alpha\,(2+\alpha)}}{2}+\mathrm{arth}\,\left(\sqrt{\frac{\alpha}{2+\alpha}}\right)\right) \\
&-\frac{\alpha\,(2+\alpha)}{2}\mathrm{th}^2\left(\frac{\tau\sqrt{\alpha\,(2+\alpha)}}{2}+\mathrm{arth}\,\left(\sqrt{\frac{\alpha}{2+\alpha}}\right)\right) \\
&+\alpha^2-\alpha\sqrt{\alpha\,(2+\alpha)}\mathrm{th}\left(\frac{\tau\sqrt{\alpha\,(2+\alpha)}}{2}+\mathrm{arth}\,\left(\sqrt{\frac{\alpha}{2+\alpha}}\right)\right)+\alpha \\
&=\frac{1}{2}\alpha^2+\alpha-\frac{\alpha\,(2+\alpha)}{2}\mathrm{th}^2\left(\frac{\tau\sqrt{\alpha\,(2+\alpha)}}{2}+\mathrm{arth}\,\left(\sqrt{\frac{\alpha}{2+\alpha}}\right)\right)
\end{aligned}
\tag{17}
$$

Consequently, this given formula holds:

$$
\mathrm{th}^2\left(\frac{\tau\sqrt{\alpha\,(2+\alpha)}}{2}+\mathrm{arth}\,\left(\sqrt{\frac{\alpha}{2+\alpha}}\right)\right)=1-\mathrm{sech}^2\left(\frac{\tau\sqrt{\alpha\,(2+\alpha)}}{2}+\mathrm{arth}\,\left(\sqrt{\frac{\alpha}{2+\alpha}}\right)\right) \tag{18}
$$

The substitution of the previous equation into the Equation 17 leads to this:

$$
\begin{aligned}
&-\frac{{\mu_0}^2}{2}\frac{\alpha\,(2+\alpha)}{2}-\alpha\mu_0+\alpha \\
&=\frac{1}{2}\alpha^2+\alpha-\frac{\alpha\,(2+\alpha)}{2}+\frac{\alpha\,(2+\alpha)}{2}\mathrm{sech}^2\left(\frac{\tau\sqrt{\alpha\,(2+\alpha)}}{2}+\mathrm{arth}\,\left(\sqrt{\frac{\alpha}{2+\alpha}}\right)\right) \\
&=\frac{\alpha\,(2+\alpha)}{2}\mathrm{sech}^2\left(\frac{\tau\sqrt{\alpha\,(2+\alpha)}}{2}+\mathrm{arth}\,\left(\sqrt{\frac{\alpha}{2+\alpha}}\right)\right)
\end{aligned}
\tag{19}
$$

The last line of the equation is identical to the final part of Equation 14. So Equation 5.7 gives a unique solution of the ordinary differential equation seen in Equation 5.6. Therefore, it is definitely the only solution.

Proof of Equation 5.9

Applying the well-known procedure for the linear, first-order ordinary differential equations can give the solution. Again, it is also less time-consuming to prove that the equation really determines the soluton. For the case $i = 1$:

$$c_1 = \alpha - \alpha\ \mathrm{e}^{-\mu_0/\alpha} \tag{20}$$

The initial condition can be tested by substituting $\mu_0 = 0$ (which gives $c_i = 0$), and it is satisfied. Moreover:

$$\frac{\mathrm{d}c_1}{\mathrm{d}\mu_0} = \mathrm{e}^{-\mu_0/\alpha} \tag{21}$$

$$1 - \frac{c_1}{\alpha} = 1 - \left(1 - \mathrm{e}^{-\mu_0/\alpha}\right) = \mathrm{e}^{-\mu_0/\alpha} \tag{22}$$

The last part of the previous two equations seem to be identical, so this function can be the actual solution of the ordinary differential equation. For the case $i > 1$:

$$c_i\,(0) = \alpha - \alpha\ \mathrm{e}^{-0/\alpha}\sum_{j=0}^{i-1}\frac{1}{j!}\left(\frac{0}{\alpha}\right)^j = \alpha - \alpha\ \mathrm{e}^{0}\frac{1}{0!}\left(\frac{0}{\alpha}\right)^0 = 0 \tag{23}$$

In this case, the initial condition is satisfied, as well. Furthermore:

$$\begin{aligned}\frac{\mathrm{d}c_i}{\mathrm{d}\mu_0} &= \mathrm{e}^{-\mu_0/\alpha}\sum_{j=0}^{i-1}\frac{1}{j!}\left(\frac{\mu_0}{\alpha}\right)^j - \alpha\ \mathrm{e}^{-\mu_0/\alpha}\sum_{j=1}^{i-1}\frac{1}{\alpha\,(j-1)!}\left(\frac{\mu_0}{\alpha}\right)^{j-1} \\ &= \mathrm{e}^{-\mu_0/\alpha}\sum_{j=0}^{i-1}\frac{1}{j!}\left(\frac{\mu_0}{\alpha}\right)^j - \mathrm{e}^{-\mu_0/\alpha}\sum_{j=0}^{i-2}\frac{1}{(j-1)!}\left(\frac{\mu_0}{\alpha}\right)^j \\ &= \frac{\mathrm{e}^{-\mu_0/\alpha}}{(i-1)!}\left(\frac{\mu_0}{\alpha}\right)^{i-1}\end{aligned} \tag{24}$$

$$\frac{c_{i-1}}{\alpha} - \frac{c_i}{\alpha} = 1 - \mathrm{e}^{-\mu_0/\alpha}\sum_{j=0}^{i-2}\frac{1}{j!}\left(\frac{\mu_0}{\alpha}\right)^j - 1 + \mathrm{e}^{-\mu_0/\alpha}\sum_{j=0}^{i-1}\frac{1}{j!}\left(\frac{\mu_0}{\alpha}\right)^j = \frac{\mathrm{e}^{-\mu_0/\alpha}}{(i-1)!}\left(\frac{\mu_0}{\alpha}\right)^{i-1} \tag{25}$$

Aagin, the last parts of the previous two equations are identical, so Equation 5.9 is indeed the solution.

Proof of Equation 5.14

First, the initial conditions are substituted into the Equation 5.14 directly:

$$2\sqrt{\frac{\alpha}{4-\alpha}}\arctan(\infty) = \pi\sqrt{\frac{\alpha}{4-\alpha}} + \ln(1) \tag{26}$$

As the value of the tangent function approaches infinity at $\pi/2$, the equation holds, and so the $\arctan(\infty)$ can be $\pi/2$, while $\ln(1) = 0$. This derivation also proves that Equation5.14 cannot be applied at $m = 0$ directly.

Both side of Equation 5.14 are differentiated with respect to μ_0:

$$\begin{aligned} &2\sqrt{\frac{\alpha}{4-\alpha}}\frac{1}{1+\left(\sqrt{\frac{\alpha}{4-\alpha}}\frac{\mu_0+2m}{\mu_0}\right)^2}\sqrt{\frac{\alpha}{4-\alpha}}\left(-\frac{2m}{{\mu_0}^2}+\frac{2}{\mu_0}\frac{\mathrm{d}m}{\mathrm{d}\mu_0}\right) \\ &= \frac{1}{\frac{\mu_0^2}{\alpha}+m\mu_0+m^2}\left(\frac{2\mu_0}{\alpha}+m+\mu_0\frac{\mathrm{d}m}{\mathrm{d}\mu_0}+2m\frac{\mathrm{d}m}{\mathrm{d}\mu_0}\right) \end{aligned} \tag{27}$$

The transformation of this equation is taken step by step:

$$\begin{aligned} &\frac{2\alpha}{4-\alpha}\frac{1}{1+\frac{\alpha}{4-\alpha}\frac{(\mu_0+2m)^2}{{\mu_0}^2}}\left(\frac{2}{\mu_0}\frac{\mathrm{d}m}{d\mu_0}-\frac{2m}{{\mu_0}^2}\right) \\ &= \frac{1}{\frac{\mu_0^2}{\alpha}+m\mu_0+m^2}\left(\frac{2\mu_0}{\alpha}+m+\mu_0\frac{dm}{\mathrm{d}\mu_0}+2m\frac{\mathrm{d}m}{\mathrm{d}\mu_0}\right) \end{aligned} \tag{28}$$

$$\begin{aligned} &\frac{4}{\frac{4}{\alpha}{\mu_0}^2-{\mu_0}^2+(\mu_0+2m)^2}\left(\mu_0\frac{\mathrm{d}m}{\mathrm{d}\mu_0}-m\right) \\ &= \frac{1}{\frac{\mu_0^2}{\alpha}+m\mu_0+m^2}\left(\frac{2\mu_0}{\alpha}+m+\mu_0\frac{\mathrm{d}m}{\mathrm{d}\mu_0}+2m\frac{\mathrm{d}m}{\mathrm{d}\mu_0}\right) \end{aligned} \tag{29}$$

$$\begin{aligned} &\frac{1}{\frac{{\mu_0}^2}{\alpha}+m\mu_0+m^2}\left(\mu_0\frac{\mathrm{d}m}{\mathrm{d}\mu_0}-m\right) \\ &= \frac{1}{\frac{\mu_0^2}{\alpha}+m\mu_0+m^2}\left(\frac{2\mu_0}{\alpha}+m+\mu_0\frac{\mathrm{d}m}{\mathrm{d}\mu_0}+2m\frac{\mathrm{d}m}{\mathrm{d}\mu_0}\right) \end{aligned} \tag{30}$$

$$\mu_0\frac{\mathrm{d}m}{\mathrm{d}\mu_0}-m = \frac{2\mu_0}{\alpha}+m+\mu_0\frac{\mathrm{d}m}{\mathrm{d}\mu_0}+2m\frac{\mathrm{d}m}{\mathrm{d}\mu_0} \tag{31}$$

$$\frac{\mathrm{d}m}{\mathrm{d}\mu_0} = -\frac{\mu_0}{\alpha m}-1 \tag{32}$$

Since the last equation is the same as Equation 5.13, the Equation 5.14 gives the solution of Equation 5.13 indeed.

Proof of Equation 5.15

The substitution of the final value of $m(=0)$ into the Equation 5.14 gives:

$$2\sqrt{\frac{\alpha}{4-\alpha}}\arctan\left(\sqrt{\frac{\alpha}{4-\alpha}}\right) = \pi\sqrt{\frac{\alpha}{4-\alpha}} + \ln\left(\frac{\mu_{0,\infty}^2}{\alpha}\right) \tag{33}$$

The equation can be transformed in two steps:

$$\frac{\mu_{0,\infty}^2}{\alpha} = \mathrm{e}^{2\sqrt{\frac{\alpha}{4-\alpha}}\arctan\left(\sqrt{\frac{\alpha}{4-\alpha}}\right)-\pi\sqrt{\frac{\alpha}{4-\alpha}}} \tag{34}$$

$$\mu_{0,\infty} = \sqrt{\alpha}\mathrm{e}^{\sqrt{\frac{\alpha}{4-\alpha}}\arctan\left(\sqrt{\frac{\alpha}{4-\alpha}}\right)-\frac{\pi}{2}\sqrt{\frac{\alpha}{4-\alpha}}} \tag{35}$$

It is evident that the last equation is indeed equivalent to Equation 5.15.

Proof of Equation 5.24

The following equation for the mass kernel, $n = 1$, is a separable ordinary differential equation.

$$\frac{\mathrm{d}m}{\mathrm{d}\tau} = -\alpha m - m(1-m) = m^2 - (\alpha+1)m \tag{36}$$

By setting $\tau = 0$, the initial conditions can be tested:

$$m = \frac{\alpha+1}{\alpha \mathrm{e}^0 + 1} = \frac{\alpha+1}{\alpha+1} = 1 \tag{37}$$

So these are all satisfied. Then, the Equation 5.27 needs to be differentiated:

$$\frac{\mathrm{d}m}{\mathrm{d}\tau} = -\frac{(\alpha+1)^2 \alpha \mathrm{e}^{(\alpha+1)\tau}}{\left(\alpha \mathrm{e}^{(\alpha+1)\tau}+1\right)^2} \tag{38}$$

After that, the right-hand side of the first equation can be calculated:

$$\begin{aligned} m^2 - (\alpha+1)m &= \frac{(\alpha+1)^2}{\left(\alpha \mathrm{e}^{(\alpha+1)\tau}+1\right)^2} - (\alpha+1)\frac{\alpha+1}{\alpha \mathrm{e}^{(\alpha+1)\tau}+1} \\ &= \frac{(\alpha+1)^2}{\left(\alpha \mathrm{e}^{(\alpha+1)\tau}+1\right)^2} - \frac{(\alpha+1)^2\left(\alpha \mathrm{e}^{(\alpha+1)\tau}+1\right)}{\left(\alpha \mathrm{e}^{(\alpha+1)\tau}+1\right)^2} \\ &= -\frac{(\alpha+1)^2 \alpha \mathrm{e}^{(\alpha+1)\tau}}{\left(\alpha \mathrm{e}^{(\alpha+1)\tau}+1\right)^2} \end{aligned} \tag{39}$$

As the last two equations are identical, Equation 5.27 is the solution indeed.

Proof of Equation 5.27

First, the initial conditions ($m = 1 \quad \text{and} \quad c_i = 0$) are checked:

$$c_1 = \frac{\alpha - \alpha}{1 + \alpha - 1} = 0 \tag{40}$$

Then, the Equation 5.27 can be differentiated:

$$\begin{aligned} \frac{\mathrm{d}c_1}{\mathrm{d}\tau} &= \frac{-\alpha}{1 + \alpha - m} + \frac{\alpha - \alpha m}{(1 + \alpha - m)^2} \\ &= \frac{\alpha - \alpha m - \alpha - \alpha^2 + \alpha m}{(1 + \alpha - m)^2} = \frac{-\alpha^2}{(1 + \alpha - m)^2} \end{aligned} \tag{41}$$

The right-hand side of the equation is given:

$$\frac{c_1 - \alpha}{\alpha + (1 - m)} = \frac{\frac{\alpha - \alpha m}{1 + \alpha - m}}{\alpha + 1 - m} = \frac{\frac{\alpha - \alpha m - \alpha - \alpha^2 + \alpha m}{1 + \alpha - m}}{\alpha + 1 - m} = -\frac{\alpha^2}{(\alpha + 1 - m)^2} \tag{42}$$

The last two equations are considered to be identical, so the solution of Equation 5.27 is indeed the solution of Equation 5.25 for the mass kernel ($n = 1$).

Proof of Equation 5.30

The initial condition ($m = 1$) simplifies the enumerator of the original differential equation, so its differentiation gives the following solution:

$$\begin{aligned}\frac{\mathrm{d}c_i}{\mathrm{d}m} &= \frac{\alpha}{i} i \left(\frac{1-m}{\alpha+1-m}\right)^{i-1} \left(-\frac{1}{\alpha+1-m} + \frac{1-m}{(\alpha+1-m)^2}\right) \\ &= -\alpha \left(\frac{1-m}{\alpha+1-m}\right)^{i-1} \frac{1}{\alpha+1-m} + \alpha \left(\frac{1-m}{\alpha+1-m}\right)^{i} \frac{1}{\alpha+1-m} \\ &= -\frac{(i-1)c_{i-1}}{\alpha+1-m} + \frac{ic_i}{\alpha+1-m}\end{aligned} \tag{43}$$

The last line is in agreement with Equation 5.30, so the solution of Equation 5.28.

Proof of Equation 5.34

First, the initial conditions ($\mu_0 = 0 \quad \text{when} \quad \tau = 0$) are substituted:

$$\mu_0 = \alpha(\alpha+1)0 + \alpha \ln\left(\frac{1+\alpha}{1+\alpha \mathrm{e}^0}\right) = \alpha \ln(1) = 0 \tag{44}$$

The differentiation of Equation 5.32 leads to this form:

$$\begin{aligned} \frac{\mathrm{d}\mu_0}{\mathrm{d}\tau} &= \alpha(\alpha+1) + \alpha \frac{1+\alpha \mathrm{e}^{(\alpha+1)\tau}}{1+\alpha} \frac{-(1+\alpha)}{\left(1+\alpha \mathrm{e}^{(\alpha+1)\tau}\right)^2} \alpha(\alpha+1)\mathrm{e}^{(\alpha+1)\tau} \\ &= \alpha(\alpha+1)\left[1 - \frac{\alpha \mathrm{e}^{(\alpha+1)\tau}}{1+\alpha \mathrm{e}^{(\alpha+1)\tau}}\right] = \alpha \frac{(\alpha+1)}{1+\alpha \mathrm{e}^{(\alpha+1)\tau}} \end{aligned} . \tag{45}$$

If the solution for m is taken, it can be obvious that the previous equation is identical to Equation 4.16.

For the second part, the initial condition can be tested more easily ($\mu_0 = 0$ when $m = 1$):

$$\mu_0 = \alpha \ln\left(1 + \frac{1}{\alpha} - \frac{1}{\alpha}\right) = \alpha \ln(1) = 0 \tag{46}$$

The rest of the proof is given by differentiation respect to m:

$$\frac{\mathrm{d}\mu_0}{\mathrm{d}m} = \alpha \frac{1}{1+\frac{1}{\alpha} - \frac{m}{\alpha}} \frac{-1}{\alpha} = -\frac{\alpha}{1+\alpha-m} \tag{47}$$

The equation is identical to Equation 5.32 when $n = 1$.

Another possibility is a cross-check by using Equation 5.24:

$$\begin{aligned} \mu_0 &= \alpha \ln\left(1 + \frac{1}{\alpha} - \frac{m}{\alpha}\right) = \alpha \ln\left(1 + \frac{1}{\alpha} - \frac{\frac{\alpha+1}{\alpha \mathrm{e}^{(\alpha+1)\tau}+1}}{\alpha}\right) \\ &= \alpha \ln\left(\frac{(1+\alpha)(\alpha \mathrm{e}^{(\alpha+1)\tau}+1)}{\alpha(\alpha \mathrm{e}^{(\alpha+1)\tau}+1)} - \frac{\alpha+1}{\alpha(\alpha \mathrm{e}^{(\alpha+1)\tau}+1)}\right) \\ &= \alpha \ln\left(\mathrm{e}^{(\alpha+1)\tau} \frac{1+\alpha}{\alpha \mathrm{e}^{(\alpha+1)\tau}+1}\right) = \alpha \ln\left(\mathrm{e}^{(\alpha+1)\tau}\right) + \alpha \ln\left(\frac{1+\alpha}{\alpha \mathrm{e}^{(\alpha+1)\tau}+1}\right) \\ &\alpha(\alpha+1)\tau + \alpha \ln\left(\frac{1+\alpha}{1+\alpha \mathrm{e}^{(\alpha+1)\tau}}\right) \end{aligned} \tag{48}$$

Proof of Equation 5.40

First, it is proved that the inital condition is satisifed indeed:

$$m(\tau = 0) = \frac{1}{2\alpha \mathrm{e}^0 + 1 - 2\alpha} = \frac{1}{2\alpha + 1 - 2\alpha} = 1 \tag{49}$$

Then the derivative of m is determined and transformed step by step until the right-hand side of Equation 5.40 is reached:

$$\begin{aligned} \frac{\mathrm{d}m}{\mathrm{d}\tau} &= \frac{\mathrm{d}}{\mathrm{d}\tau}\left(\frac{1}{2\alpha \mathrm{e}^\tau + 1 - 2\alpha}\right) = \frac{2\alpha \mathrm{e}^\tau}{(2\alpha \mathrm{e}^\tau + 1 - 2\alpha)^2} \\ &= \frac{1 - 2\alpha - 2\alpha \mathrm{e}^\tau - 1 + 2\alpha}{(2\alpha \mathrm{e}^\tau + 1 - 2\alpha)^2} = (1 - 2\alpha)\left(\frac{1}{2\alpha \mathrm{e}^\tau + 1 - 2\alpha}\right)^2 - \frac{1}{2\alpha \mathrm{e}^\tau + 1 - 2\alpha} \\ &= (1 - 2\alpha)m^2 - m \end{aligned} \tag{50}$$

Derivation of Equation 5.42

The thought is that the following nonhomogeneous linear differential equation can be solved when c_{i-1} is known:

$$\frac{\mathrm{d}c_i}{\mathrm{d}m} = \frac{i-1}{(1-2\alpha)m-1}c_{i-1} - \frac{i}{(1-2\alpha)m-1}c_i \tag{51}$$

First, the nonhomogeneous term is cancelled to solve the differential equation (and γ_i denotes this function):

$$\frac{\mathrm{d}\gamma_i}{\mathrm{d}m} = -\frac{i}{(1-2\alpha)m-2}\gamma_i \tag{52}$$

The variables are separated as follows:

$$\frac{1}{\gamma_i}\frac{\mathrm{d}\gamma_i}{\mathrm{d}m} = \frac{i}{1-(1-2\alpha)m} \tag{53}$$

Then integrating both sides gives:

$$\ln\gamma_i = \frac{i}{\alpha-1}\ln\left[1-(1-2\alpha)m\right] \tag{54}$$

After a rearrangement, an explicit formula for γ_i can be found:

$$\gamma_i = \left[1-(1-2\alpha)m\right]^{i/(2\alpha-1)} \tag{55}$$

Then, the solution of Equation 51 is to look for in the following way:

$$c_i = f(m)\gamma_i \tag{56}$$

Substituting this into Equation 51:

$$\frac{\mathrm{d}f(m)}{\mathrm{d}m}\gamma_i + f(m)\frac{\mathrm{d}f\gamma_i}{\mathrm{d}m} = \frac{i-1}{(1-2\alpha)m-1}c_{i-1} - \frac{i}{(1-2\alpha)m-1}f(m)\gamma_i \tag{57}$$

The next step is to differentiate the γ_i function:

$$\begin{aligned}&\frac{\mathrm{d}f(m)}{\mathrm{d}m}\left[1-(1-2\alpha)m\right]^{i/(2\alpha-1)} - \frac{i}{(1-2\alpha)m-1}\gamma_i f(m)\\ &\frac{i-1}{(1-2\alpha)m-1}c_{i-1} - \frac{i}{(1-2\alpha)m-1}f(m)\gamma_i\end{aligned} \tag{58}$$

Leavig the common terms on both sides determines the following formula:

$$\frac{\mathrm{d}f(m)}{\mathrm{d}m}\left[1-(1-2\alpha)m\right]^{i/(2\alpha-1)} = \frac{i-1}{(1-2\alpha)m-1}f(m)\gamma_i \tag{59}$$

This can be rearranged to get the derivative function ($f(m)$) explicitly:

$$\frac{\mathrm{d}f(m)}{\mathrm{d}m} = -(i-1)\left[1-(1-2\alpha)m\right]^{-i/(2\alpha-1)-1}c_{i-1} \tag{60}$$

So, simple integration gives $f(m)$, from which m can be calculated by substituing back to Equation 56:

$$\begin{aligned} c_i = C\left[1-(1-2\alpha)m\right]^{i/(2\alpha-1)} - \left[1-(1-2\alpha)m\right]^{i/(2\alpha-1)}(i-1) \\ \int\left[1-(1-2\alpha)m\right]^{-i/(2\alpha-1)-1}c_{i-1}\mathrm{d}m \end{aligned} \tag{61}$$

Proof of Equation 5.43

First, it is tested that the initial condition is satisifed:

$$\begin{aligned} c_2(m=1) &= -\frac{\alpha(1+2)}{4\alpha-6}\frac{3\alpha}{4\alpha-6}\left(\frac{1-1}{2\alpha}+1\right)^{2/(2\alpha-1)} \\ &= -\frac{3\alpha}{4\alpha-6}+\frac{3\alpha}{4\alpha-6}=0 \end{aligned} \tag{62}$$

Then the derivative of the function is determined and rearranged step by step until the right-hand side of Equation 5.43 is obtained:

$$\begin{aligned} &\frac{\mathrm{c}_2}{\mathrm{d}m} = -\frac{2\alpha}{4\alpha-6}+\frac{3\alpha}{4\alpha-6}\left(\frac{1-m}{2\alpha}+m\right)^{(2/2\alpha-1)-1}\left(1-\frac{1}{2\alpha}\right)\frac{2}{2\alpha-1} \\ &= -\frac{2\alpha}{4\alpha-6}+\frac{3}{4\alpha-6}\left(\frac{1-m}{2\alpha}+m\right)^{(2/2\alpha-1)-1} \\ &= \frac{(1-2\alpha)m-1}{(1-2\alpha)m-1}\left[-\frac{2\alpha}{4\alpha-6}+\frac{3}{4\alpha-6}\left(\frac{1-m}{2\alpha}+m\right)^{(2/2\alpha-1)-1}\right] \\ &\frac{-1}{(1-2\alpha)m-1}2\alpha\left(\frac{1-m}{2\alpha}+m\right)\left[-\frac{2\alpha}{4\alpha-6}+\frac{3}{4\alpha-6}\left(\frac{1-m}{2\alpha}+m\right)^{(2/2\alpha-1)-1}\right] \\ &= \frac{1}{(1-2\alpha)m-1}\left[-\frac{2\alpha(1-2\alpha)m-2\alpha}{4\alpha-6\alpha}-\frac{6\alpha}{4\alpha-6}\left(\frac{1-m}{2\alpha}+m\right)^{2/(2\alpha-1)}\right] \\ &= \frac{1}{(1-2\alpha)m-1}\left[\frac{4\alpha^2m+2\alpha-2\alpha m}{4\alpha-6}-\frac{6\alpha}{4\alpha-6}\left(\frac{1-m}{2\alpha}+m\right)^{2/(2\alpha-1)}\right] \\ &= \frac{1}{(1-2\alpha)m-1}\left[\frac{4\alpha^4m-6\alpha m}{4\alpha-6}+\frac{2\alpha+4\alpha m}{4\alpha-6}-\frac{6\alpha}{4\alpha-6}\left(\frac{1-m}{2\alpha}+m\right)^{2/(2\alpha-1)}\right] \\ &= \frac{1}{(1-2\alpha)m-1}[\alpha m-2c_2] = \frac{\alpha m-2c_2}{(1-2\alpha)m-1} \end{aligned} \tag{63}$$

Proof of Equation 5.44

First, it is tested that the initial condition is satisfied:

$$c_3 = -\frac{\alpha(-3+\alpha-3)}{3(\alpha-2)(2\alpha-3)} + \frac{3\alpha}{(2\alpha-3)}\left(\frac{1-1}{2\alpha}+1\right)^{2/(2\alpha-1)} - \frac{4\alpha}{3(\alpha-2)}\left(\frac{1-1}{2\alpha}+1\right)^{3/(2\alpha-1)} \tag{64}$$

Then the derivative of the function is determined and rearranged step by step until the right-hand side of Equation 5.44 is obtained:

$$\begin{aligned}
&\frac{\mathrm{d}c_3}{\mathrm{d}m} = \frac{\alpha}{(\alpha-2)(2\alpha-3)} + \frac{3\alpha}{2\alpha-3}\left(\frac{1-m}{2\alpha}+m\right)^{2/(2\alpha-1)-1}\frac{2}{2\alpha-1}\frac{2}{2\alpha-1}\left(1-\frac{1}{2\alpha}\right)\\
&-\frac{4\alpha}{3(\alpha-2)}\left(\frac{1-m}{2\alpha}+m\right)^{3/(2\alpha-1)-1}\frac{3}{2\alpha-1}\left(1-\frac{1}{2\alpha}\right)\\
&=\frac{\alpha}{(\alpha-2)(2\alpha-3)} + \frac{3}{2\alpha-3}\left(\frac{1-m}{2\alpha}+m\right)^{2/(2\alpha-1)-1}\\
&-\frac{2\alpha}{\alpha-2}\left(\frac{1-m}{2\alpha}+m\right)^{3/(2\alpha-1)-1}\\
&=\frac{(1-2\alpha)m-1}{(1-2\alpha)m-1}\\
&\left[\frac{\alpha}{(\alpha-2)(2\alpha-3)} + \frac{3}{2\alpha-3}\left(\frac{1-m}{2\alpha}+m\right)^{2/(2\alpha-1)-1} - \frac{2\alpha}{\alpha-2}\left(\frac{1-m}{2\alpha}+m\right)^{3/(2\alpha-1)-1}\right]\\
&=\frac{1}{(1-2\alpha)m-1}\\
&\left[\frac{\alpha m-2\alpha^2 m-\alpha}{(\alpha-2)(2\alpha-3)} - \frac{6\alpha}{2\alpha-3}\left(\frac{1-m}{2\alpha}+m\right)^{2/(2\alpha-1)} + \frac{4\alpha}{\alpha-2}\left(\frac{1-m}{2\alpha}+m\right)^{3/(2\alpha-1)}\right]\\
&=\frac{1}{(1-2\alpha)m-1}\left[\frac{4\alpha m-2\alpha^2 m+2\alpha-\alpha^2}{(\alpha-2)(2\alpha-3)} + \frac{3\alpha}{2\alpha-3}\left(\frac{1-m}{2\alpha}+m\right)^{2/(2\alpha-1)}\right]\\
&+\frac{1}{(1-2\alpha)m-1}\\
&\left[3\frac{\alpha(-3+\alpha-3m)}{3(\alpha-2)(2\alpha-3)} - 3\frac{3\alpha}{2\alpha-3}\left(\frac{1-m}{2\alpha}+m\right)^{2/(2\alpha-1)} + 3\frac{4\alpha}{3(\alpha-2)}\left(\frac{1-m}{2\alpha}+m\right)^{3/(2\alpha-1)}\right]\\
&=\frac{1}{(1-2\alpha)m-1}\left[-2\alpha\frac{2m(\alpha-2)+\alpha-2}{(\alpha-2)(4\alpha-6)} + 2\frac{3\alpha}{4\alpha-6}\left(\frac{1-m}{2\alpha}+m\right)^{2/(2\alpha-1)} - 3c_3\right]\\
&=\frac{2c_2-3c_3}{(1-2\alpha)m-1}
\end{aligned} \tag{65}$$

Proof of Equation 5.45

First, it is tested that the initial condition is satisfied:

$$
\begin{aligned}
c_4\left(m=1\right) &= \frac{\alpha\left(-30+11\alpha-2\alpha^2\right)}{4\left(2\alpha-5\right)\left(2\alpha-3\right)\left(\alpha-2\right)} + \frac{9\alpha}{2\left(2\alpha-3\right)} - \frac{4\alpha}{\left(\alpha-2\right)} + \frac{15\alpha}{4\left(2\alpha-5\right)} \\
&= \alpha\frac{\left(-30+11\alpha-2\alpha^2\right)+18\left(2\alpha-5\right)\left(\alpha-2\right)-16\left(2\alpha-5\right)\left(2\alpha-3\right)+15\left(2\alpha-3\right)\left(\alpha-2\right)}{4\left(2\alpha-5\right)\left(2\alpha-3\right)\left(\alpha-2\right)} \\
&= \alpha\frac{\left(-30+11\alpha-2\alpha^2\right)+\left(180-162\alpha+36\alpha^2\right)+\left(-240+256\alpha-64\alpha^2\right)+\left(90-105\alpha+30\alpha^2\right)}{4\left(2\alpha-5\right)\left(2\alpha-3\right)\left(\alpha-2\right)} \\
&= \alpha\frac{\left(-2+36-64+30\right)\alpha^2+\left(11-162+256-105\right)\alpha+\left(-30+180-240+90\right)}{4\left(2\alpha-5\right)\left(2\alpha-3\right)\left(\alpha-2\right)} = 0
\end{aligned}
\tag{66}
$$

Then the derivative of the function is determined and rearranged step by step until the right-hand side of Equation 5.45 is obtained:

$$
\begin{aligned}
&\frac{\mathrm{d}c_4}{\mathrm{d}m} = \frac{-12\alpha}{4\left(2\alpha-5\right)\left(2\alpha-3\right)\left(\alpha-2\right)} + \frac{9\alpha}{2\left(2\alpha-3\right)}\left(\frac{1-m}{2\alpha}+m\right)^{2/(2\alpha-1)-1}\frac{2}{2\alpha-1}\left(-\frac{1}{2\alpha}+1\right) - \frac{4\alpha}{\left(\alpha-2\right)} \\
&\left(\frac{1-m}{2\alpha}+m\right)^{3/(2\alpha-1)-1}\frac{3}{2\alpha-1}\left(-\frac{1}{2\alpha}+1\right) + \frac{15\alpha}{4\left(2\alpha-5\right)}\left(\frac{1-m}{2\alpha}+m\right)^{4/(2\alpha-1)-1}\frac{4}{2\alpha-1}\left(-\frac{1}{2\alpha}+1\right) \\
&\frac{-12\alpha}{4\left(2\alpha-5\right)\left(2\alpha-3\right)\left(\alpha-2\right)} + \frac{9}{2\left(2\alpha-3\right)}\left(\frac{1-m}{2\alpha}+m\right)^{2/(2\alpha-1)-1} - \frac{6}{\left(\alpha-2\right)}\left(\frac{1-m}{2\alpha}+m\right)^{3/(2\alpha-1)-1} \\
&+ \frac{15}{2\left(2\alpha-5\right)}\left(\frac{1-m}{2\alpha}+m\right)^{4/(2\alpha-1)-1} \\
&\frac{\left(1-2\alpha\right)m-1}{\left(1-2\alpha\right)m-1}\left[\frac{-12\alpha}{4\left(2\alpha-5\right)\left(2\alpha-3\right)\left(\alpha-2\right)} + \frac{9}{2\left(2\alpha-3\right)}\left(\frac{1-m}{2\alpha}+m\right)^{2/(2\alpha-1)-1}\right] \\
&+ \frac{\left(1-2\alpha\right)m-1}{\left(1-2\alpha\right)m-1}\left[-\frac{6}{\left(\alpha-2\right)}\left(\frac{1-m}{2\alpha}+m\right)^{3/(2\alpha-1)-1} + \frac{15}{2\left(2\alpha-5\right)}\left(\frac{1-m}{2\alpha}+m\right)^{4/(2\alpha-1)-1}\right] \\
&= \frac{1}{\left(1-2\alpha\right)m-1}\left[\alpha\frac{-12m+24\alpha m+12}{4\left(2\alpha-5\right)\left(2\alpha-3\right)\left(\alpha-2\right)} - \frac{9\alpha}{\left(2\alpha-3\right)}\left(\frac{1-m}{2\alpha}+m\right)^{2/(2\alpha-1)}\right] \\
&+ \frac{1}{\left(1-2\alpha\right)m-1}\left[\frac{12\alpha}{\left(\alpha-2\right)}\left(\frac{1-m}{2\alpha}+m\right)^{3/(2\alpha-1)} - \frac{15\alpha}{\left(2\alpha-5\right)}\left(\frac{1-m}{2\alpha}+m\right)^{4/(2\alpha-1)}\right] \\
&= \frac{1}{\left(1-2\alpha\right)m-1}\left[\alpha\frac{72-44\alpha+8\alpha^2+48m}{4\left(2\alpha-5\right)\left(2\alpha-3\right)\left(\alpha-2\right)} - \alpha\frac{60-44\alpha+8\alpha^2+60m-24\alpha m}{4\left(2\alpha-5\right)\left(2\alpha-3\right)\left(\alpha-2\right)}\right] \\
&+ \frac{1}{\left(1-2\alpha\right)m-1}\left[\left(3\frac{3\alpha}{\left(2\alpha-3\right)} - 4\frac{9\alpha}{2\left(2\alpha-3\right)}\right)\left(\frac{1-m}{2\alpha}+m\right)^{2/(2\alpha-1)}\right]\frac{1}{\left(1-2\alpha\right)m-1} \\
&\left[\left(-3\frac{4\alpha}{3\left(\alpha-2\right)} + 4\frac{4\alpha}{\left(\alpha-2\right)}\right)\left(\frac{1-m}{2\alpha}+m\right)^{3/(2\alpha-1)} - 4\frac{15\alpha}{4\left(2\alpha-5\right)}\left(\frac{1-m}{2\alpha}+m\right)^{4/(2\alpha-1)}\right] \\
&\frac{1}{\left(1-2\alpha\right)m-1}\left[4\alpha\frac{18-11\alpha+2\alpha^2+12m}{4\left(2\alpha-5\right)\left(2\alpha-3\right)\left(\alpha-2\right)} - \alpha\frac{2\alpha^2-5\alpha-6\alpha+15-6\alpha m+15m}{\left(2\alpha-5\right)\left(2\alpha-3\right)\left(\alpha-2\right)}\right] + \\
&\frac{1}{\left(1-2\alpha\right)m-1}\left[\left(3\frac{3\alpha}{\left(2\alpha-3\right)} - 4\frac{9\alpha}{2\left(2\alpha-3\right)}\right)\left(\frac{1-m}{2\alpha}+m\right)^{2/(2\alpha-1)}\right] \\
&+ \frac{1}{\left(1-2\alpha\right)m-1}\left[\left(-3\frac{4\alpha}{3\left(\alpha-2\right)} + 4\frac{4\alpha}{\left(\alpha-2\right)}\right)\left(\frac{1-m}{2\alpha}+m\right)^{3/(2\alpha-1)}\right] \\
&+ \frac{1}{\left(1-2\alpha\right)m-1}\left[-4\frac{15\alpha}{4\left(2\alpha-5\right)}\left(\frac{1-m}{2\alpha}+m\right)^{4/(2\alpha-1)}\right] = \frac{3c_3-4c_4}{\left(1-2\alpha\right)m-1}
\end{aligned}
\tag{67}
$$

Proof of Equation 5.46

First, it is tested that the initial condition is satisfied:

$$\begin{aligned} c_i\left(m=1\right) &= \frac{\alpha\left(i-1\right)!\left(-1\right)^{i-1}\left(1-1\right)}{\prod_{j=2}^{i}\left(2\alpha-j-1\right)} \\ &+ \sum_{j=2}^{i}\frac{\alpha\left(j^2-1\right)}{j\left(2\alpha-j-1\right)}\left(\binom{i-1}{j-1}\right)\left(-1\right)^j\left[\left(\frac{1-1}{2\alpha}+1\right)^{j/(2\alpha-1)}-1\right] \\ &= 0+\sum_{j=2}^{i}\frac{\alpha\left(j^2-1\right)}{j\left(2\alpha-j-1\right)}\left(\binom{i-1}{j-1}\right)\left(-1\right)^j\left[1^{j/(2\alpha-1)}-1\right]=0 \end{aligned} \tag{68}$$

Before going on, a few identities of the binomial coefficients must be proved:
Lemma:

$$\sum_{j=0}^{i}\binom{i}{j}(-1)^j=0 \tag{69}$$

$$\sum_{j=0}^{i}j\binom{i}{j}(-1)^j=0 \tag{70}$$

$$\sum_{j=2}^{i}\frac{(j-1)}{j}\binom{i-1}{j-1}(-1)^j=\frac{1}{i} \tag{71}$$

$$\sum_{j=0}^{i-1}\frac{(-1)^j(j+2)j}{(2\alpha-j-2)}\binom{i-1}{j}=2\alpha\frac{(i-1)!(-1)^{i-1}}{\prod_{j=1}^{i-1}(2\alpha-j-2)} \tag{72}$$

The proof of the first one can be obtained easily by the binomial theorem directly:

$$\sum_{j=0}^{i}\binom{i}{j}(-1)^j=(1-1)^i=0 \tag{73}$$

For the second one, the function $(1-x)^i$ must be differentiated:

$$\frac{\mathrm{d}}{\mathrm{d}x_i}(1-x)^i=\frac{\mathrm{d}}{\mathrm{d}x_i}\sum_{j=0}^{i}x^j\binom{i}{j}(-1)^j=\sum_{j=0}^{i}\binom{i}{j}(-1)^j \tag{74}$$

The differentiation can also be done without the binomial theorem:

$$\frac{\mathrm{d}}{\mathrm{d}x}(1-x)^i=-i(1-x)^{i-1} \tag{75}$$

Comparing the right-hand side of the last two equations at $x = 1$ determines the Equation 70 considering $i \geq 1$:

$$\sum_{j=0}^{i} j \binom{i}{j} (-1)^j = -i(1-1)^{i-1} = 0 \tag{76}$$

The proof of Equation 71 relies on the formulas of the Equation 70 and 69:

$$\begin{aligned}
&\sum_{j=2}^{i} \frac{j-1}{j} \binom{i-1}{j-1} (-1)^j = \sum_{j=1}^{i} \frac{j-1}{j} \binom{i-1}{j-1} (-1)^j = \\
&\sum_{j=1}^{i} \frac{(j-1)\,i}{ji} \binom{i-1}{j-1} (-1)^j = \frac{1}{i} \sum_{j=1}^{i} (j-1) \binom{i}{j} (-1)^j \\
&= \frac{1}{i} \left[\sum_{j=1}^{i} j \binom{i}{j} (-1)^j - \sum_{j=1}^{i} \binom{i}{j} (-1)^j \right] \\
&= \frac{1}{i} \left[\sum_{j=0}^{i} j \binom{i}{j} (-1)^j - \left\{ \sum_{j=0}^{i} \binom{i}{j} (-1)^j - \binom{i}{0} \right\} \right] \\
&= \frac{1}{i} \left[0 - -1 \right] = \frac{1}{i}
\end{aligned} \tag{77}$$

For proving Equation 72, mathematical induction is applied:

$$\begin{aligned}
&\sum_{j=0}^{i} \frac{(-1)^j\,(j+2)\,j}{(2\alpha-j-2)} \binom{i}{j} = \sum_{j=1}^{i} \frac{(-1)^j\,(j+2)\,j}{(2\alpha-j-2)} \binom{i}{j} = i \sum_{j=1}^{i} \frac{(-1)^j\,(j+2)}{(2\alpha-j-2)} \binom{i-1}{j-1} \\
&= \frac{i}{2\alpha-i-2} \sum_{j=1}^{i} \frac{(-1)^j\,(j+2)\,(2\alpha-i-2)}{(2\alpha-j-2)} \binom{i-1}{j-1} = \frac{i}{2\alpha-i-2} \sum_{j=1}^{i} (-1)^j\, \frac{2\alpha j - ij - 2j + 4\alpha - 2i - 4}{(2\alpha-j-2)} \binom{i-1}{j-1} \\
&= \frac{i}{2\alpha-i-2} \sum_{j=1}^{i} (-1)^j\, \frac{4\alpha - 2j - 4 + 2\alpha j - j^2 - 2j + j^2 + 2j - ji - 2i}{(2\alpha-j-2)} \binom{i-1}{j-1} \\
&= \frac{i}{2\alpha-i-2} \left[2 \sum_{j=1}^{i} (-1)^j \binom{i}{j-1} + \sum_{j=1}^{i-1} (-1)^j\, j \binom{i-1}{j-1} - \sum_{j=1}^{i} (-1)^j\, \frac{(j+2)\,(i-j)}{(2\alpha-j-2)} \binom{i-1}{j-1} \right] \\
&= \frac{i}{2\alpha-i-2} \left[2 \sum_{j=1}^{i} (-1)^j \binom{i-1}{j-1} + \sum_{j=1}^{i} (-1)^j\, [(j-1)+1] \binom{i-1}{j-1} - \sum_{j=1}^{i-1} (-1)^j\, \frac{(j+2)\,(i-j)}{(2\alpha-j-2)} \binom{i-1}{j-1} \right] \\
&= \frac{i}{2\alpha-i-2} \left[3 \sum_{j=1}^{i} (-1)^j \binom{i-1}{j-1} + \sum_{j=1}^{i} (-1)^j\, (j-1) \binom{i-1}{j-1} - \sum_{j=1}^{i-1} (-1)^j\, \frac{(j+2)\,j}{(2\alpha-j-2)} \binom{i-1}{j} \right] \\
&= \frac{-i}{2\alpha-i-2} \left[\sum_{j=0}^{i-1} (-1)^j\, \frac{(j+2)\,j}{(2\alpha-j-2)} \binom{i-1}{j} \right]
\end{aligned} \tag{78}$$

From the last line, it can be obvious that if the formula is true for a positive integer of i, then it must be true for $i+1$, as well. For $i = 3$ the formula is tested to be

true because:

$$\begin{aligned}
&\sum_{j=0}^{3-1}\frac{(-1)^j\,(j+2)\,j}{(2\alpha-j-2)}\binom{3-1}{j}=\sum_{j=0}^{2}\frac{(-1)^j\,(j+2)\,j}{(2\alpha-j-2)}\binom{2}{j}=\frac{-3}{(2\alpha-3)}\binom{2}{1}+\frac{8}{(2\alpha-4)}\binom{2}{2}\\
&=\frac{-6\,(2\alpha-4)+8\,(2\alpha-3)}{(2\alpha-3)\,(2\alpha-4)}=\frac{4\alpha}{(2\alpha-3)\,(2\alpha-4)}=2\alpha\frac{(3-1)!\,(-1)^{3-1}}{\prod_{j=1}^{3-1}(2\alpha-j-2)}
\end{aligned}\tag{79}$$

Now returning to the proof of Equation 5.46, the derivative of c_i is determined and rearranged step by step until the right-hand side of Equation 5.46 is reached:

$$\begin{aligned}
&\frac{\mathrm{d}c_i}{\mathrm{d}m}=\frac{\alpha\,(i-1)!\,(-1)^{i-1}}{\prod_{j=2}^{i}(2\alpha-j-1)}+\sum_{j=2}^{i}\frac{\left(j^2-1\right)}{2\,(2\alpha-j-1)}\binom{i-1}{j-1}(-1)^j\left(\frac{1-m}{2\alpha}+m\right)^{j/(2\alpha-1)-1}\\
&=\frac{(1-2\alpha)\,m-1}{(1-2\alpha)\,m-1}\left[\frac{\alpha\,(i-1)!\,(-1)^{i-1}}{\prod_{j=2}^{i}(2\alpha-j-1)}+\sum_{j=2}^{i}\frac{\left(j^2-1\right)}{2\,(2\alpha-j-1)}\binom{i-1}{j-1}(-1)^j\left(\frac{1-m}{2\alpha}+m\right)^{j/(2\alpha-1)-1}\right]\\
&=\frac{1}{(1-2\alpha)\,m-1}\\
&\left[\frac{(1-2\alpha)\,m\alpha\,(i-1)!\,(-1)^{i-1}-\alpha\,(i-1)!\,(-1)^{i-1}}{\prod_{j=2}^{i}(2\alpha-j-1)}-\sum_{j=2}^{i}\frac{\alpha\left(j^2-1\right)}{(2\alpha-j-1)}\binom{i-1}{j-1}(-1)^j\left(\frac{1-m}{2\alpha}+m\right)^{j/(2\alpha-1)}\right]\\
&=\frac{1}{(1-2\alpha)\,m-1}\left[\frac{(1-2\alpha)\,m\alpha\,(i-1)!\,(-1)^{i-1}-\alpha\,(i-1)!\,(-1)^{i-1}}{\prod_{j=2}^{i}(2\alpha-j-1)}\right]\\
&+\frac{1}{(1-2\alpha)\,m-1}\left[\sum_{j=2}^{i-1}\frac{\alpha\left(j^2-1\right)}{(2\alpha-j-1)}\left\{\frac{i-1}{j}\binom{i-1}{j-1}-\frac{i}{j}\binom{i-1}{j-1}\right\}(-1)^j\left(\frac{1-m}{2\alpha}+m\right)^{j/(2\alpha-1)}\right]\\
&+\frac{1}{(1-2\alpha)\,m-1}\left[-\frac{i\alpha\left(i^2-1\right)}{i\,(2\alpha-i-1)}(-1)^i\left(\frac{1-m}{2\alpha}+m\right)^{i/(2\alpha-1)}\right]\\
&=\frac{1}{(1-2\alpha)\,m-1}\left[\frac{(1-2\alpha)\,m\alpha\,(i-1)!\,(-1)^{i-1}-\alpha\,(i-1)!\,(-1)^{i-1}}{\prod_{j=2}^{i}(2\alpha-j-1)}\right]\\
&+\frac{1}{(1-2\alpha)\,m-1}\left[(i-1)\sum_{j=2}^{i-1}\frac{\alpha\left(j^2-1\right)}{j\,(2\alpha-j-1)}\binom{i-2}{j-1}(-1)^j\left(\frac{1-m}{2\alpha}+m\right)^{j/(2\alpha-1)}\right]\\
&+\frac{1}{(1-2\alpha)\,m-1}\left[-i\sum_{j=2}^{i}\frac{\alpha\left(j^2-1\right)}{j\,(2\alpha-j-1)}\binom{i-1}{j-1}(-1)^j\left(\frac{1-m}{2\alpha}+m\right)^{j/(2\alpha-1)}\right]
\end{aligned}\tag{80}$$

At this point, the last two lines are dealt separately:

$$
\begin{aligned}
&(i-1)\sum_{j=2}^{i-1}\frac{\alpha\left(j^2-1\right)}{j\left(2\alpha-j-1\right)}\binom{i-2}{j-1}(-1)^j - i\sum_{j=2}^{i}\frac{\alpha\left(j^2-1\right)}{j\left(2\alpha-j-1\right)}\binom{i-1}{j-1}(-1)^j \\
&=\sum_{j=2}^{i-1}\frac{(i-1)\,\alpha\left(j^2-1\right)}{j\left(2\alpha-j-1\right)}\binom{i-1}{j-1}(-1)^j - \sum_{j=2}^{i}\frac{i\alpha\left(j^2-1\right)}{j\left(2\alpha-j-1\right)}\binom{i-1}{j-1}(-1)^j \\
&=\sum_{j=2}^{i-1}\frac{\alpha\left(j^2-1\right)}{j\left(2\alpha-j-1\right)}\left[(i-1)\binom{i-2}{j-1} - i\binom{i-1}{j-1}\right](-1)^j - \frac{\alpha\left(i^2-1\right)}{(2\alpha-i-1)}(-1)^i \\
&=-\alpha\sum_{j=2}^{i}\frac{\left(j^2-1\right)}{(2\alpha-j-1)}\binom{i-1}{j-1}(-1)^j = \alpha\sum_{j=0}^{i-1}\frac{(-1)^j\,(j+2)\,j}{(2\alpha-j-2)}\binom{i-1}{j} \\
&=\alpha^2\frac{2\,(i-1)!\,(-1)^{i-1}}{\prod_{j=1}^{i-1}(2\alpha-j-2)}
\end{aligned}
\tag{81}
$$

The identity given in Equation 72 is used in the last line.

The proof is continued by substituting the last line of Equation 81 back into

Equation 80:

$$
\begin{aligned}
&\frac{\mathrm{d}c_i}{\mathrm{d}m} = \frac{1}{(1-2\alpha)\,m-1}\left[\frac{(1-2\alpha)\,m\alpha\,(i-1)!\,(-1)^{i-1}-\alpha\,(i-1)!\,(-1)^{i-1}}{\prod_{j=2}^{i}(2\alpha-j-1)}\right]\\
&+\frac{1}{(1-2\alpha)\,m-1}\left[(i-1)\sum_{j=2}^{i-1}\frac{\alpha\left(j^2-1\right)}{j\,(2\alpha-j-1)}\binom{i-2}{j-1}(-1)^j\left(\frac{1-m}{2\alpha}+m\right)^{j/(2\alpha-1)}\right]\\
&+\frac{1}{(1-2\alpha)\,m-1}\left[-i\sum_{j=2}^{i}\frac{\alpha\left(j^2-1\right)}{j\,(2\alpha-j-1)}\binom{i-1}{j-1}(-1)^j\left(\frac{1-m}{2\alpha}+m\right)^{j/(2\alpha-1)}\right]\\
&=\frac{1}{(1-2\alpha)\,m-1}\left[\frac{(1-2\alpha)\,m\alpha\,(i-1)!\,(-1)^{i-1}-\alpha\,(i-1)!\,(-1)^{i-1}}{\prod_{j=2}^{i}(2\alpha-j-1)}\right]\\
&+\frac{1}{(1-2\alpha)\,m-1}\left[(i-1)\sum_{j=2}^{i-1}\frac{\alpha\left(j^2-1\right)}{j\,(2\alpha-j-1)}\binom{i-2}{j-1}(-1)^j\left(\frac{1-m}{2\alpha}+m\right)^{j/(2\alpha-1)}\right]\\
&+\frac{1}{(1-2\alpha)\,m-1}\left[-i\sum_{j=2}^{i}\frac{\alpha\left(j^2-1\right)}{j\,(2\alpha-j-1)}\binom{i-1}{j-1}(-1)^j\left(\frac{1-m}{2\alpha}+m\right)^{j/(2\alpha-1)}\right]\\
&+\frac{1}{(1-2\alpha)\,m-1}\\
&\left[-(i-1)\sum_{j=2}^{i-1}\frac{\alpha\left(j^2-1\right)}{j\,(2\alpha-j-1)}\binom{i-2}{j-1}(-1)^j+i\sum_{j=2}^{i}\frac{\alpha\left(j^2-1\right)}{j\,(2\alpha-j-1)}\binom{i-1}{j-1}(-1)^j\right]\\
&+\frac{1}{(1-2\alpha)\,m-1}\alpha^2\frac{2\,(i-1)!\,(-1)^{i-1}}{\prod_{j=1}^{i-1}(2\alpha-j-2)}\\
&=\frac{1}{(1-2\alpha)\,m-1}\\
&\left[\frac{(1-2\alpha)\,\alpha m\,(i-1)!\,(-1)^{i-1}-\alpha\,(i-1)!\,(-1)^{i-1}}{\prod_{j=2}^{i}(2\alpha-j-1)}+\alpha^2\frac{2\,(i-1)!\,(-1)^{i-1}}{\prod_{j=2}^{i}(2\alpha-j-1)}\right]\\
&+\frac{(i-1)}{(1-2\alpha)\,m-1}\\
&\left[\sum_{j=2}^{i-1}\frac{\alpha\left(j^2-1\right)}{j\,(2\alpha-j-1)}\binom{i-2}{j-1}(-1)^j\left(\frac{1-m}{2\alpha}+m\right)^{j/(2\alpha-1)}-\sum_{j=2}^{i-1}\frac{\alpha\left(j^2-1\right)}{j\,(2\alpha-j-1)}\binom{i-2}{j-1}(-1)^j\right]\\
&+\frac{-i}{(1-2\alpha)\,m-1}\\
&\left[\sum_{j=2}^{i}\frac{\alpha\left(j^2-1\right)}{j\,(2\alpha-j-1)}\binom{i-1}{j-1}(-1)^j\left(\frac{1-m}{2\alpha}+m\right)^{j/(2\alpha-1)}-\sum_{j=2}^{i}\frac{\alpha\left(j^2-1\right)}{j\,(2\alpha-j-1)}\binom{i-1}{j-1}(-1)^j\right]
\end{aligned}
\tag{82}
$$

For the final transformations:

$$
\begin{aligned}
&\frac{\mathrm{d}c_i}{\mathrm{d}m} = \frac{(i-1)!\,(-1)^{i-1}}{(1-2\alpha)\,m-1}\left[\frac{m\alpha-2\alpha^2m-\alpha+2\alpha^2}{\prod_{j=2}^{i}(2\alpha-j-1)}\right]\\
&+\frac{(i-1)}{(1-2\alpha)\,m-1}\left[\sum_{j=2}^{i-1}\frac{\alpha\left(j^2-1\right)}{j\,(2\alpha-j-1)}\binom{i-2}{j-1}(-1)^j\left[\left(\frac{1-m}{2\alpha}+m\right)^{j/(2\alpha-1)}-1\right]\right]\\
&\frac{-i}{(1-2\alpha)\,m-1}\left[\sum_{j=2}^{i}\frac{\alpha\left(j^2-1\right)}{j\,(2\alpha-j-1)}\binom{i-1}{j-1}(-1)^j\left[\left(\frac{1-m}{2\alpha}+m\right)^{j/(2\alpha-1)}-1\right]\right]\\
&=\frac{\alpha\,(i-1)!\,(-1)^{i-1}}{(1-2\alpha)\,m-1}\left[\frac{-im+i+m-1+im-i-2\alpha m+2\alpha}{\prod_{j=2}^{i}(2\alpha-j-1)}\right]\\
&+\frac{(i-1)}{(1-2\alpha)\,m-1}\left[\sum_{j=2}^{i-1}\frac{\alpha\left(j^2-1\right)}{j\,(2\alpha-j-1)}\binom{i-2}{j-1}(-1)^j\left[\left(\frac{1-m}{2\alpha}+m\right)^{j/(2\alpha-1)}-1\right]\right]\\
&\frac{-i}{(1-2\alpha)\,m-1}\left[\sum_{j=2}^{i}\frac{\alpha\left(j^2-1\right)}{j\,(2\alpha-j-1)}\binom{i-1}{j-1}(-1)^j\left[\left(\frac{1-m}{2\alpha}+m\right)^{j/(2\alpha-1)}-1\right]\right]\\
&=\frac{\alpha\,(i-1)!\,(-1)^{i-1}}{(1-2\alpha)\,m-1}\left[\frac{-i\,(m-1)+(m-1)\,(1+i-2\alpha)}{\prod_{j=2}^{i}(2\alpha-j-1)}\right]\\
&+\frac{(i-1)}{(1-2\alpha)\,m-1}\left[\sum_{j=2}^{i-1}\frac{\alpha\left(j^2-1\right)}{j\,(2\alpha-j-1)}\binom{i-2}{j-1}(-1)^j\left[\left(\frac{1-m}{2\alpha}+m\right)^{j/(2\alpha-1)}-1\right]\right]\\
&\frac{-i}{(1-2\alpha)\,m-1}\left[\sum_{j=2}^{i}\frac{\alpha\left(j^2-1\right)}{j\,(2\alpha-j-1)}\binom{i-1}{j-1}(-1)^j\left[\left(\frac{1-m}{2\alpha}+m\right)^{j/(2\alpha-1)}-1\right]\right]\\
&=\frac{1}{(1-2\alpha)\,m-1}\left[\frac{-i\alpha\,(i-1)!\,(-1)^{i-1}\,(m-1)}{\prod_{j=2}^{i}(2\alpha-j-1)}+\frac{(i-1)\,\alpha\,(i-2)!\,(-1)^{i-2}\,(m-1)}{\prod_{j=2}^{i-1}(2\alpha-j-1)}\right]\\
&+\frac{(i-1)}{(1-2\alpha)\,m-1}\left[\sum_{j=2}^{i-1}\frac{\alpha\left(j^2-1\right)}{j\,(2\alpha-j-1)}\binom{i-2}{j-1}(-1)^j\left[\left(\frac{1-m}{2\alpha}+m\right)^{j/(2\alpha-1)}-1\right]\right]\\
&\frac{-i}{(1-2\alpha)\,m-1}\left[\sum_{j=2}^{i}\frac{\alpha\left(j^2-1\right)}{j\,(2\alpha-j-1)}\binom{i-1}{j-1}(-1)^j\left[\left(\frac{1-m}{2\alpha}+m\right)^{j/(2\alpha-1)}-1\right]\right]\\
&=\frac{(i-1)\,c_{i-1}-ic_i}{(1-2\alpha)\,m-1}
\end{aligned}
\tag{83}
$$

Quod erat demonstrandum.

Derivation of Equation 5.48

If $\alpha << 1$ is assumed, the approximation $1 \pm \alpha = 1 \pm 2\alpha = 1$ can be applied, and gives the following:

$$\begin{aligned}
\lim_{\tau\to\infty} c_i &\cong \frac{-\alpha\,(i-1)!\,(-1)^{i-1}}{\prod_{j=2}^{i} -(j+1)} + \sum_{j=2}^{i} \frac{\alpha\,(j+1)\,(j-1)}{j\,(j+1)} \binom{i-1}{j-1} (-1)^j \\
&= \frac{-\alpha\,(i-1)!2\,(-1)^{i-1}}{(i+1)!} + \sum_{j=2}^{i} \frac{\alpha\,(j+1)\,(j-1)}{j\,(j+1)} \binom{i-1}{j-1} (-1)^j \\
&= \alpha \frac{-2}{i\,(i+1)} + \alpha \sum_{j=2}^{i} \frac{(j-1)}{j} \binom{i-1}{j-1} (-1)^j \\
&= \alpha \frac{-2}{i\,(i+1)} + \alpha \frac{1}{i} = \alpha \frac{i-1}{i(i+1)}
\end{aligned} \tag{84}$$

The identity given in Equation 71 is used in the last line.

Proof of Equation 5.50

First, it is tested that the initial condition ($\mu_0 = 0$ when $\tau = 0$) is satisfied:

$$\mu_0 = \frac{\alpha}{(1-2\alpha)(1-2\alpha+2\alpha)} + \frac{-\alpha+2\alpha^2}{(1-2\alpha)^2} - \frac{\alpha\ln(1-2\alpha+2\alpha)}{(1-2\alpha)^2} = \frac{\alpha}{1-2\alpha} - \frac{\alpha}{1-2\alpha} = 0 \tag{85}$$

Differentiation of the first part of Equation 5.50 gives:

$$\begin{aligned}\frac{\mathrm{d}\mu_0}{\mathrm{d}\tau} &= \frac{-2\alpha^2\mathrm{e}^\tau}{(1-2\alpha)(1-2\alpha+2\alpha\mathrm{e}^\tau)^2} + \frac{\alpha}{(1-2\alpha)^2} - \frac{2\alpha^2\mathrm{e}^\tau}{(1-2\alpha)^2(1-2\alpha+2\alpha\mathrm{e}^\tau)} \\ &= \frac{-2\alpha^2\mathrm{e}^\tau}{(1-2\alpha)(1-2\alpha+2\alpha\mathrm{e}^\tau)^2} + \frac{\alpha}{(1-2\alpha)(1-2\alpha+2\alpha\mathrm{e}^\tau)} \\ &= \frac{\alpha-2\alpha^2}{(1-2\alpha)(1-2\alpha+2\alpha\mathrm{e}^\tau)^2} = \frac{\alpha}{(1-2\alpha)(1-2\alpha+2\alpha\mathrm{e}^\tau)^2}\end{aligned} \tag{86}$$

The last part is in agreement with Equation 5.32.
The initial condition is tested for the second part, as well:

$$\mu_0 = \frac{\alpha-\alpha}{1-2\alpha} + \frac{\alpha\ln\left(\frac{1}{2\alpha}-\frac{1}{2\alpha}+1\right)}{(1-2\alpha)^2} = 0 \tag{87}$$

Then the differentiation of the second part gives:

$$\begin{aligned}\frac{\mathrm{d}\mu_0}{\mathrm{d}m} &= \frac{\alpha}{1-2\alpha} + \frac{\alpha\frac{-\frac{1}{2\alpha}+1}{\frac{1}{2\alpha}-\frac{m}{2\alpha}+m}}{(1-2\alpha)^2} = \frac{\alpha}{1-2\alpha} - \frac{\alpha}{(1-2\alpha)(1-m+2\alpha m)} \\ &= \frac{\alpha}{1-2\alpha}\left(\frac{-m+2\alpha m}{1-m+2\alpha m}\right) = -\frac{-\alpha}{2\alpha+(1-m)m^{-1}}\end{aligned} \tag{88}$$

The last part is in agreement with Equation 5.49 at $n = 2$. The cross-check can be obtained by the following:

$$\begin{aligned}\mu_0 &= \frac{\frac{\alpha}{1-2\alpha+2\alpha\mathrm{e}^\tau}-\alpha}{1-2\alpha} + \frac{\alpha\ln\left(\frac{1}{2\alpha}-\frac{\frac{1}{1-2\alpha+2\alpha\mathrm{e}^\tau}}{2\alpha}+\frac{1}{1-2\alpha+2\alpha\mathrm{e}^\tau}\right)}{(1-2\alpha)^2} \\ &= \frac{\alpha}{(1-2\alpha)(1-2\alpha+2\alpha\mathrm{e}^\tau)} - \frac{\alpha}{(1-2\alpha)} + \frac{\alpha\ln\left(\frac{2\alpha\mathrm{e}^\tau}{2\alpha(1-2\alpha+2\alpha\mathrm{e}^\tau)}\right)}{(1-2\alpha)^2} \\ &= \frac{\alpha}{(1-2\alpha)(1-2\alpha+2\alpha\mathrm{e}^\tau)} - \frac{\alpha}{(1-2\alpha)} + \frac{\alpha^\tau}{(1-2\alpha)^2} - \frac{\alpha\ln(1-2\alpha+2\alpha\mathrm{e}^\tau)}{(1-2\alpha)^2}\end{aligned} \tag{89}$$

The final part is indeed the same as the first part of Equation 5.50.

Proof of Equation 5.52

First, it is tested that the initial condition is satisfied:

$$0 = \frac{1}{\sqrt{1-12\alpha}}\left[\operatorname{arth}\left(\frac{6\alpha-1}{\sqrt{1-12\alpha}}\right) - \operatorname{arth}\left(\frac{6\alpha-1}{\sqrt{1-12\alpha}}\right)\right] + \frac{1}{2}\ln\left(1-\frac{1}{3\alpha}+\frac{1}{3\alpha^2}\right) \tag{90}$$

The term in the parantheses after the logarithm sign is 1, so the equation is satisfied. In order to test the validity of the differential equation, the derivative of the inverse hyperbolic function must be recalled as follows:

$$\frac{\mathrm{darthz}}{\mathrm{dz}} = \frac{1}{1-\mathrm{z}^2} \tag{91}$$

The differentiation of Equation 5.52 with respect to τ:

$$1 = \frac{1}{\sqrt{1-12\alpha}}\frac{1}{1-\left(\frac{6\alpha m-1}{\sqrt{1-12\alpha}}\right)^2}\frac{6\alpha}{\sqrt{1-12\alpha}}\frac{\mathrm{d}m}{\mathrm{d}\tau} + \frac{1}{2}\frac{1}{1-\frac{1}{3\alpha m}+\frac{1}{3\alpha m^2}}\left(\frac{1}{3\alpha m^2}-\frac{2}{3\alpha m^3}\right)\frac{\mathrm{d}m}{\mathrm{d}\tau} \tag{92}$$

Then, it is transformed gradually:

$$1 = \frac{6\alpha}{1-12\alpha}\frac{1}{1-\frac{(6\alpha m-1)}{1-12\alpha}}\frac{\mathrm{d}m}{\mathrm{d}\tau} + \frac{1}{2}\frac{3\alpha m^2}{3\alpha m^2-m+1}\frac{m-2}{3\alpha m^3}\frac{\mathrm{d}m}{\mathrm{d}\tau} \tag{93}$$

$$1 = \frac{6\alpha}{1-12\alpha-(6\alpha m-1)^2}\frac{\mathrm{d}m}{\mathrm{d}\tau} + \frac{m-2}{6\alpha m^3-2m^3+2m}\frac{\mathrm{d}m}{\mathrm{d}\tau} \tag{94}$$

$$1 = \frac{-m}{6\alpha m^3-2m^2+2m}\frac{\mathrm{d}m}{\mathrm{d}\tau} + \frac{m-2}{6\alpha m^3-2m^2+2m}\frac{\mathrm{d}m}{\mathrm{d}\tau} \tag{95}$$

$$1 = \frac{-1}{3\alpha m^3-m^2+m}\frac{\mathrm{d}m}{\mathrm{d}\tau} \tag{96}$$

It can be seen that the last equation is equivalent to Equation 5.51. So Equation 5.52 is indeed the solution.

Proof of Equation 5.54

First, it is tested that the initial condition is satisfied ($\mu_0 = 0$ when $m = 1$):

$$\begin{aligned}\mu_0 &= \frac{1-1}{3} + \frac{(1-6\alpha)}{9\alpha\sqrt{1-12\alpha}}\operatorname{arth}\left(\frac{(1-1)\sqrt{1-12\alpha}}{1+6\alpha-1}\right) - \frac{1}{18\alpha}\ln\left(\frac{1}{3\alpha} - \frac{1}{3\alpha} + 1\right) \\ &= 0 + 0 - 0 = 0\end{aligned} \tag{97}$$

Then, the differentiation leads to:

$$\begin{aligned}&\frac{\mathrm{d}\mu_0}{\mathrm{d}m} = -\frac{1}{3} + \frac{(1-6\alpha)}{9\alpha\sqrt{1-12\alpha}} \frac{1}{1-\left(\frac{(1-m)\sqrt{1-12\alpha}}{1+6\alpha m-m}\right)^2} \left(\frac{-\sqrt{1-12\alpha}}{1+6\alpha m-m} + \frac{(1-6\alpha)(1-m)\sqrt{1-12\alpha}}{(1+6\alpha m-m)^2}\right) \\ &- \frac{1}{18\alpha}\frac{1}{\frac{1}{3\alpha} - \frac{m}{3\alpha} + m^2}\left(-\frac{1}{3\alpha} + 2m\right) \\ &= -\frac{1}{3} - \frac{1}{18\alpha}\frac{6\alpha m - 1}{1 - m + 3\alpha m^2} \\ &+ \frac{(1-6\alpha)}{9\alpha\sqrt{1-12\alpha}} \frac{\sqrt{1-12\alpha}}{(1+6\alpha m-m)^2 - (1-m)^2(1-12\alpha)} \left(-1 - 6\alpha m + m + (1-6\alpha)(1-m)\right) \\ &= -\frac{1}{3} - \frac{1}{18\alpha}\frac{6\alpha m - 1}{1 - m + 3\alpha m^2} + \frac{(1-6\alpha)}{9\alpha}\frac{(-6\alpha)}{36\alpha^2 m^2 - 12\alpha m + 12\alpha} \\ &= -\frac{1}{3} - \frac{1}{18\alpha}\frac{6\alpha m - 1}{1 - m + 3\alpha m^2} - \frac{1-6\alpha}{18\alpha}\frac{1}{3\alpha m^2 - m + \alpha} \\ &= \frac{1 - m - 1 + m - 9\alpha m^2}{3 - 3m + 9\alpha m^2} = \frac{-3\alpha m^2}{1 - m + 3\alpha m^2}\end{aligned} \tag{98}$$

The last part is in agreement with Equation 5.53.

Proof of Equation 5.62

First, the differential equation is rearranged:

$$\frac{\mathrm{d}\mu_0}{\mathrm{d}m} = -\frac{\alpha m^{n-1}}{\mu_0} \tag{99}$$

Then, it is differentiated step by step:

$$\frac{\mathrm{d}}{\mathrm{d}m}\left(\sqrt{\frac{2\alpha}{n}\left(1-m^n\right)}\right) = -\frac{\alpha m^{n-1}}{\sqrt{\frac{2\alpha}{n}\left(1-m^n\right)}} \tag{100}$$

$$\frac{1}{2\sqrt{\frac{2\alpha}{n}\left(1-m^n\right)}}\left(-2\alpha m^{n-1}\right) = -\frac{\alpha m^{n-1}}{\sqrt{\frac{2\alpha}{n}\left(1-m^n\right)}} \tag{101}$$

$$\frac{-\alpha m^{n-1}}{\sqrt{\frac{2\alpha}{n}\left(1-m^n\right)}} = \frac{-\alpha m^{n-1}}{\sqrt{\frac{2\alpha}{n}\left(1-m^n\right)}} \tag{102}$$

Proof of Equation 5.74

First, Equation 5.71 is rearranged:

$$\frac{\mathrm{d}\mu_0}{\mathrm{d}m} = -\alpha\ m^{n-1}\mu_0^{-\frac{1}{3}}\,(1-m)^{-\frac{2}{3}} \tag{103}$$

Then, it is differentiated step by step:

$$\frac{\mathrm{d}}{\mathrm{d}m}\left(\alpha^{\frac{3}{4}}\,(1-m)^{\frac{1}{4}}\left(\sum_{i=0}^{n-1}\left(\frac{4}{3n}\prod_{j=i+1}^{n}\frac{3j}{3j-2}\right)m^i\right)^{\frac{3}{4}}\right) = \alpha^{\frac{3}{4}}\,(1-m)^{\frac{1}{4}} \tag{104}$$

$$\begin{aligned}
&-\alpha^{\frac{3}{4}}\frac{1}{4}\,(1-m)^{-\frac{3}{4}}\left(\sum_{i=0}^{n-1}\left(\frac{4}{3n}\prod_{j=i+1}^{n}\frac{3j}{3j-2}\right)m^i\right)^{\frac{3}{4}}\\
&+\frac{3}{4}\alpha^{\frac{3}{4}}\,(1-m)^{\frac{1}{4}}\left(\sum_{i=0}^{n-1}\left(\frac{4}{3n}\prod_{j=i+1}^{n}\frac{3j}{3j-2}\right)m^i\right)^{-\frac{1}{4}}\left(\sum_{i=1}^{n-1}\left(\frac{4i}{3n}\prod_{j=i+1}^{n}\frac{3j}{3j-2}\right)m^{i-1}\right) =\\
&-\alpha\ m^{n-1}\alpha^{-\frac{1}{4}}\,(1-m)^{-\frac{1}{12}}\left(\sum_{i=0}^{n-1}\left(\frac{4}{3n}\prod_{j=i+1}^{n}\frac{3j}{3j-2}\right)m^i\right)^{-\frac{1}{4}}(1-m)^{-\frac{2}{3}}\\
&-\frac{1}{3n}\left(\sum_{i=0}^{n-1}\left(\prod_{j=i+1}^{n}\frac{3j}{3j-2}\right)m^i\right)+\frac{1}{n}\,(1-m)\left(\sum_{i=1}^{n-1}\left(i\prod_{j=i+1}^{n}\frac{3j}{3j-2}\right)m^{i-1}\right) = -m^{n-1}
\end{aligned} \tag{105}$$

Specific function form Equation 5.74 for small values of n:

$n = 1$:

$$\mu_0 = 4^{\frac{3}{4}} \alpha^{\frac{3}{4}} (1-m)^{\frac{1}{4}} \tag{106}$$

$$\mu_{\frac{2}{3}} = 4^{\frac{1}{4}} \alpha^{\frac{1}{4}} (1-m)^{\frac{3}{4}} \tag{107}$$

$$\lim_{m \to 0} \mu_0 = 4^{\frac{3}{4}} \alpha^{\frac{3}{4}} \tag{108}$$

$n = 2$:

$$\mu_0 = \alpha^{\frac{3}{4}} (3+m)^{\frac{3}{4}} (1-m)^{\frac{1}{4}} \tag{109}$$

$$\mu_{\frac{2}{3}} = \alpha^{\frac{1}{4}} (3+m)^{\frac{1}{4}} (1-m)^{\frac{3}{4}} \tag{110}$$

$$\lim_{m \to 0} \mu_0 = 3^{\frac{3}{4}} \alpha^{\frac{3}{4}} \tag{111}$$

$n = 3$:

$$\mu_0 = \left(\frac{2}{7}\right)^{\frac{3}{4}} \alpha^{\frac{3}{4}} \left(9 + 3m + 2m^2\right)^{\frac{3}{4}} (1-m)^{\frac{1}{4}} \tag{112}$$

$$\mu_{\frac{2}{3}} = \left(\frac{2}{7}\right)^{\frac{1}{4}} \alpha^{\frac{1}{4}} \left(9 + 3m + 2m^2\right)^{\frac{1}{4}} (1-m)^{\frac{3}{4}} \tag{113}$$

$$\lim_{m \to 0} \mu_0 = \left(\frac{18}{7}\right)^{\frac{3}{4}} \alpha^{\frac{3}{4}} \tag{114}$$

$n = 4$:

$$\mu_0 = \left(\frac{1}{35}\right)^{\frac{3}{4}} \alpha^{\frac{3}{4}} \left(81 + 27m + 18m^2 + 14m^3\right)^{\frac{3}{4}} (1-m)^{\frac{1}{4}} \tag{115}$$

$$\mu_{\frac{2}{3}} = \left(\frac{1}{35}\right)^{\frac{1}{4}} \alpha^{\frac{1}{4}} \left(81 + 27m + 18m^2 + 14m^3\right)^{\frac{1}{4}} (1-m)^{\frac{3}{4}} \tag{116}$$

$$\lim_{m \to 0} \mu_0 = \left(\frac{81}{35}\right)^{\frac{3}{4}} \alpha^{\frac{3}{4}} \tag{117}$$

$n = 5$:

$$\mu_0 = \left(\frac{4}{455}\right)^{\frac{3}{4}} \alpha^{\frac{3}{4}} \left(243 + 81m + 54m^2 + 42m^3 + 35m^4\right)^{\frac{3}{4}} (1-m)^{\frac{1}{4}} \tag{118}$$

$$\mu_{\frac{2}{3}} = \left(\frac{4}{455}\right)^{\frac{1}{4}} \alpha^{\frac{1}{4}} \left(243 + 81m + 54m^2 + 42m^3 + 35m^4\right)^{\frac{1}{4}} (1-m)^{\frac{3}{4}} \tag{119}$$

$$\lim_{m \to 0} \mu_0 = \left(\frac{972}{455}\right)^{\frac{3}{4}} \alpha^{\frac{3}{4}} \tag{120}$$

Proof of Equation 5.85

First, Equation 5.82 is rearranged:

$$\frac{\mathrm{d}\mu_0}{\mathrm{d}m} = -\alpha\, m^{n-1}\mu_0^{-\frac{2}{3}}\,(1-m)^{-\frac{1}{3}} \tag{121}$$

Then, it is differentiated step by step:

$$\begin{aligned}
&-\frac{2}{5}\alpha^{\frac{3}{5}}\,(1-m)^{-\frac{3}{5}}\left(\sum_{i=0}^{n-1}\left(\frac{5}{3n}\prod_{j=i+1}^{n}\frac{3j}{3j-1}\right)m^i\right)^{\frac{3}{5}}\\
&+\frac{3}{5}\alpha^{\frac{3}{5}}\,(1-m)^{\frac{2}{5}}\left(\sum_{i=0}^{n-1}\left(\frac{5}{3n}\prod_{j=i+1}^{n}\frac{3j}{3j-1}\right)m^i\right)^{-\frac{2}{5}}\left(\sum_{i=1}^{n-1}\frac{5i}{3n}\left(\prod_{j=i+1}^{n}\frac{3j}{3j-1}\right)m^{i-1}\right)\\
&=-\alpha\, m^{n-1}\alpha^{-\frac{2}{5}}\,(1-m)^{-\frac{4}{15}}\left(\sum_{i=0}^{n-1}\left(\frac{5}{3n}\prod_{j=i+1}^{n}\frac{3j}{3j-1}\right)m^i\right)^{-\frac{2}{5}}(1-m)^{-\frac{1}{3}}
\end{aligned} \tag{122}$$

$$\begin{aligned}
&-\frac{2}{5}\alpha^{\frac{3}{5}}\left(\sum_{i=0}^{n-1}\left(\frac{5}{3n}\prod_{j=i+1}^{n}\frac{3j}{3j-1}\right)m^i\right)\\
&+\frac{3}{5}\alpha^{\frac{3}{5}}\,(1-m)\left(\sum_{i=1}^{n-1}\frac{5i}{3n}\left(\prod_{j=i+1}^{n}\frac{3j}{3j-1}\right)m^{i-1}\right)=-m^{n-1}\alpha^{\frac{3}{5}}
\end{aligned} \tag{123}$$

$$-\frac{1}{3n}\alpha^{\frac{3}{5}}\left(\sum_{i=0}^{n-1}\left(2\prod_{j=i+1}^{n}\frac{3j}{3j-1}\right)m^i\right)+\frac{1}{3n}\alpha^{\frac{3}{5}}\,(1-m)\left(\sum_{i=1}^{n-1}3i\left(\prod_{j=i+1}^{n}\frac{3j}{3j-1}\right)m^{i-1}\right)=-m^{n-1}\alpha^{\frac{3}{5}} \tag{124}$$

$$-\sum_{i=0}^{n-1}\left(2m^i\prod_{j=i+1}^{n}\frac{3j}{3j-1}\right)+\sum_{i=1}^{n-1}\left(3im^{i-1}\prod_{j=i+1}^{n}\frac{3j}{3j-1}\right)-\sum_{i=1}^{n-1}\left(3im^i\prod_{j=i+1}^{n}\frac{3j}{3j-1}\right)=-3nm^{n-1} \tag{125}$$

$$\begin{aligned}
&-2m^{n-1}\frac{3n}{3n-1}-\sum_{i=0}^{n-2}\left(m^i\frac{6i+6}{3i+2}\prod_{j=i+2}^{n}\frac{3j}{3j-1}\right)\\
&+\sum_{i=0}^{n-2}\left(3\,(i+1)\,m^i\prod_{j=i+2}^{n}\frac{3j}{3j-1}\right)-\sum_{i=1}^{n-1}\left(3im^i\prod_{j=i+1}^{n}\frac{3j}{3j-1}\right)=-3nm^{n-1}
\end{aligned} \tag{126}$$

$$\begin{aligned}
&-2m^{n-1}\frac{3n}{3n-1}-\sum_{i=0}^{n-2}\left(m^i\frac{6i+6}{3i+2}\prod_{j=i+2}^{n}\frac{3j}{3j-1}\right)+\sum_{i=0}^{n-2}\left(3\,(i+1)\,m^i\prod_{j=i+2}^{n}\frac{3j}{3j-1}\right)\\
&-3\,(n-1)\,m^{n-1}\frac{3n}{3n-1}-\sum_{i=1}^{n-2}\left(3im^i\frac{3+3}{3i+2}\prod_{j=i+2}^{n}\frac{3j}{3j-1}\right)=-3nm^{n-1}
\end{aligned} \tag{127}$$

$$
\begin{aligned}
&-3nm^{n-1}-\frac{6}{2}\prod_{j=2}^{n}\frac{3j}{3j-1}+3\prod_{j=i+2}^{n}\frac{3j}{3j-1}\\
&+\sum_{i=1}^{n-2}\left(m^i\left(-\frac{6i+6}{3i+2}+3\left(i+1\right)-3i\frac{3i+3}{3i+2}\right)\prod_{j=i+2}^{n}\frac{3j}{3j-1}\right)=-3nm^{n-1}
\end{aligned}
\tag{128}
$$

$$
\begin{aligned}
&-3nm^{n-1}+\sum_{i=1}^{n-2}\left(m^i\left(\frac{-6i-6-9i^2-9i+9i^2+6i+9i+6}{3i+2}\right)\prod_{j=i+2}^{n}\frac{3j}{3j-1}\right)\\
&=-3nm^{n-1}
\end{aligned}
\tag{129}
$$

Specific function form Equation 5.85 for small values of n:

$n = 1$:

$$\mu_0 = \left(\frac{5}{2}\right)^{\frac{3}{5}} \alpha^{\frac{3}{5}} (1-m)^{\frac{2}{5}} \tag{130}$$

$$\mu_{\frac{1}{3}} = \left(\frac{5}{2}\right)^{\frac{2}{5}} \alpha^{\frac{2}{5}} (1-m)^{\frac{3}{5}} \tag{131}$$

$$\lim_{m\to 0} \mu_0 = \left(\frac{5}{2}\right)^{\frac{3}{5}} \alpha^{\frac{3}{5}} \tag{132}$$

$n = 2$:

$$\mu_0 = \alpha^{\frac{3}{5}} \left(\frac{3}{2}+m\right)^{\frac{3}{5}} (1-m)^{\frac{2}{5}} \tag{133}$$

$$\mu_{\frac{1}{3}} = \alpha^{\frac{2}{5}} \left(\frac{3}{2}+m\right)^{\frac{2}{5}} (1-m)^{\frac{3}{5}} \tag{134}$$

$$\lim_{m\to 0} = \alpha^{\frac{3}{5}} \left(\frac{3}{2}\right)^{\frac{3}{5}} \tag{135}$$

$n = 3$:

$$\mu_0 = \left(\frac{1}{8}\right)^{\frac{3}{5}} \alpha^{\frac{3}{5}} \left(9+6m+5m^2\right)^{\frac{3}{5}} (1-m)^{\frac{2}{5}} \tag{136}$$

$$\mu_{\frac{1}{3}} = \left(\frac{1}{8}\right)^{\frac{2}{5}} \alpha^{\frac{2}{5}} \left(9+6m+5m^2\right)^{\frac{2}{5}} (1-m)^{\frac{3}{5}} \tag{137}$$

$$\lim_{m\to 0} \mu_0 = \left(\frac{9}{8}\right)^{\frac{3}{5}} \alpha^{\frac{3}{5}} \tag{138}$$

$n = 4$:

$$\mu_0 = \left(\frac{1}{88}\right)^{\frac{3}{5}} \alpha^{\frac{3}{5}} \left(81+54m+45m^2+40m^3\right)^{\frac{3}{5}} (1-m)^{\frac{2}{5}} \tag{139}$$

$$\mu_{\frac{1}{3}} = \left(\frac{1}{88}\right)^{\frac{2}{5}} \alpha^{\frac{2}{5}} \left(81+54m+45m^2+40m^3\right)^{\frac{2}{5}} (1-m)^{\frac{3}{5}} \tag{140}$$

$$\lim_{m\to 0} \mu_0 = \left(\frac{81}{88}\right)^{\frac{3}{5}} \alpha^{\frac{3}{5}} \tag{141}$$

$n = 5$:

$$\mu_0 = \left(\frac{1}{308}\right)^{\frac{3}{5}} \alpha^{\frac{3}{5}} \left(243+162m+135m^2+120m^3+110m^4\right)^{\frac{3}{5}} (1-m)^{\frac{2}{5}} \tag{142}$$

$$\mu_{\frac{1}{3}} = \left(\frac{1}{308}\right)^{\frac{2}{5}} \alpha^{\frac{2}{5}} \left(243 + 162m + 135m^2 + 120m^3 + 110m^4\right)^{\frac{2}{5}} (1-m)^{\frac{3}{5}} \tag{143}$$

$$\lim_{m\to 0} \mu_0 = \left(\frac{243}{308}\right)^{\frac{3}{5}} \alpha^{\frac{3}{5}} \tag{144}$$

Proof of Equations 5.93 and 5.94

First, the differential equation is rearranged:

$$\frac{\mathrm{d}\mu_0}{\mathrm{d}m} = -\frac{\alpha m^{n-1}}{\alpha n + 1 - m} \tag{145}$$

Then, it is differentiated step by step:

$$\begin{aligned} &\frac{\mathrm{d}}{\mathrm{d}m}\left(\alpha\left(1+\alpha n\right)^{n-1}\ln\left(\frac{\alpha n+1-m}{\alpha n}\right)+\alpha\sum_{i=1}^{n-1}\frac{1}{i}\left(1+\alpha n\right)^{n-1-i}\left(m^i-1\right)\right) \\ &=-\frac{\alpha m^{n-1}}{\alpha n+1-m} \end{aligned} \tag{146}$$

$$-\frac{\alpha\left(1+\alpha n\right)^{n-1}}{\alpha n+1-m}+\alpha\sum_{i=1}^{n-1}\left(1+\alpha n\right)^{n-1-i}m^{i-1}=-\frac{\alpha m^{n-1}}{\alpha n+1-m} \tag{147}$$

$$-\frac{\alpha\left(1+\alpha n\right)^{n-1}}{\alpha n+1-m}+\alpha\left(1+\alpha n\right)^{n-2}\sum_{i=0}^{n-2}\left(\frac{m}{1+\alpha n}\right)^i=-\frac{\alpha m^{n-1}}{\alpha n+1-m} \tag{148}$$

$$-\frac{\alpha\left(1+\alpha n\right)^{n-1}}{\alpha n+1-m}+\alpha\left(1+\alpha n\right)^{n-2}\frac{1-\left(\frac{m}{1+\alpha n}\right)^{n-1}}{1-\frac{m}{1+\alpha n}}=-\frac{\alpha m^{n-1}}{\alpha n+1-m} \tag{149}$$

$$-\alpha\frac{\left(1+\alpha n\right)^{n-1}}{\alpha n+1-m}+\alpha\frac{\left(1+\alpha n\right)^{n-1}-m^{n-1}}{\alpha n+1-m}=-\frac{\alpha m^{n-1}}{\alpha n+1-m} \tag{150}$$

$$\alpha\frac{-m^{n-1}}{\alpha n+1-m}=-\frac{\alpha m^{n-1}}{\alpha n+1-m} \tag{151}$$

Specific function form Equation 5.94

$n = 2$:

$$\mu_0 = \alpha\,(m-1) + \alpha\,(1+2\alpha)\ln\left(\frac{2\alpha+1-m}{2\alpha}\right) \tag{152}$$

$n = 3$:

$$\mu_0 = \frac{\alpha}{2}\left(m^2-1\right) + \alpha\,(1+3\alpha)\,(m-1) + \alpha\,(1+3\alpha)^2\ln\left(\frac{3\alpha+1-m}{3\alpha}\right) \tag{153}$$

$n = 4$:

$$\begin{aligned}\mu_0 = {} & \frac{\alpha}{3}\left(m^3-1\right) + \frac{\alpha}{2}\,(1+4\alpha)\left(m^2-1\right) \\ & + \alpha\,(1+4\alpha)^2\,(m-1) + \alpha\,(1+4\alpha)^3\ln\left(\frac{4\alpha+1-m}{4\alpha}\right)\end{aligned} \tag{154}$$

$n = 5$:

$$\begin{aligned}\mu_0 = {} & \frac{\alpha}{4}\left(m^4-1\right) + \frac{\alpha}{3}\,(1+5\alpha)\left(m^3-1\right) + \frac{\alpha}{2}\,(1+5\alpha)^2\left(m^2-1\right) \\ & + \alpha\,(1+5\alpha)^3\,(m-1) + (1+5\alpha)^4\ln\left(\frac{5\alpha+1-m}{5\alpha}\right)\end{aligned} \tag{155}$$

Derivation of Equation 5.118

Equation 5.116 is substituted into Equation 5.117 and setting the initial condition ($\mu_0 = 0$):

$$\frac{\mathrm{d}\mu_0}{\mathrm{d}\tau} = \beta\ p_0 \mathrm{e}^{-\beta\tau} \tag{156}$$

The solution can be found by a simple integration, since μ_0 does not appear on the right hand side of the above equation:

$$\mu_0 = C - p_0 \mathrm{e}^{-\beta\tau} \tag{157}$$

C denotes the integration constant which can be determined by the initial conditions ($c_i(\tau = 0) = 0$, so $\mu_0(\tau = 0) = 0$).

Proof of Equation 5.121

First, it is tested that the initial conditon is satisfied ($m = 1$ when $\tau = 0$):

$$1 = \mathrm{e}^{p_0/\beta - p_0/\beta} - n\beta\ p_0 \mathrm{e}^{-p_0/\beta} \int_0^0 \mathrm{e}^{p_0 \mathrm{e}^{-\beta\xi}/\beta + p_0\xi - \beta\xi} \mathrm{d}\xi \tag{158}$$

The equation holds indeed, since the value of the integration on the right-hand side is zero.

Then, it is differntiated step by step:

$$\begin{aligned} &\frac{\mathrm{d}m}{\mathrm{d}\tau} = \left(p_0 \mathrm{e}^{-\beta\tau} - p_0\right) \mathrm{e}^{p_0/\beta - p_0 \mathrm{e}^{-\beta\tau}/\beta - p_0\tau} - n\beta\ p_0 \left(p_0 \mathrm{e}^{-\beta\tau} - p_0\right) \mathrm{e}^{-p_0 \mathrm{e}^{-\beta\tau}/\beta - p_0\tau} \\ &\int_0^\tau \mathrm{e}^{p_0 \mathrm{e}^{-\beta\xi}/\beta + p_0\xi - \beta\xi} \mathrm{d}\xi - n\beta\ p_0 \mathrm{e}^{-p_0 \mathrm{e}^{-\beta\tau}/\beta - p_0\tau} \mathrm{e}^{p_0 \mathrm{e}^{-\beta\tau}/\beta + p_0\tau - \beta\tau} \\ &= p_0 \left(\mathrm{e}^{-\beta\tau} - 1\right) \mathrm{e}^{p_0/\beta - p_0 \mathrm{e}^{-\beta\tau}/\beta - p_0\tau} - n\beta\ p_0 \mathrm{e}^{-\beta\tau} \\ &- p_0 \left(\mathrm{e}^{-\beta\tau} - 1\right) n\beta\ p_0 \mathrm{e}^{-p_0 \mathrm{e}^{-\beta\tau}/\beta - p_0\tau} \int_0^\tau \mathrm{e}^{p_0 \mathrm{e}^{-\beta\xi}/\beta + p_0\xi - \beta\xi} \mathrm{d}\xi \end{aligned} \tag{159}$$

The last integral in the above equation can be given from Equation 5.121:

$$n\beta\ p_0 \mathrm{e}^{-p_0 \mathrm{e}^{-\beta\tau}/\beta - p_0\tau} \int_0^\tau \mathrm{e}^{p_0 \mathrm{e}^{-\beta\xi}/\beta + p_0\xi - \beta\xi} \mathrm{d}\xi = \mathrm{e}^{p_0/\beta - p_0 \mathrm{e}^{-\beta\tau}/\beta - p_0\tau} - m \tag{160}$$

This formula is substituted back into Equation 159:

$$\begin{aligned} &\frac{\mathrm{d}m}{\mathrm{d}\tau} = p_0 \left(\mathrm{e}^{-\beta\tau} - 1\right) \mathrm{e}^{p_0/\beta - p_0 \mathrm{e}^{-\beta\tau}/\beta - p_0\tau} - n\beta\ p_0 \mathrm{e}^{-\beta\tau} - p_0 \left(\mathrm{e}^{-\beta\tau} - 1\right) \\ &\left(\mathrm{e}^{p_0/\beta - p_0 \mathrm{e}^{-\beta\tau}/\beta - p_0\tau} - m\right) = -n\beta\ p_0 \mathrm{e}^{-\beta\tau} - m p_0 \left(1 - \mathrm{e}^{-\beta\tau} - 1\right) \end{aligned} \tag{161}$$

Therefore, Equation 5.121 is indeed the solution of the ordinary differential equation given as Equation 5.120.

Remark on solving Equation 5.122

```
In[1]:= FullSimplify[DSolve[y'[x] == -c * Exp[-b * x] - y[x] * (1 - y[x]), y[x], x]]
Out[1]= {{y[x] → (e^(-b x) (c c1 Hypergeometric0F1[2 - 1/b, c e^(-b x)/b^2]/(-1 + b) + 1/b^2 (-1)^(1/b) (Sqrt[c] Sqrt[e^(-b x)]/b)^(2/b) Gamma[1/b]
(b e^(b x) Hypergeometric0F1Regularized[1 + 1/b, c e^(-b x)/b^2] + c Hypergeometric0F1Regularized[2 + 1/b, c e^(-b x)/b^2]))) /
((-1)^(1/b) (Sqrt[c] Sqrt[e^(-b x)]/b)^(2/b) Hypergeometric0F1[1 + 1/b, c e^(-b x)/b^2] + c1 Hypergeometric0F1[(-1 + b)/b, c e^(-b x)/b^2])}}
```

The more readable form of the solution is the following:

$$\frac{C\frac{n\beta p_0}{\beta-1}\,{}_0F_1\left(;2-\frac{1}{\beta};\frac{np_0}{\beta}\mathrm{e}^{-\beta\tau}\right)+\left(-\frac{np_0}{\beta}\mathrm{e}^{-\beta\tau}\right)^{\frac{1}{\beta}}\Gamma\left(\frac{1}{\beta}\right)\left(\beta\mathrm{e}_0^{\beta\tau}\bar{F}_1\left(;1+\frac{1}{\beta};\frac{np_0}{\beta}\mathrm{e}^{-\beta\tau}\right)+\frac{np_0}{\beta}\,{}_0\bar{F}_1\left(;2+\frac{1}{\beta};\frac{np_0}{\beta}\mathrm{e}^{-\beta\tau}\right)\right)}{\mathrm{e}^{\beta\tau}\left(-\frac{np_0}{\beta}\mathrm{e}^{-\beta\tau}\right)_0^{\frac{1}{\beta}}F_1\left(;1+\frac{1}{\beta};\frac{np_0}{\beta}\mathrm{e}^{-\beta\tau}\right)+C\mathrm{e}_0^{\beta\tau}F_1\left(;1-\frac{1}{\beta};\frac{np_0}{\beta}\mathrm{e}^{-\beta\tau}\right)} \tag{162}$$

where ${}_0F_1$ refers to a confluent hyperbolic function, ${}_0\bar{F}_1$ means the regularized confluent hyperbolic function, Γ denotes the gamma function.

Appendices

Important Matlab codes

Listing 7.1: Matlab code for implementing the Gillespie algorithm for the diffusion kernel and $n = 1$

```
clear;
n=10000000; %initial number of monomer units
alpha=1e-6; %ratio of nucleation and growth rate constant
s=1; %the minimum number of monomer units in the smallest
viable seed
a=n; %initial number of nanoparticles
i=0; %initial number of steps

while a > 100, %loop until the number of nanoparticles
is 100
a=0; %initial number of nanoparticles
i=i+1; %increment number of steps
m=n; %current number of monomer units
tau=0; %dimensionless time
np=0; %increment number of nanoparticles

prsum=alpha*n; %initial sum of propensities
tau=tau-log(rand)/prsum/m; %initial time leap
a=a+1; %increment number of nanoparticles
np(a)=s;m=m-s; %decrement number of monomer units

while m > 0, %loop until the number of monomer units is 0
```

```
 prsum=alpha*n+a; %sum of propensities
 tau=tau-log(rand)/prsum/m; %time leap
 prob=rand*prsum; %random variable for step selection
 aux=alpha*n; %auxiliary variable
 if prob < aux, m=m-s;a=a+1;np(a)=s; %nucleation step
 selected
 else aux2=0; %second auxiliary variable for random
selection
       while prob > aux, aux2=aux2+1; aux=aux+1; end;
       np(aux2)=np(aux2)+1; m=m-1; %particle growth step
       selected
 end;
end;
np=np'; %the number of monomer units in the increment
'a'number of NPs
size=n/a; %average number of monomer units
var=sqrt(ones(1,a)*(np.*np)/a-size*size);    %variance
nprad=np.^(1/3); %size of the increment 'a' number of NPs
 radsize=sum(nprad)/a; %radius size
 radvar=sqrt(ones(1,a)*(nprad.*nprad)/a-radsize*radsize);
 %variance
 Res(a+5,i)=0;
 Res(1,i)=alpha;
 Res(2,i)=size;
 Res(3,i)=var;
 Res(4,i)=radsize;
 Res(5,i)=radvar;
 Res(6:(a+5),i)=np;
 csvwrite('Res.txt',Res);
 alpha=alpha/1.1;
end;
```

Listing 7.2: Matlab code for implementing the Gillespie algorithm for the mass kernel and $n = 5$

```
clear;
n=10000000;%initial number of monomer units
alpha=1e-3;%ratio of nucleation and growth rate constant
s=5; %the minimum number of monomer units in the smallest
viable seed
a=n; %initial number of nanoparticles
i=0;%initial number of steps

while alpha > 1e-6, %loop until the alpha
is 1e-6
 a=0;%initial number of nanoparticles
 i=i+1;%increment number of steps
m=n;%current number of monomer units
 tau=0;%dimensionless time
 np=0;%increment number of nanoparticles

 prsum=alpha*(m-1)*(m-2)*(m-3)*(m-4)/n/n/n;%initial sum of
 propensities
 tau=tau-log(rand)/prsum/m;%initial time leap
 a=a+1;%increment number of nanoparticles
 np(a)=s;m=m-s;%decrement number of monomer units

 while m > 0, %loop until the number of monomer units is 0
  prsum=alpha*(m-1)*(m-2)*(m-3)*(m-4)/n/n/n+sum(np);%sum of
  propensities
  tau=tau-log(rand)/prsum/m; %time leap
  prob=rand*prsum; %random variable for step selection
  aux=alpha*(m-1)*(m-2)*(m-3)*(m-4)/n/n/n;%auxiliary variable
  if prob < aux, m=m-s;a=a+1;np(a)=s;%nucleation step
  selected
   else aux2=0; %second auxiliary variable for random
    selection
      while prob > aux, aux2=aux2+1; aux=aux+np(aux2); end;
      np(aux2)=np(aux2)+1; m=m-1;%particle growth step
      selected
```

```
  end;
 end;
 np=np';%the number of monomer units in the increment
 'a'number of NPs
 size=n/a;%average number of monomer units
 var=sqrt(ones(1,a)*(np.*np)/a-size*size);%variance
 nprad=np.^(1/3); %size of the increment 'a' number of NPs
 radsize=sum(nprad)/a; %radius size
 radvar=sqrt(ones(1,a)*(nprad.*nprad)/a-radsize*radsize);
 %variance
 Res(a+5,i)=0;
 Res(1,i)=alpha;
 Res(2,i)=size;
 Res(3,i)=var;
 Res(4,i)=radsize;
 Res(5,i)=radvar;
 Res(6:(a+5),i)=np;
 csvwrite('Res.txt',Res);
 alpha=alpha/1.1;
end;
```

Listing 7.3: Matlab code for implementing the Gillespie algorithm for the surface kernel and $n = 3$

```
clear;
n=10000000; %initial number of monomer units
alpha=1e-6; %ratio of nucleation and growth rate constant
s=3; %the minimum number of monomer units in the smallest
viable seed
a=n; %initial number of nanoparticles
i=0; %initial number of steps

while a > 100, %loop until the number of nanoparticles is 100
 a=0; %initial number of nanoparticles
 i=i+1; %increment number of steps
 m=n; %current number of monomer units
 tau=0; %dimensionless time
 np=0; %increment number of nanoparticles

 prsum=alpha*(m-1)*(m-2)/n; %initial sum of propensities
 tau=tau-log(rand)/prsum/m; %initial time leap
 a=a+1; %increment number of nanoparticles
 np(a)=s;m=m-s; %decrement number of monomer units

 while m > 0, %loop until the number of monomer units is 0
  prsum=alpha*(m-1)*(m-2)/n+sum(np.^(2/3)); %sum
  of propensities
  tau=tau-log(rand)/prsum/m; %time leap
  prob=rand*prsum; %random variable for step selection
  aux=alpha*(m-1)*(m-2)/n; %auxiliary variable
  if prob < aux, m=m-s;a=a+1;np(a)=s; %nucleation step selected
    else aux2=0; %second auxiliary variable for random selection
      while prob > aux, aux2=aux2+1; aux=aux+np(aux2)^(2/3); end;
      np(aux2)=np(aux2)+1; m=m-1; %particle growth step selected
  end;
 end;
 np=np';%the number of monomer units in the increment
'a'number of NPs
 size=n/a;%average number of monomer units
```

```
  var=sqrt(ones(1,a)*(np.*np)/a-size*size);%variance
  nprad=np.^(1/3); %size of the increment 'a' number of NPs
  radsize=sum(nprad)/a; %radius size
  radvar=sqrt(ones(1,a)*(nprad.*nprad)/a-radsize*radsize);
  %variance
  Res(a+5,i)=0;
  Res(1,i)=alpha;
  Res(2,i)=size;
  Res(3,i)=var;
  Res(4,i)=radsize;
  Res(5,i)=radvar;
  Res(6:(a+5),i)=np;
  csvwrite('Res3.txt',Res);
  alpha=alpha/1.1;
end;
```

Listing 7.4: Matlab code for implementing the Gillespie algorithm for the Brownian kernel and $n = 2$

```
clear;
n=10000000; %initial number of monomer units
alpha=1e-6; %ratio of nucleation and growth rate constant
s=2; %the minimum number of monomer units in the
smallest viable seed
a=n; %initial number of nanoparticles
i=0; %initial number of steps

while alpha > 1e-7, %loop until the alpha is 1e-7
 a=0; %initial number of nanoparticles
 i=i+1; %increment number of steps
 m=n; %current number of monomer units
 tau=0; %dimensionless time
 np=0; %increment number of nanoparticles

 prsum=alpha*(m-1); %initial sum of propensities
 tau=tau-log(rand)/prsum/m; %initial time leap
 a=a+1; %increment number of nanoparticles
 np(a)=s;m=m-s; %decrement number of monomer units

 while m > 0, %loop until the number of monomer units is 0
  prsum=alpha*(m-1)+sum(np.^(1/3)); %sum of propensities
  tau=tau-log(rand)/prsum/m; %time leap
  prob=rand*prsum; %random variable for step selection
  aux=alpha*(m-1); %auxiliary variable
  if prob < aux, m=m-s;a=a+1;np(a)=s; %nucleation step selected
    else aux2=0; %second auxiliary variable for random selection
        while prob > aux, aux2=aux2+1; aux=aux+np(aux2)^(1/3); end;
        np(aux2)=np(aux2)+1; m=m-1; %particle growth step selected
  end;
 end;
 np=np';%the number of monomer units in the increment
 `a`number of NPs
 size=n/a;%average number of monomer units
 var=sqrt(ones(1,a)*(np.*np)/a-size*size);%variance
```

```
  nprad=np.^(1/3); %size of the increment 'a' number of NPs
  radsize=sum(nprad)/a; %radius size
  radvar=sqrt(ones(1,a)*(nprad.*nprad)/a-radsize*radsize);
  %variance
  Res(a+5,i)=0;
  Res(1,i)=alpha;
  Res(2,i)=size;
  Res(3,i)=var;
  Res(4,i)=radsize;
  Res(5,i)=radvar;
  Res(6:(a+5),i)=np;
  csvwrite('Res2.txt',Res);
  alpha=alpha/1.1;
end;
```